REDUCTION OF A SINGLE E3 UBIQUITIN LIGASE ALTERS NEURAL-SPECIFIC GLYCOSYLATION IN *DROSOPHILA MELANOGASTER*

by

NICKITA MEHTA

(Under the Direction of Michael Tiemeyer)

ABSTRACT

The regulatory pathways that control tissue-specific glycan expression are not well understood. A mutagenesis screen was undertaken in *Drosophila* to identify mutants that are deficient in the expression of a family of structurally related, neural-specific N-linked glycans known as HRP-epitopes. These epitopes are detectable by anti-HRP antibody staining. To date, three mutants have been recovered, each in different genes. Each mutant lacks HRP-epitope expression during embryonic stages and, as a group, the mutants exhibit genetic interactions with each other in regards to the loss of HRP-epitope. Additionally, all three mutants exhibit a similar neuromotor defect as adults. While mutant adults are motile and can right themselves when flipped over, they all fail to exhibit spontaneous climbing activity, which is a robust behavior in wildtype adults. One of these mutants, originally designated ms16, affects the expression level of an E3 ubiquitin ligase known as roc2, which has previously been demonstrated to be essential for neural development. In addition to altered HRP-epitope expression, the total glycan profile of *roc2*^{ms16} embryos was shifted toward increased abundance of complex glycans in comparison to wildtype embryos. In addition, Golgi compartmentation was also shifted such that the overlap between markers for early and late Golgi was increased, suggesting that augmented glycan complexity may arise from altered access of processing enzymes and substrates. Differential proteomic analysis,

by LC-MS/MS and validated subsequently by orthogonal approaches, detected significantly increased (2-fold) expression of ATPalpha (Na^+/K^+ pump-alpha subunit) in *roc2*^{ms16} mutants compared to wildtype. Conversely, quantification of HRP-epitope expression by ELISA detected increased expression of the neural-specific glycan class in a deficiency line that partially reduced ATPalpha expression. Therefore, increased ATPalpha expression (*roc2*^{ms16}) reduced HRP-epitope abundance while decreased ATPalpha expression (ATPalpha deficiency line) increased HRP-epitope abundance, indicating a role for ATPalpha in the regulation of glycoprotein glycosylation. Other components of the membrane excitability machinery were also impacted in *roc2*^{ms16}. Notably, expression of the excitatory glutamate receptor at the neuromuscular junction, dGluRIII, was increased in *roc2*^{ms16} larvae, perhaps in response to altered ionic fluxes induced by increased ATPalpha activity. Thus, altered roc2 activity impacts neural-specific glycosylation and key functions of excitable cells.

INDEX WORDS: HRP-epitope, glycosylation, neural development, ubiquitination, ion homeostasis, glutamate receptor, Na^+/K^+ ATPase

REDUCTION OF A SINGLE E3 UBIQUITIN LIGASE ALTERS NEURAL-SPECIFIC GLYCOSYLATION IN *DROSOPHILA MELANOGASTER*

by

NICKITA MEHTA

BS, Michigan State University, 2008

A Dissertation Submitted to the Graduate Faculty of The University of Georgia in Partial Fulfillment of the Requirements for the Degree

DOCTOR OF PHILOSOPHY

ATHENS, GEORGIA

2016

© 2016

NICKITA MEHTA

All Rights Reserved

REDUCTION OF A SINGLE E3 UBIQUITIN LIGASE ALTERS NEURAL-SPECIFIC GLYCOSYLATION IN *DROSOPHILA MELANOGASTER*

by

NICKITA MEHTA

Major Professor: Michael Tiemeyer

Committee: Richard Steet
Lance Wells
Michael Pierce

Electronic Version Approved:

Suzanne Barbour
Dean of the Graduate School
The University of Georgia
May 2016

To my grandfather, the man who taught me that everything non-science is “non-sense”

and to my mom, the brightest star in the sky that’s always shining over me.

You left this world too soon.

ACKNOWLEDGEMENTS

I would like to start by thanking my advisor Michael Tiemeyer for the constant support and for being patient with me through the years. Thank you for being such a great role model – if I can be half as smart and enthusiastic as you are someday, I will consider myself super lucky. Thank you for being available for all my stupid questions while never letting me feel dumb, for giving me the freedom to do whatever I wanted and for being the best mentor I could have ever asked for. I would also like to thank my committee members, Lance Wells, Michael Pierce and Richard Steet for all your insightful suggestions and questions. Thank you for helping me through this process and for all your advice. I could not have done this without you all.

I will forever be grateful to Katie Tiemeyer aka “Western/Elisa Robot”, the sweetest 17 year old I know. I still remember your first summer in the lab 3 years ago and I am so proud of the beautiful and intelligent scientist you have become today. Thank you for everything you did for me, from sorting to beheading flies to being such a good friend and bringing me chocolate when I am down. I consider myself lucky to have you in my life. I wish you so much success in your future and know that you will be nothing short of amazing. I guess that is one more thing I should thank your dad for..his good genes!

A good support system is key in graduate school and I could not have gotten through it without my amazing friends at the CCRC and outside (you know who you are) and of course the Tiemeyer lab members. I seriously lucked out with all of you. You guys are the only people that can get on my nerves and make me laugh all at the same time. Thank you for keeping me sane through the years and putting up with me. I will always remember the good times we had and I cannot imagine not seeing you all (almost)

everyday. I have learned something new and exciting every single day being around you and cannot thank you enough. I would like to thank my personal support crew, Mindy and Simone. Thank you for being such amazing coworkers and friends. For always being there for me and bringing so much positivity into my life. I will miss your smiling faces. I love you guys!

I must thank my family for all their unconditional love and support in the last six years. Especially my dad and sister, who are a true inspiration to me and motivate me on a daily basis to be a better person and work hard. I love that you are so proud of me even though you don't have a clue what my research is about. You have been instrumental in me gaining any sort of confidence in who I am today and I can never thank you enough.

Lastly and most importantly, the best thing that happened to me during the last 6 years was marrying my best friend and soul mate, Shiraz. Thank you for being my biggest cheerleader, for always encouraging me to follow my dreams and loving me through the good times and the bad. You have been there for me through thick and thin and I thank you with all my heart for that (even when I am super cranky and we both know those are BAD days). Thank you for coming to lab with me at odd hours of the night and weekends and listen to me blab on for hours talking about things you don't understand. Thank you for believing in me on days when I didn't believe in myself. I love you.

TABLE OF CONTENTS

Page

ACKNOWLEDGEMENTS v

LIST OF TABLES ix

LIST OF FIGURES x

CHAPTER

1 INTRODUCTION AND LITERATURE REVIEW 1

Summary and scope of dissertation 42

References 44

2 REDUCTION OF A SINGLE E3 UBIQUITIN LIGASE ALTERS NEURAL-SPECIFIC GLYCOSYLATION IN *DROSOPHILA MELANOGASTER* 53

Abstract 54

Introduction 55

Experimental Procedure 58

Results 64

Discussion 84

References 90

3 MASS SPECTROMETRIC QUANTIFICATION OF N-LINKED GLYCANS BY REFERENCE TO EXTERNAL STANDARDS 94

Abstract 95

Introduction 96

Experimental Procedure 98

Results and Discussion 103

Conclusions 126

References 128

4 CONCLUSIONS AND FUTURE DIRECTIONS 131

Closing Remarks 138

References 141

APPENDICES

A Appendix Tables (S1-S6) 143

B Appendix Figures (S1-S7) 149

LIST OF TABLES

Page

Table 1.1: *Drosophila* specific mutations in N- and O-linked glycosylation and their phenotypes 11

Table 1.2: Mutants that affect HRP-epitope fall into two classes 23

Table 2.1: P-element recombination mapping suggested that the mutation was between nucleotide 6141579 and 9637727 67

Table 3.1: N-glycan and malto-series oligosaccharide standards for glycan modification 104

LIST OF FIGURES

Page

Figure 1.1: Biosynthesis of the Dolichol P-P precursor and initial N-glycan synthesis 6

Figure 1.2: Classes of N-glycans 7

Figure 1.3: N-glycosylation in *Drosophila* 9

Figure 1.4: Neuroblast formation in *Drosophila* 13

Figure 1.5: Engrailed expressing cells in stage 12 embryos.....15

Figure 1.6: Anatomy of the muscles at the NMJ in third instar larvae..... 18

Figure 1.7: HRP-epitopes found in *Drosophila* 22

Figure 1.8: HRP-epitope mutants 26

Figure 1.9: The Ubiquitination process 28

Figure 1.10: Ion exchange through the Sodium-Potassium pump..... 34

Figure 1.11: Golgi compartmentalization and localization of glycosyltransferases..... 41

Figure 2.1: HRP epitopes in Drosophila are decreased in m16..... 65

Figure 2.2: A mutation in Roc2, an E3 ubiquitin ligase is responsible for the ms16 phenotype 70

Figure 2.3: Insertion of Roc2 in ms16 background rescues HRP-epitope expression in specific cells 70

Figure 2.4: *Roc2*^{ms16} interacts with other players of the pathway, Tollo and sff..... 71

Figure 2.5: Overall N-glycosylation is altered in the mutant and shifted to an increase of a subset of complex sialylated glycans using PNGaseF..... 73

Figure 2.6: Golgi architecture and integrity is altered in the mutant..... 75

Figure 2.7: Several proteins are affected by the absence of a ubqituin ligase including Na+/K+-ATPase*, which alters HRP-epitope expression* 78

Figure 2.8: *Roc2*^{ms16} mutants are deficient in negative geotaxis, have reduced viability at increased temperatures and have altered neural muscular junctions (NMJ) 82
Figure 2.9: Golgi architecture and overall glycosylation is altered in the mutant 89
Figure 3.1: Heterogeneity and mass purity of N-glycan standards 107
Figure 3.2: Linearity of MS responses for N-glycan standards 108
Figure 3.3: Linearity of MS/MS responses for major N-glycan standard fragments 109
Figure 3.4: Constant ratio of major MS/MS fragments for N-glycan standards 111
Figure 3.5: Linearity of MS responses for malto-series standards..... 114
Figure 3.6: Molar responses for permethylated N-glycan and malto-series standards are independent of glycan mass 115
Figure 3.7: Comparability of signal responses for malto-series standards across three analytic platforms 117
Figure 3.8: Molar response factors for malto-series standards measured by HPLC-fluorescence detection and by mass spectrometry 118
Figure 3.9: Permethylation of malto-series standards with methyliodide containing stable isotopes of carbon or hydrogen yields equivalent MS responses 120
Figure 3.10: Recovery of MS signal responses for external standards mixed into a biological matrix..... 122
Figure 3.11: Quantification of mouse brain N-glycans by reference to external standards.....125
Figure 4.1: Roc2 regulates glycan expression by controlling synaptic homeostasis and neural membrane potential 140

CHAPTER 1

INTRODUCTION AND LITERATURE REVIEW

Although protein glycosylation is essential for normal development and viability in all-multicellular organisms, the pathways and mechanisms that control tissue-specific glycan expression are not well understood. This is due to the complexity of glycans on proteins and a lack of animal models with tissue specific glycosylation defects. *Drosophila melanogaster* embryos express a family of neural-specific, core α3-fucosylated N-linked oligosaccharides called HRP epitopes, which can be used as a reporter to study the role of glycosylation in neural development. The scope of this dissertation highlights the importance of the underlying mechanisms that control tissue-specific glycosylation through which we can understand its role in neural development.

In this chapter, general properties of glycoprotein glycosylation will be discussed including the many functions of glycans. Since the main focus of this project deals with N-glycosylation in the developing *Drosophil*a embryo, these topics will be discussed in length. This will be followed by an introduction into the vast field of Golgi trafficking, signaling and ubiquitination. Finally, Na^+/K^+ ATPase, which is an ion pump involved in signaling and trafficking, another focus of my research, will also be discussed.

Glycoprotein glycosylation

Glycans cover the surface of all animal cells and are found in the form of glycolipids and glycoproteins. They form a coat, which is the outermost layer of the cell called the glycocalyx; this ultimately becomes the interface between the cells. Glycosylation is ubiquitous and glycans can be added post-translationally to proteins and post-synthetically to lipids. The process starts in the Endoplasmic Reticulum (ER) and then continues into the Golgi where further modifications take place. Different subgroups

of glycans are built in the Golgi that create various classes of glycans, after which they get transported to their final destination. There are certain themes of glycans that differ based on how they are initiated; most glycans are either N-linked, i.e., they are attached to an Asparagine residue, O-linked (attached to a Ser/Thr) or C-linked (mannose attached to a tryptophan residue). If they are O-linked they are predominantly initiated by N-acetylgalactoseamine (GalNAc), Mannose or Fucose, and in case of N-linked they are initiated by N-acetylglucosamine (GlcNAc) (Varki et al., 2009). Glycosylation can be species, tissue and cell specific.

In addition to linkage differences, glycans are also extremely complex due to variation in branching and assembly of monosaccharides. Even a specific site can have different glycans, called microheterogeneity (Schachter, 2014). The intricacies in understanding glycosylation also lie in the fact that it requires a lot of machinery. There are a myriad of proteins (~700) required for building all the different possible glycans in mammals, which not only include enzymes and glycosyltransferases, but also availability and localization of substrates and donors (Moremen et al., 2012).

Glycosylation is crucial in both biological and physiological roles from protein folding to development and disease (Varki et al., 2009). Cell surface glycans are essential in several ways; not only in cell-cell interaction and communication, but also for signaling as they can be ligands, receptors and interactors, all of which directly influence function and activity (Varki, 1993). Recent studies have also provided evidence of glycosylation playing roles in immunity, in recognizing viral infections as well as neuronal functions; the failure of which leads to diseases like Alzheimers.

Glycosylation in development and disease

The diversity of glycans and assembly during development emphasizes their importance throughout the process (Haltiwanger and Lowe, 2004). Glycans on cell surfaces mediate interactions throughout development and consequently play a role in

cell-cell interaction. This function makes glycosylation a vital process and its defects have been shown to lead to cognitive disabilities, muscular dystrophy, congenital disorders of glycosylation, immunodeficiency and defects in protein maturation (Freeze, 2002; Varki, 1993; Haltiwanger and Lowe, 2004; Grewal and Hewitt, 2003). As cells differentiate, the glycans they possess change, making glycosylation in each tissue and cell unique, thus imparting discrete functions. As such, tissue specific glycosylation is shown to have serious implications for signal modulation, cell-migration, recognition and adhesion (Acheson et al., 1991; Storan et al., 2004; Zhang et al., 1992; Stanley and Okajima, 2010). A well studied example of tissue specific glycosylation is the role that Notch plays in development. Notch is a family of proteins that contain O-fucose modifications and is fundamental for development in metazoans as a signaling molecule that drives differentiation. There are four Notch receptors in mammals and one in *Drosophila melanogaster* (Takeuchi and Haltiwanger, 2010). Notch plays a role in several tissues in *Drosophila*, including neurons, heart and muscle (Fortini, 2009; Fortini, 2012). In order for its ligands, Delta and Serrate to interact with it, Notch needs to be glycosylated on its Epidermal Growth Factor (EGF) repeats. Failure of Notch activity leads to altered neurogenesis (de la Pompa et al., 1997) and embryonic lethality in mice (Swiatek et al., 1994). Mutations in Notch and its pathway are also associated with several diseases like multiple sclerosis and colon cancer (Takeuchi and Haltiwanger, 2010) demonstrating once more the importance of glycosylation in development. Notch got its name from *Drosophila* through its phenotype of “notched” wings.

N-glycosylation

The synthesis of glycans has been a subject of extensive investigation by studying the multitude of signaling pathways that direct glycan biosynthesis. Since this dissertation mainly focuses on N-glycosylation, its synthesis will be discussed in full detail. The biosynthesis of N-glycans starts at the cytoplasmic side of the ER where a

specific glycosyltransferase, GlcNAc-1-phosphotransferase, utilizes UDP-GlcNAc to add a phosphate and a GlcNAc onto a membrane bound Dolichol-Phosphate (Dol-P) causing the release of UMP. Using another UDP-GlcNAc, a second GlcNAc residue is transferred to the Dol-P-GlcNAc, which is followed by the addition of five mannose residues, step-wise, from GDP-Man to result in $Man_5GlcNAc_2$-P-P-Dol. This precursor then flips into the lumen of the ER for further modification (**Fig 1.1**). The Dol-P-P glycan precursor gets further decorated by four Mannose residues and three Glucose residues by Dol-P-Man and Dol-P-Glc, respectively. All monosaccharide additions in building this precursor are catalyzed by specific glycosyltransferases. In animals, the $Glc_3Man_9GlcNAc_2$ precursor glycan is highly conserved and ultimately gets added to an asparagine residue on a nascent protein that is in the lumen of the ER. This process requires a specific Oligosaccharyltransferase complex (OST).

Once transferred onto a protein, a series of stepwise cleavages occur to remove the glucose residues, followed by the removal of a mannose residue by the ER mannosidase I. This is a crucial step in the synthesis pathway as quality control through the chaperone proteins, calnexin and calreticulin, determine the fate of glycoproteins that can either exit the ER to get further processed in the Golgi or get degraded (Xu and Ng, 2015; Ellgaard and Helenius, 2003). In the Cis-Golgi, glycans are trimmed down to $Man_5GlcNAc_2$-Asn, which now acts as a precursor to form the three classes of N-glycans. The addition of GlcNAc through N-acetylglucosamine transferase (GlcNAcT-1 or GnTI) starts the N-glycan branching process through which glycans shift toward complexity. For complex glycosylation, monosaccharides like fucose (Fuc) using GDP-Fuc as a donor, Galactose (Gal) using UDP-Gal and sialic Acid (SA) using CMP-SA are added after the action of GnTI, II, III and IV. Glycans are considered high mannose when there is no further addition to the $Man_5GlcNAc_2$-Asn except terminal mannose residues. A hybrid structure as the name suggests is a branched glycan with a mix of one arm

containing only terminal mannose residues while the other arm has complex sugars (**Fig 1.2**).

Figure 1.1: Biosynthesis of the Dolichol P-P precursor and initial N-glycan synthesis.
The synthesis of N-glycans starts in the cytoplasm of a cell. The process starts with the building of a Dolichol linked precursor, followed by the addition of GlcNAc (2) donated by UDP-GlcNAc and mannose residues (5) through GDP-Man. This glycan then flips into the lumen the Endoplasmic Reticulum, where additional mannoses are added. This process is completed by the addition of three glucose residues before the $Glc_3Man_9GlcNAc_2$ precursor glycan is transferred onto a nascent protein using the OST complex. Adapted from Varki et al., 1999.

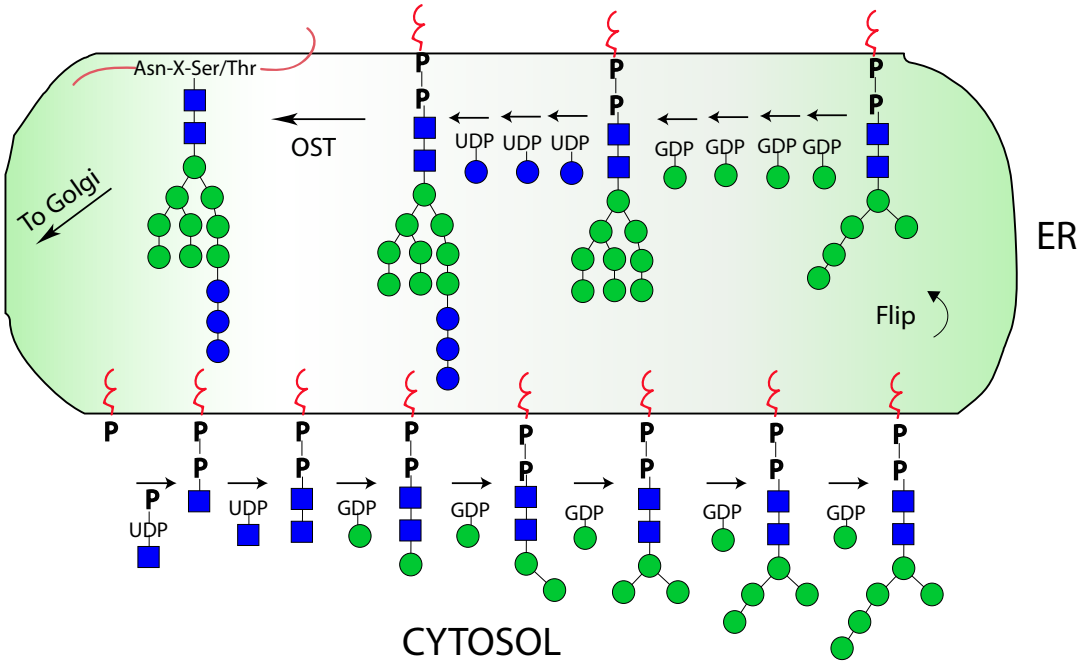

Figure 1.2: Classes of N-glycans.
There are three classes of N-glycans based on the enzyme interactions and the substrate: high mannose (terminal oligomannose stay unmodified), hybrid (when one branch has terminal oligomannoses and the other has been modified by enzymes like GnTI-IV, GalT or SiaT) and complex (both branches are modified). Adapted from Varki et al., 1999.

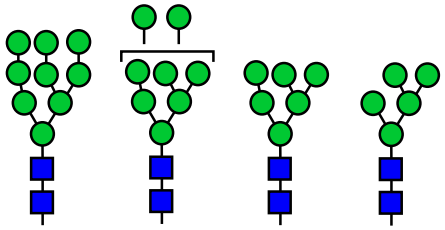

High mannose glycans (left-right): Man9, MAn8, Man6 and Man5

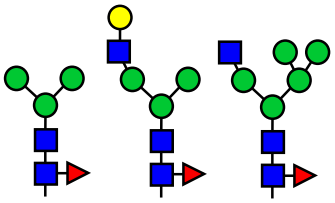

Paucimannose (left) and hybrid glycans (middle and right)

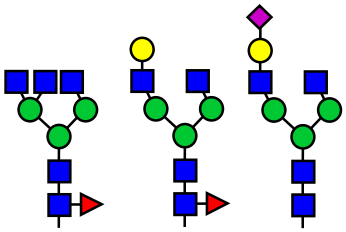

complex glycans

Drosophila as a model system

To understand tissue-specific glycosylation in its entirety, studying glycosylation in whole organisms is necessary, making *Drosophila* a valuable model (Seppo and Tiemeyer, 2000; Tiemeyer et al., 2009). *Drosophila* has been the major model system for several decades in genetics because it has several advantages; some of which include a fully sequenced genome, a complex neural system and a regulated and short developmental cycle. The *Drosophila* life cycle spans approximately two weeks starting with 17 embryonic stages (24 hours), three larval stages, a pupal stage which finally become an adult approximately nine days later (Hartenstein and Campos-Ortega, 1985). Most experiments discussed in this thesis are performed in the developing embryo; however, there are also experiments in larval and adult stages.

N-glycosylation in *Drosophila*

Glycosylation is conserved across species for the most part; however, there are some variations in insects compared to eukaryotes and these will be highlighted here in detail. The most abundant glycans in *Drosophila* are high mannose type glycans, but the insect does make other glycans too (Aoki et al., 2007). The presence of an Arthropod specific hexosaminidase, Fused Lobes (Fdl), contributes to the abundance of high mannose glycans (Léonard et al., 2006). (**Fig 1.3**) Fdl removes the GlcNAc that is added by GnTI to the α1,3-linked mannose on the non-reducing end and gives rise to paucimannosidic as well as high mannose structures by eliminating the option for these glycans to be further modified. Nonetheless, some glycans are able to bypass the action of Fdl and can become more complex by the action of enzymes like GnTI-IV, Galactosyltransferase (GalT), Sialyltransferase (SiaT) and fucosyltransferases (FucT), all of which are present in *Drosophila* but not as well studied. Since *Drosophila* only possesses a single SiaT (DSiaT), with significant homology to mammalian a2,6 sialyltransferases, it is a good system to study the roles of protein sialylation.

Figure 1.3: N-glycosylation in *Drosophila*.

Glycosylation between species is relatively conserved, however, there are some specific changes in *Drosophila*. In the fly, there is an enzyme called Fdl, that keeps a balance of glycans between paucimannose (green) and complex structues (blue). In the presence of this enzyme, the terminal GlcNAc added by GnTI, is removed to prevent the glycan from getting further modified. In addition to Fdl, another *Drosophila* specific modification is added by FucTA, which adds a fucose monosaccharide in α1,3 linkage to the proximal GlcNAc residue adjacent to the asparagine (red). So far, sialylated complex glycans (purple) are only seen in the presence of a single core α1,6-linked fucose.

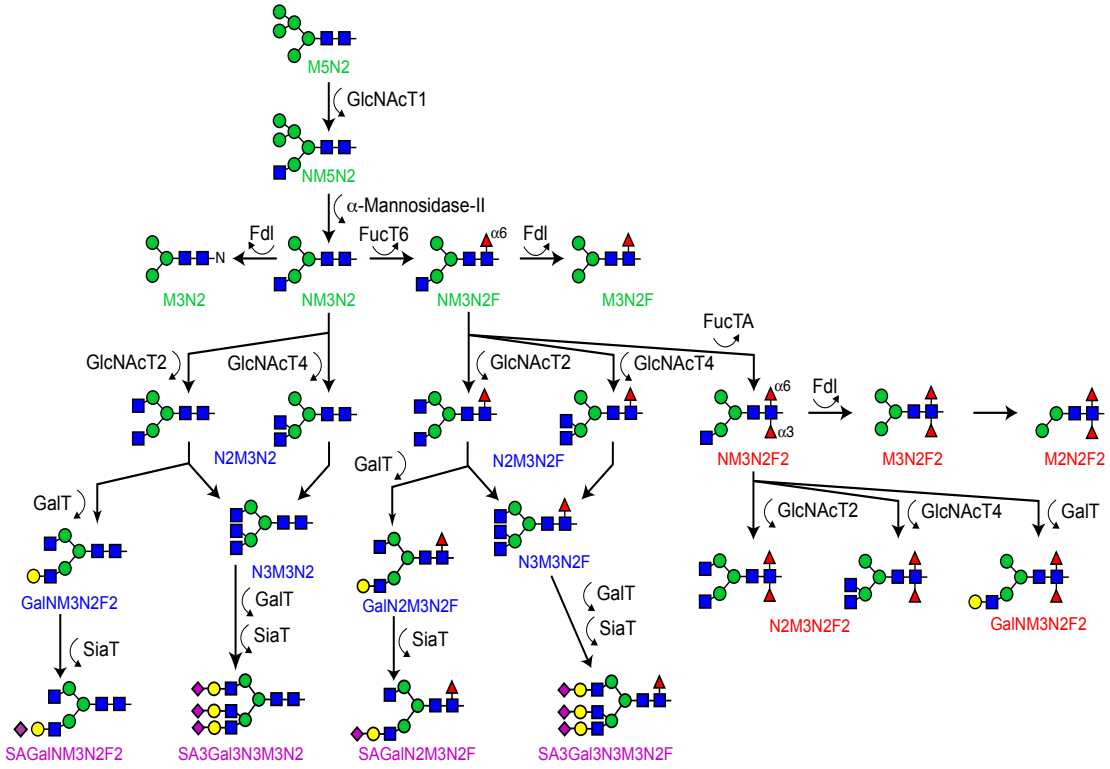

To this end, mutations in DSiaT, which is only expressed in a subset of CNS neurons, have led to several neurological and behavioral defects, including shorter life span and paralysis (Repnikova et al., 2010). Furthermore, mutations in other glycosyltransferases, like mgat1 and O-fut-1, have also been studied and demonstrated phenotypes ranging from reduced viability to altered cellular differentiation, respectively (**Table 1.1**). These phenotypes address the importance of complex glycans as well as their associated enzymes in development.

Another unique characteristic of arthropod N-glycans is the ability to decorate the chitobiose core with both α1,3 and α1,6 linked fucose modifications, whereas mammals solely bear α1,6 linked fucose residues at the proximal reducing GlcNAc residue. The α1,3 linked core fucose is found on proteins whose expression is restricted to neural tissue. This fucose residue is the antigenic determinant for antibodies generated against the plant glycoprotein horseradish peroxidase (HRP); these antibodies have been used for decades as markers to study neural development. HRP-epitopes also appear early in development and therefore it can be used as a reporter throughout the development of the nervous system. This thesis uses HRP-epitopes as markers to understand the underlying mechanisms that control neural glycosylation and will be discussed in more detail later in this chapter.

Neural development in *Drosophila*

The nervous system can be divided into the Central Nervous system (CNS) and Peripheral Nervous System (PNS); in *Drosophila*, the CNS is comprised of the ventral nerve cord (VNC) and the brain. In this section, formation of the VNC will be reviewed as the next chapter discusses a mutation in neural tissue, including the VNC. After fertilization, embryogenesis starts with cellularization and blastoderm formation. This is followed by gastrulation around stage 8, which ends approximately 5 hours post

Table 1.1: *Drosophila* specific mutations in N- and O-linked glycosylation and their phenotypes.

Mutant	Affected Protein	Phenotype
mas1	a-Mannosidase I	peripheral nervous system, wing, and eye morphology
fused lobe (*fdl*)	glycoprotein glycan processing β-hexosaminidase	larval and adult brain lobe morphology
mgat1	GlcNAcT-I	reduced viability and locomotor activity
tollo/toll-8	Toll-like receptor 8	altered glycosylation in embryonic central nervous system
neurally altered carbohydrate/GFR (nac/GFR)	GDP-Fuc transporter in the Golgi	altered glycosylation in larval, pupal, and adult central nervous system
fuctA	α3-fucosyltransferase	altered glycosylation in larval, pupal, and adult central nervous system
sugar-free frosting (sff)	Sff/SAD serine/threonine protein kinase	altered glycosylation in embryonic nervous system, adult locomotor defects, Golgi organization defects
dSiaT	α6-sialyltransferase	adult locomotor defects, temperature-sensitive seizures, altered neuronal membrane excitability
pgant3	Polypeptide GalNAcT	cell adhesion deficits
pgant4	Polypeptide GalNAcT	Golgi trafficking
pgant5, pgant7 & 35g	Polypeptide GalNAcT	pupal lethality
rotated abdomen (*rt*)	Protein-*O*-mannosyltransferase I	abdominal morphology
twisted (*tw*)	Protein-*O*-mannosyltransferase II	abdominal morphology
OFUT-1	*O*-fucosyltransferase I	*notch*-like defects in cellular differentiation
efr	GDP-Fuc transporter in the ER	*notch*-like defects in cellular differentiation
fringe (*fng*)	Fuc-specific β3GlcNAcT	pattern formation defects resulting from altered Notch activation
rumi	protein *O*-glucosyl and *O*-xylosyltransferase activity	*notch*-like defects in cellular differentiation

fertilization (Jan and Jan, 1982). During gastrulation, cells at the ventral midline involute and migrate dorsally into the embryo, resulting in the formation of mesoderm, endoderm, and ectodermal layers. After gastrulation, the neurogenic ectoderm gives rise to either the ventral neuroectoderm or the procephalic neuroectoderm with the latter determining where the brain hemispheres emerge. However, the organization of these cells is still unclear. The precursor cells of the VNC come from the ventral neurogenic ectoderm, which either gives rise to neuroblasts (NBs) or epidermoblasts (controlled by proteins like Notch) (Campos-Ortega, 1994; Campos-Ortega, 1988). NBs continuously divide asymmetrically, generating ganglion mother cells (GMC) from the basal side and then get pushed dorsally into embryos between stages 9 through 13 (Fuerstenberg et al., 1998; Doe and Goodman, 1985). GMCs divide into approximately 400 neurons (5% motor neurons or ~90% interneurons) and/or ~5% glia at the midline VNC. Glial cells can become midline glial cells or lateral glial cells while the interneurons are formed. Interneurons extend axons within the nerve cord (Campos-Ortega, 1994; Skeath and Thor, 2003) and motor neurons extend their axons into the periphery. Neuroblast formation is a continuous process and starts with the appearance of NB 3-5 and 2-5, followed by a sequential series of 12 NBs, all of which are considered “early NBs” forming the first three columns. Next, the eight “middle NBs” arise in between the 2nd and 3rd column and finally, the last nine NBs (considered the “late NBs”) along with segment specific median neuroblast (aMNB) and NB 5-5 are formed. In total, NBs form seven rows and three columns along with a dorsal MNB (Doe and Goodman, 1985) (**Fig 1.4**). Each of the NBs gives rise to GMCs of different sizes and with different gene expression, which makes *Drosophila* a powerful model to study neurogenesis. This organ system is very complex and needs regulatory genes for proper development as can be seen by the distinct properties of each cell and the expression of their ion channels, neurotransmitters and neuropeptides.

Figure 1.4: Neuroblast formation in *Drosophila*.
In *Drosophila*, neurogenesis starts with the division of neuroblasts into GMCs. The "early" NBs are light yellow and get darker as the "late" NBs come up. These neuroblasts are organized into seven rows and three columns, 25 hours after the first NB formation. The fate of each of these neuroblasts is genetically predetermined. The image below displays only half a segment. Figure adapted by(Doe and Goodman, 1985)

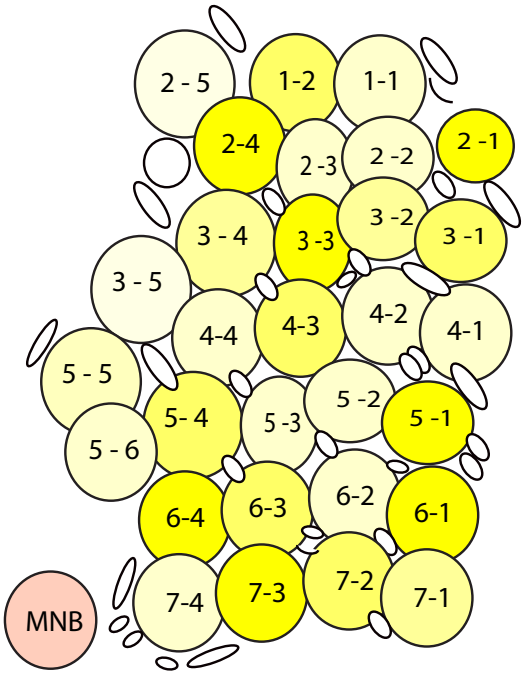

Since these genes and transcription factors drive the fate of the neurons and the glia, this system can be used to genetically manipulate expression of genes in specific neurons. An elegant portrayal of this system is seen with Prospero protein that is needed for GMCs to activate GMC specific gene expression (e.g., *even-skipped*). During NB mitosis, *prospero* gets first transported to the basal side of the NB, and then into the nucleus of the GMC where it plays an essential role for GMC cell fate. *Prospero* is needed for GMC cell fate. In the second chapter of this dissertation, we have used a similar system where we are able to drive expression of HRP-epitopes in a specific subset of nerve cells to show rescue of our mutant. For our experiments, we use a transcription factor called *engrailed* (*en*), which is expressed in the posterior midline glial cells starting around embryo stage 10. Specifically, the expression is seen in median neuroblasts (MNB) of rows six and seven, that eventually become ventral unpaired median (VUM) and midline precursors (MPs) (Schmid et al., 1999) (**Fig 1.5**).

The midline cells of the ventral nerve cord develop independently compared to the rest of the nerve cord. The precursor cells start to assemble around stage 5 and by stage 8, they assemble into a single row (Hartenstein and Campos-Ortega, 1985). Around stage 12, the VNC commissures are formed and development continues through a series of events through stage 14 where axon tracks are fully complete and mature. This is when nerve condensation (9-10 hours) starts as well as the curling over of the brain lobe towards the axon scaffold (Jan and Jan, 1982). This contraction continues through the development of the embryo. Staining with antibodies against the HRP-epitope in the *Drosophila* embryo beautifully demonstrates the nerve cord development and brain lobes through out development, as it appears early on in development (**Fig 1.5**).

Figure 1.5: Engrailed expressing cells in stage 12 embryos
In *Drosophila* embryos, neural fate is determined by the transcription factors it possesses. Therefore, its possible to genetically manipulate the neurons to drive expression of specific genes in specific cells. (A) Embryo stained with anti-HRP showing commissures, segments and brain lobes. (B) Engrailed is expressed in the posterior neuroblasts of each segment, as shown below. Figure demonstrates cells within ONE segment.

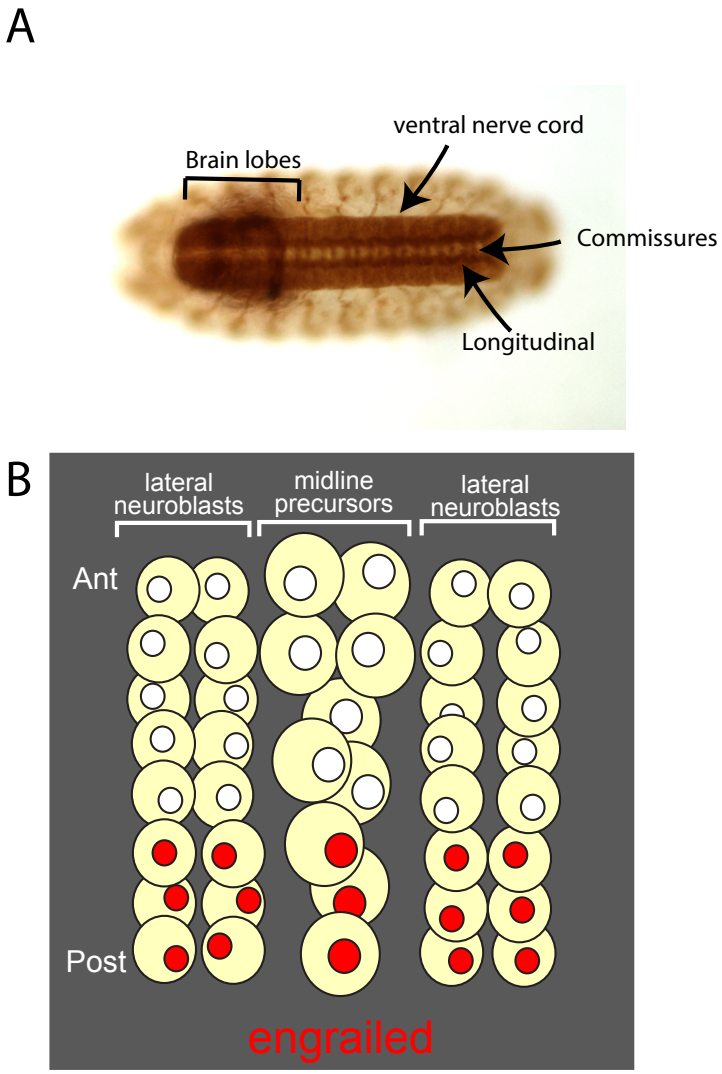

Neuromuscular Junction

Neural activity is transmitted from cell to cell through a synapse, which can either be between two neurons or a neuron and a target cell. Hence, a synapse can be defined as an area between two cells, which could be nerve and nerve or nerve and target, which in the case of the NMJ is a muscle fiber. Motor neurons are derived from different NBs, which at embryonic stage 15 extend their axons into the musculature (Landgraf et al., 1997; Landgraf and Thor, 2006). As previously mentioned, the path of the neurons are predetermined using transcription factors that drive neural fate (Ruiz-Cañada and Budnik, 2006). One side is the pre-synaptic side, which is where the neurotransmitter is stored and eventually released from and the other is called a post-synaptic density (PSD); this is the neural or non-neural region where the receptors that bind the neurotransmitters are located. In neuron-neuron communication, the dendrites on the post-synaptic neuron accept the signal passed by the pre-synaptic neuron. Once the growth cones of developing axons connect to targets, PSD form and receptors are recruited to the surface; this usually happens at the end of embryonic development. At approximately the same time, growth cones become the pre-synaptic neuronal boutons. Motor nerve terminals differentiate to pre-synaptic active zones where vesicles dock and the neurotransmitter is emitted. A bouton contains an active zone on the pre-synapse and a receptor on the post-synaptic cell.

In *Drosophila*, there are only 32 known motor neurons in each segment and its NMJ is studied extensively (Menon et al., 2013). The muscle pattern consists of a collection of 6 segmental repeats, and each of the segments is made up of exactly 30 identifiable muscles (Keshishian et al., 1996) (**Fig 1.6**). The NMJ uses different neurotransmitters across different species. Unlike humans, whose NMJ utilize acetylcholine as their primary neurotransmitter, *Drosophila* NMJs are glutamatergic and use ionotropic glutamate receptors (homolog of AMPA receptors in human brain). The

simplicit, accessibility, and resemblances to human systems make *Drosophila* a good model to study NMJs.

Once an action potential is fired and reaches the pre-synaptic bouton, a voltage dependent calcium channel is activated, causing the influx of calcium and leading to the fusion of vesicles containing neurotransmitter to the membrane; this fusion causes exocytosis of the neurotransmitter into the synaptic cleft (region in between pre- and post-synapse). Pre-synaptic active zones consist of a collection of proteins, called cytomatrix proteins, which work together and are responsible for proper neurotransmitter release as well as regulating the required machinery. Some of these proteins include Actin (Blunk et al., 2014), protein phosphatase 2A and GSK-3β (Viquez et al., 2009), spectrin (Featherstone et al., 2001) and Bruchpilot (Brp) (Fouquet et al., 2009; Kittel et al., 2006; Matkovic et al., 2013; Wagh et al., 2006). The alignment of the neurotransmitter release region and the receptor on the PSD is essential for efficient function and uptake (Marrus et al., 2004), and is carried out by the collection of proteins found at the active zone. For example, mutations in *Drosophila* Actin 57B, cause impaired alignment and spacing of the active zones, alters function of post-synaptic spectrin and causes mislocalization of other proteins (Blunk et al., 2014). Alterations in spectrin localization and function lead to disruptions in presynaptic vesicle tethering and post-synaptic receptor aggregation (Featherstone et al., 2001). *Drosophila* NMJs also have approximately 500 independent active zones which are near a cluster of glutamate receptors (DGluR's) normally correlated with the amount of Brp present at the active zone (Viquez et al., 2009).

Figure 1.6: Anatomy of the muscles at the NMJ in third instar larvae.
(A) The NMJ in *Drosophila* is composed of six identical segments. (B) Each of these segments contains 30 muscles in a highly organized fashion. The muscles that have the most identified NMJs are between muscles 6 and 7. (C) Boutons and active zones branch off the NMJ as indicated in the picture below. Figure adapted from (Menon et al., 2013).

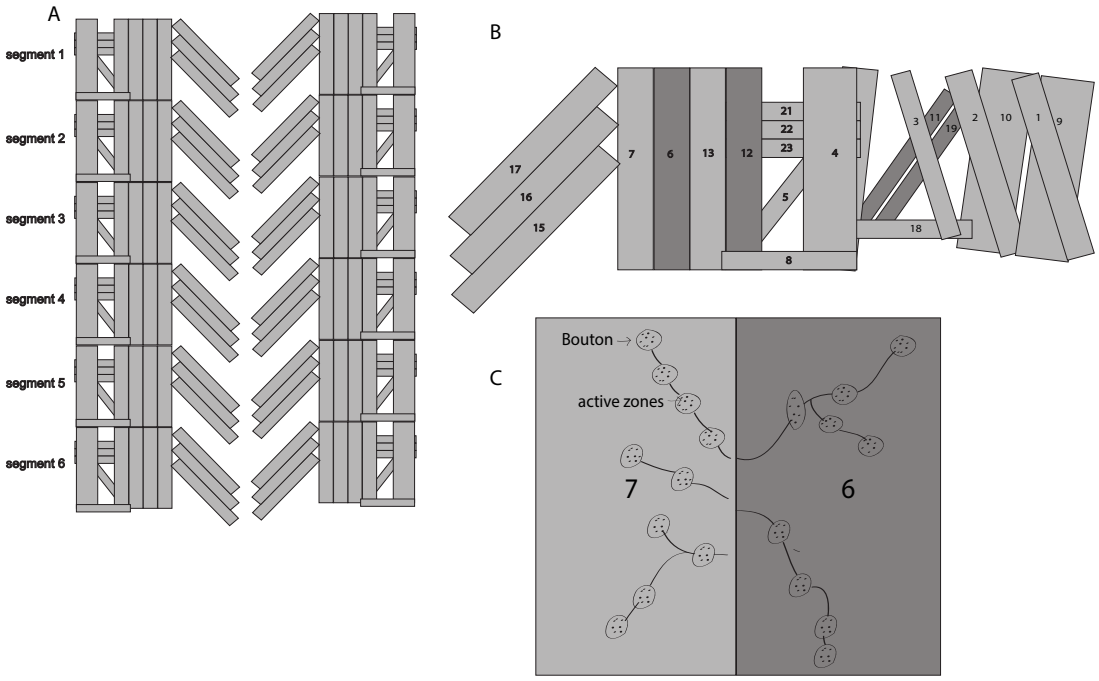

Glycoproteins are part of the synaptomatrix and are essential for NMJ development. Their functions include differentiation of the active zone. Altered glycosylation of key components of the NMJ, such as Wnt protein wingless and BMP proteins, result in complete disruption leading to improper NMJ development (Kamimura et al., 2013). In addition, *Mgat1* mutants give rise to NMJs that are increased in size because of increased bouton area and branching (Parkinson et al., 2013). HRP-carrying proteins, like Fasiclin II cell adhesion molecule, are also present at the NMJ and regulate GluR assembly (Beumer et al., 2002).

The response of the PSD to the signal is key in shaping synaptic strength, which is determined by the receptors receiving the neurotransmitter (Marrus et al., 2004). Therefore, understanding of the receptor subunits is extremely crucial. There are seven known ionotropic receptors in *Drosophila*; four of these are expressed exclusively in the CNS (Vèolkner et al., 2000), and the other three in somatic muscles (Schuster et al., 1991; Marrus et al., 2004). The family of receptors discussed in chapter 2 is glutamate receptors. There are six of these known in *Drosophila*: DGluRIIA-E and DGluRIII. These receptors are expressed at the NMJ and even though DGluRIIA and DGluRIIB are redundant in viability, they function independently and have different physiological properties (DiAntonio et al., 1999). DGluRIII is required for synaptic localization and transmission of DGluRIIA and IIB, while only one of the two, DGluRIIA or IIB, is needed for the localization of DGluRIII (Marrus et al., 2004). DGluRIIA and B are found in the form of heterotetramers at the NMJ, however whether DGluRIII heterotetramerizes with DGluRII's is not known.

HRP-epitope

As briefly discussed in the previous sections, the HRP-epitopes are N-linked oligosaccharides expressed throughout development of the nervous system in *Drosophila* embryos. The antigenic determinant is an α1,3-linked fucose on the reducing

end of the chitobiose core added by fucosyltransferase A (FucTA) (Paschinger et al., 2009; Rendic et al., 2010). So far, all the HRP-epitopes found in *Drosophila* have been identified (Aoki et al., 2007) (**Fig 1.7**). This modification represents a hallmark on plant and various invertebrate derived N-glycans. As it is foreign to vertebrates, humans and rabbits can generate antibodies against this epitope. In *Drosophila*, anti-HRP-epitopes are expressed in the ventral nerve cord (VNC), and peripheral nervous system (PNS) and some non-neural tissues like the garland gland (gg), posterior hindgut (phg) and anal pads (ap). HRP-epitope staining is not seen in NB but does start to appear in 6-hour embryos (Jan and Jan, 1982). There are several known proteins that carry the HRP-epitope found numerous years ago by using affinity chromatography and reverse phase HPLC (Desai et al., 1994). Some of these proteins include Fasciclin I, II (FasI and II), Neurotactin and Neuroglian (Jan and Jan, 1982) and some protein tyrosine kinases. Fas I and II are both, as the name suggests, expressed on fasiculating axon pathways as neural recognition molecules in the CNS during development, and are two of the most highly expressed HRP-epitope carrying proteins found thus far. Fas II is a homolog of the neural cell adhesion molecule (NCAM); and neurotactin is another adhesion molecule expressed in the CNS. Whether these epitopes regulate the adhesive functions of these glycoproteins remains still unclear. It is unlikely that all of the proteins bearing HRP-epitopes have been identified.

The restricted expression of HRP-epitope in the nervous system suggests a neural specific function and researchers are making tremendous effort in identifying its specific role. So far, several mutations with respect to HRP-epitope have been discovered. These fall into two classes as shown in Table 1.2. The first group falls under the Biosynthetic gene class, which includes loss of FucTA, the glycosyltransferase responsible for the addition of the α1,3-fucose on the proximal GlcNAc of the chitobiose core (Rendic et al., 2010). Second, *neutrally altered carbohydrate* (*nac*), a mutation

found in the GDP-fucose transporter needed for fucose addition (Katz et al., 1988; Geisler et al., 2012) and finally MGAT1, a mutation in the enzyme GnT1 which is required for complex glycosylation including HRP-epitope formation (Sarkar et al., 2006). All of the above are necessary for the proper biosynthesis of HRP-epitope. To identify mutations that would most likely regulate HRP-epitope expression, we performed a genetic screen to look for non-biosynthetic derived HRP mutants, which led to the second class of genes that can be categorized into the cell interaction and signaling class. Mutant embryos were stained with Concanavalin A (ConA), which is known to recognize high mannose structures, to assess whether N-glycosylation is occurring at a normal level. All of these identified mutants work in parallel pathways and interact with each other through different cell types, but unfortunately the complete pathway still needs to be resolved. The first identified mutant of this genetic screen was Tollo, which is expressed in the ectoderm and not in the neuron. The second one was a Ser/Thr kinase, which is regulated by the ectodermal cell but expressed in the neural cell. Both of them will be discussed in more detail below as the next chapter discusses an additional mutant (ms16), which was also found in this genetic screen and interacts with the first two mutants.

Figure 1.7: HRP-epitopes found in *Drosophila*.
HRP-epitope expression is a hallmark of plants and many invertebrates including arthropods. In Drosophila, it is restricted to neural expression providing a great tool to study the role of glycosylation in the developing nervous system., but its restricted neural expression makes it a good tool to study the role of glycosylation in the developing nervous system. Depicted below are the epitopes that have been discovered so far. The antigenic determinant is highlighted (red circle) which is a fucose linkage that is not common in mammals.

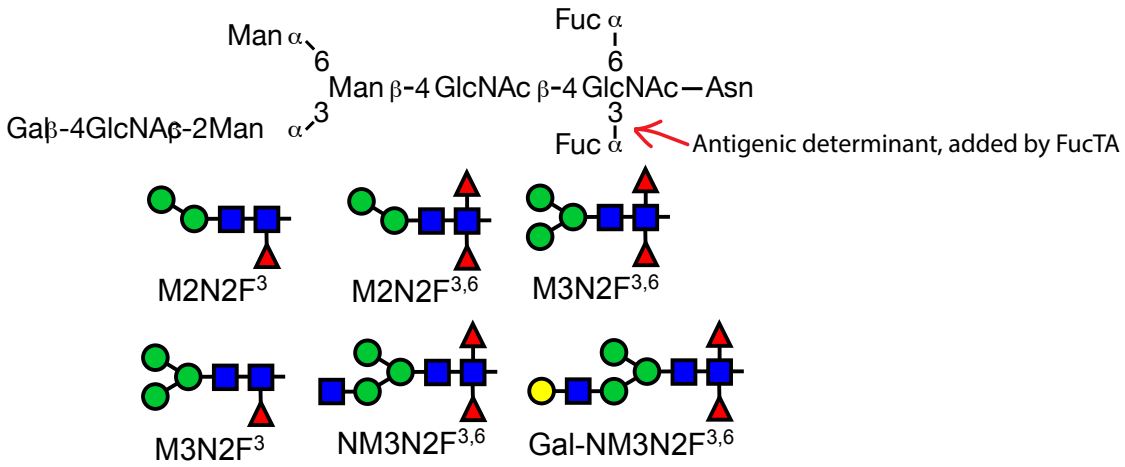

Table 1.2: Mutants that affect HRP-epitope fall into two classes.

Gene Name	Gene Class
Golgi FucTA (Fucosyltransferase A)	Biosynthetic
GFR/*nac* (GDP fucose transporter)	Biosynthetic
MGAT1 (GlcNAcT1)	Biosynthetic
Tollo-toll-8 (Toll-like receptor 8)	Cell signaling/interaction
Sff/SAD kinase (Neural specific kinase)	Cell signaling/interaction
Ms16/*Roc2* (E3-ubiqtuin ligase)	Cell signaling/interaction

Regulation of HRP-epitope expression

As mentioned above, a forward genetic screen was performed to identify genes that alter HRP-epitope expression. The first gene found in this screen was *Tollo,* which is a mutation in toll-8. Mutations in *Tollo*/toll-8, a member of the *Drosophila* Toll-like Receptor (TLR) family, reduce neural expression of the HRP-epitope and generate behavioral defects. The gene was named *Tollo*, which in Finnish translates to "stupid" in the sense of being a "bumpkin" since the adults were unable to free themselves from food and lingered around the bottom of the vial. The *Tollo* mutation is located on the TM3 balancer chromosome and mutant embryos lack HRP expression in the VNC and PNS, but demonstrate HRP-epitopes being expressed on a subset of non-neural tissues: ap, gg and hg, suggesting a role in tissue-specific glycosylation (Seppo et al., 2003) (**Fig 1.8**). The *tollo* mutation revealed a non-canonical signaling pathway affecting neural specific glycan expression. This adds a new function for TLRs in inducing tissue specific glycosylation, in addition to the already known TLR functions in innate immunity and dorsal ventral patterning (Belvin and Anderson, 1996; Takeda and Akira, 2004; Bilak et al., 2003; Medzhitov et al., 1997). Even though their role is defined, only a fraction of TLRs in *Drosophila* are involved in innate immunity, with most others being responsible for developmental functions (Bilak et al., 2003; Imler and Zheng, 2004). The canonical TLR signaling pathway is conserved in *Drosophila* and mammals, and hence, share common signaling components. The human and mammalian TLRs are both type I transmembrane proteins with common extracellular leucine-rich repeat (LLR) domains and a cytoplasmic domain of human interleukin-1 (IL) receptor also called the TIR (Toll/IL-1R) domain (Bilak et al., 2003; Medzhitov et al., 1997).

The second mutation analyzed from this screen was named "sugar-free frosting" (*sff*) because of the slight residual anti-HRP staining detected on the dorsal aspect of the ventral nerve cord that appeared like a frosting. *Sff* shows temperature sensitivity, with

lower temperatures decreasing HRP-epitope expression even further. This third chromosome mutation is a partial loss-of-function mutation and was mapped to the *Drosophila* homolog of “Synapses of the Amphid Defective” (SAD), a Ser/Thr kinase previously shown to affect NMJ morphology and neural polarity in *C. elegans* (Baas et al., 2011; Crump et al., 2001; Kishi et al., 2005). Furthermore, this mutation uncovers the significance of Golgi regulation and processing in glycan expression, which is in agreement with the presence of an increase in complex glycans in these mutants. This mutations identified a role of protein kinases in affecting Golgi function (Baas et al., 2011). Finally, it was revealed through *in-situ* hybridization that *sff* mRNA is expressed in the embryonic nervous system and reduced in *sff* mutants, placing it in the neuron of the pathway that regulates HRP-epitope expression. A similar NMJ defect as seen with SAD mutants in *C. elegans* is seen in *sff* mutant flies. NMJ morphology is significantly less complex and is reduced in both bouton and branch numbers as compared to wild type. Negative geotaxis is the ability of flies to climb upwards, away from the food; homozygous *sff* flies are deficient in negative geotaxis and are hesitant to climb to the top of their culture vials. The mutants all have this behavioral phenotype but heterozygous *sff* flies (*sff*/+) are normal. This behavior is shared with *Tollo*/toll-8 mutants.

Figure 1.8: HRP-epitope mutants.
Anti-HRP as well as ConA staining for HRP-epitope mutants identified in the genetic screen are shown compared to wildtype OreR embryos. In OreR, HRP-epitope expression was observed mainly in the neural tissues such as the ventral nerve cord (arrow, VNC) and the peripheral nervous system (PNS), but also in some non-neural tissues including the hindgut (hg) and garland gland (gg) (arrows). In comparison, *Tollo* mutants solely express the epitope in the non-neural tissues, while *sff (B22)* and ms16 mutants demonstrate reduced ventral nerve cord staining. As seen by ConA staining, core glycosylation in all these mutants remains intact.

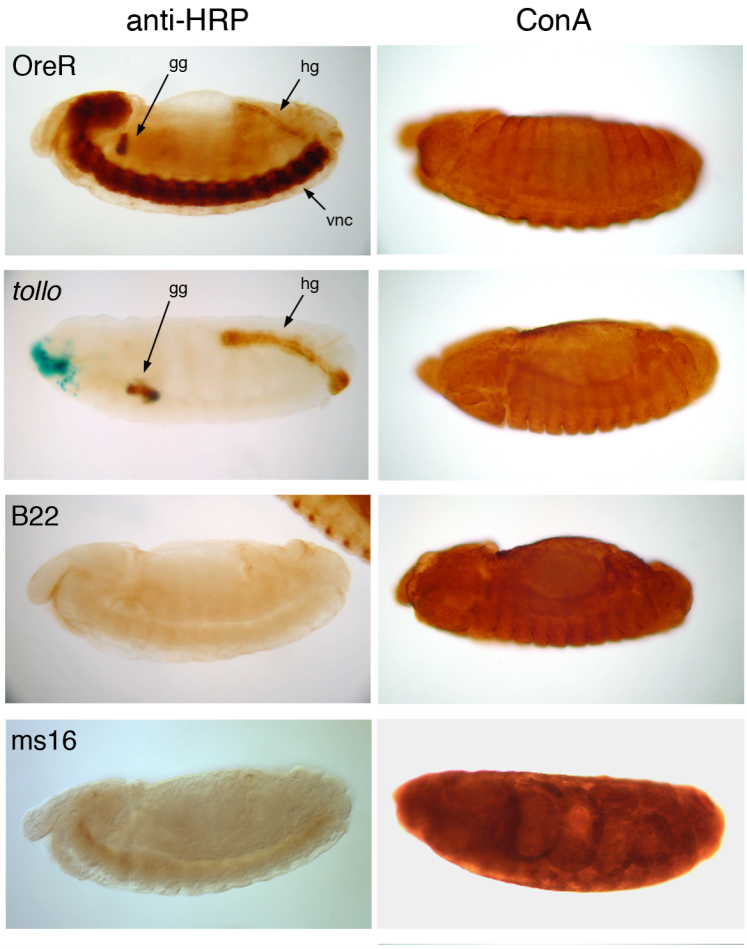

Ubiquitination

The results presented in the next chapter demonstrate for the first time how a mutation in an E3 ubiquitin ligase affects neural development by altering glycosylation. Therefore, this section will review ubiquitination and its functions as well as the previously known roles of ubiquitin ligases to understand how it could be involved with glycosylation.

Ubiquitination is a post-translational modification used by many cells to regulate protein expression. It involves the addition of the 76-amino acid, ubiquitin, onto lysine residues of a protein through an isopeptide bond. Once ubiquitinated, the protein can either get degraded (if it is polyubiquitinated) or in the case of monoubiquitination, proteins can use this tag for cellular localization or signaling (Pickart, 2001). The process of ubiquitination requires three sets of proteins families: the E1 activator protein, E2 conjugators and the E3 ligases (Hershko and Ciechanover, 1998). The ubiquitination process starts with the activation of ubiquitin using ATP, followed by the addition of a single ubiquitin molecule in thioester linkage to the sulfhydryl group of E1. The E1 then transfers the ubiquitin to the E2 protein family, which can act as a conjugator when charged and bind to their E3 ligase counterpart that is associated with a specific protein substrate (**Fig 1.9**). Once complexed with E3, the E2 conjugation enzyme transfers the ubiquitin to the substrate. The transfer of ubiquitin from E2 to substrate-bound E3 is a continuous process and can lead to polyubiquitination, which as mentioned earlier represents a tag for proteosomal protein degradation. There are very few known E1 enzymes. However, there are significantly more E2 and E3 present creating a diversity in recognition of protein or substrate (Reynolds et al., 2008). While the E3 ligases maybe redundant in function, they are especially important not only because they aid the transfer of the ubiquitin from E2 to a specific protein substrate, but also contain the protein characteristics that determine substrate specificity (Jackson et al., 2000).

Figure 1.9: The ubiquitination process.
Ubiquitination is a process used by every cell in most animals. The process starts with the activation of the ubiquitin, using ATP. Once the ubiquitin monomer is attached to the E1 complex, it can pass the ubiquitin to the catalytically active E2 conjugator complex. The charged E2 then binds to the E3 ligase, which is bound on its other end to a specific protein substrate and is used to ligate the ubiquitin monomer from the E2 to the substrate. This process can happen over and over again to produce a polyubiquitin chain.

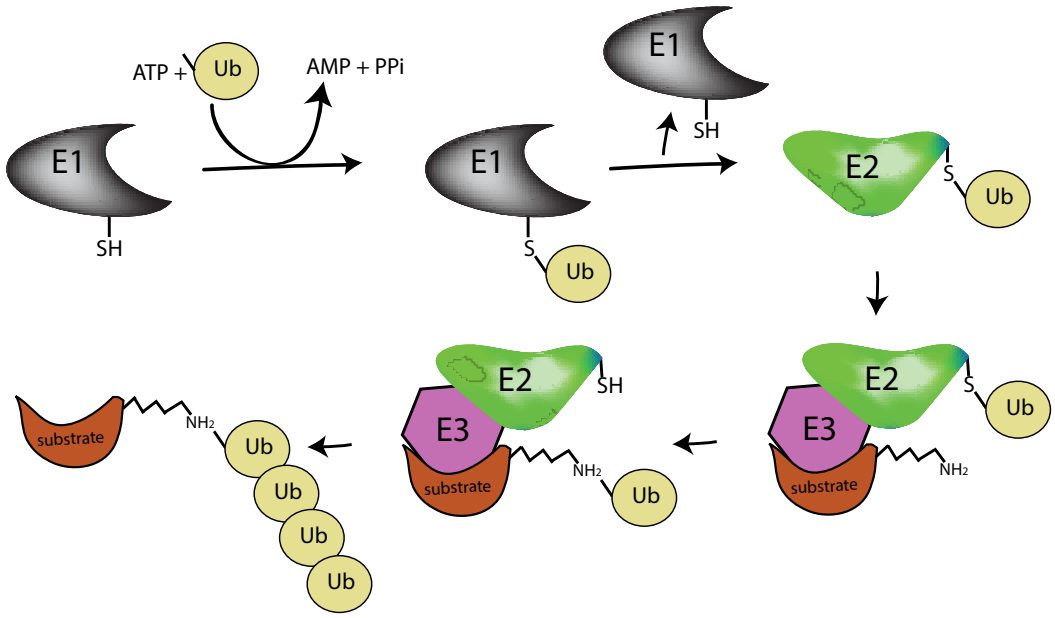

The Skp, Cullin, F-box containing (SCF) family of ubiquitin ligases is the largest family of ubiquitin ligases. They regulate protein stability by ubiquitination and targeting to the 26S proteasome. Protein ubiquitination, particularly through the SCF ligases are important in several cell processes such as apoptosis, signaling pathways and DNA replication (Hiramatsu et al., 2006). Its structure is comprised of an S-phase-kinase associated protein 1 (skp1), a cullin protein, an F-box protein, and a RING protein (Tan et al., 2011). In Humans, the RING protein is called RBX1/2 or regulators of Cullins (ROC). The *Drosophila* homolog is Roc1 although there are three members in the fly: Roc1a, Roc1b and Roc2. The mouse homolog is *sensitive to apoptosis* gene (SAG) and budding yeast also contains a single *Roc1* gene called *Hrt1*. These cross-species homologues have been shown to possess conserved functions. The skp1 protein serves as an adaptor between the F-box domain of the F-box protein and the Cullin protein. Cullins bind the F-box protein and the E2 enzyme together. Each of the RING domains has binding preferences for specific cullins, although the factors driving the specificity are not completely understood. The F-box protein is essential for determining substrate specificity and recruiting particular proteins for the transfer of the ubiquitin from the catalytically active E2 to the substrate. A *Drosophila* specific example of this can be seen with the F-box protein, Slimb, whose targets are Cubitus interruptus (Ci) and Armadillo (Arm), which are transcription factors in the hedgehog and wingless signaling pathways, respectively (Jiang and Struhl, 1998). Substrate phosphorylation is important for recognition by F-box proteins (Donaldson et al., 2004).

Ubiquitin ligases

To provide context for results to be presented later in this thesis, this section will focus on some of the already identified roles for ubiquitination in secretory pathway trafficking and localization.

A well-designed screen looking for interactors of a particular ubiquitin ligase, Kelch-like protein 20 (KLHL20), which is found at the Trans Golgi Network (TGN) revealed its association with coronin7 (CRN7), a protein involved in post-Golgi trafficking. These experiments illustrated that proper ubiquitination of CRN7, an F-actin regulator, is a key promoter of post-Golgi transport (Yuan et al., 2014) and results in altered protein trafficking (Baumann, 2014). A similar study, performed in the Wang and Zerial laboratory, revealed that another ubiquitin ligase, HACE1, previously identified as a tumor suppressor, is a regulator of Golgi membrane dynamics during the cell cycle. HACE1 interacts directly with Rab1 to target it to the Golgi membrane. In the absence of this ubiquitin ligase, Golgi stacks are altered and the lengths of cisternae are shortened indicating that HACE1 ubiquitin ligase is necessary for Golgi membrane assembly and disassembly (Tang et al., 2011). A third example of a ubiquitin ligase in regulating Golgi morphology is the Cul7 Fbxw8 E3 ligase (Litterman et al., 2011). Cul7 specific ubiquitin ligase localizes to the Golgi complex in mammalian brains and controls growth and elongation of dendrites along with altered trafficking through the Golgi by impairing signaling in neurons. Upon further investigations, Grasp65, a protein involved in Golgi stacking (Barr et al., 1997) was identified to be a direct substrate of this ubiquitin ligase, thereby affecting Golgi morphology and dendrite patterning. In addition to the three examples described here, there are many others exemplifying the importance of ubiquitin ligases in the secretory pathway in terms of protein trafficking, quality control and mislocalization in the absence of ubiquitin ligases (Risinger and Kaiser, 2008; Guerriero et al., 2013). Therefore, ubiquitin ligases play a role in Golgi dynamics, as many of their substrates are membrane bound proteins that are part of the secretory pathway. Altered Golgi dynamics leads to altered protein trafficking through the secretory pathway, which ultimately affects cell function, differentiation, and viability.

Trafficking of glycoproteins through the Golgi and secretory pathway will be discussed in more detail later.

Roc2 in trafficking

The three members of the Roc family in *Drosophila* have been proposed to be functionally non-redundant. Male sterility caused by Roc1b disruption is not rescued by Roc2 and is only partially rescued by Roc1a expression (Donaldson et al., 2004). Deletion of *Roc1a* in *Drosophila* causes larval death through cell cycle arrest (Noureddine et al., 2002). Furthermore, expression of *Roc1b* driven by the *Roc1a* promoter did not rescue this phenotype despite their sequence similarities suggesting that *Roc1a* and *Roc1b* present functional non-complementation. Even though they bind to some of the same Cullins, which bind to specific F-box proteins, it is thought that their non-redundancy imparts specificity to ubiquitination reactions (Jin and Harper, 2002). As predicted, *Roc2* is expressed throughout development in *Drosophila*, but is most abundant in pupae. In adults, it is predominantly expressed in the brain (Noureddine et al., 2002). In humans, RBX1/Roc1 and RBX2/Roc2 are also ubiquitously expressed with most abundant expression in the heart and skeletal muscle as well as some expression in the brain, lungs and kidneys (Swaroop et al., 2001). In mice, RBX1 is expressed in the ovaries, testis and prostate; RBX2 is mostly expressed in the brain (Sun et al., 2001) and both RBX1 and RBX2 are expressed throughout embryogenesis.

Several functions of Rocs have been described, making *Roc1 and Roc2* essential for development. The tumor suppressor gene, neurofibromatosis type 1 (*NF1*) is a direct target of Roc2/SAG and studies performed in mice show that *sag* is essential for neural and vascular development by controlling *NF1*. Accumulation of NF1 leads to the inhibition of Ras, which ultimately blocks differentiation and proliferation of cells. Mice mutants for *sag* are embryonic lethal and have several neural development abnormalities through *NF1* accumulation (Tan et al., 2011). SAG/ROC2 in mice also

degrades targets like c-Jun (Gu et al., 2007b), IκBα (Gu et al., 2007a) and additionally inhibits proliferation and abolishes immortalization by inducing senescence (Tan et al., 2015). As mentioned before, ubiquitin tags can be added as a single molecule (monoubiquitin) and as a chain of several ubiquitins together (polyubiquitin). However, the exact reaction mechanism of Roc2 ligating with the protein substrate and E2 enzymes is yet to be determined.

Roc2 has proven to be essential for development, important in cancer and useful as cancer drug targets (Huang et al., 2001); *Roc2* also plays a role in cell survival and apoptosis. This, along with the number of E3 ubiquitin ligases present in nature, highlights the importance of its regulation in development. The next chapter provides results revealing for the first time that *Drosophila* Roc2 regulates a membrane and vesicular pump and thereby alters N-glycosylation.

Sodium-Potassium ATPase, Na^+/K^+ pump

The sodium potassium ATPase (Na^+/K^+ pump) is found primarily in the plasma membrane and consists of two subunits with the alpha subunit being 110 kDa and the beta subunit approximately 38 kDa in size; the subunits are synthesized independently in the ER but must heterodimerize before they can exit and be transported to the plasma membrane. There are four known alpha subunits and three beta subunits in humans, and only one of each in *Drosophila,* called ATPalpha (ATPα) and Nervana, respectively. In humans, the α1 isoform is ubiquitously expressed everywhere (Mobasheri et al., 2000), whereas the α3 isoform is found in the heart and the neurons (Hilgenberg et al., 2006). In *Drosophila*, ATPα is expressed throughout development in the embryo, including the nervous system and trachea, at the larval NMJ and in larval brains, as well as in adult heads, thorax, abdomen and nervous system (Lebovitz et al., 1989). Interestingly, the most abundant Roc2 expression is also seen in adult heads, which correlates with ATPα expression in adults. The alpha subunit is catalytic and consists of

10 transmembrane domains and an ATP binding domain. The beta subunit represents a single transmembrane domain and its function is to regulate the pump for maturation and membrane transport (Doi and Iwasaki, 2008; Horisberger, 1994). However, it also has been proposed to have additional functions as a cell adhesion molecule (Geering, 1991b; Geering, 1991a).

The Na^+/K^+ pump creates ion gradients across membranes by moving three Na^+ ions out of the cell and two K^+ ions into the cell to maintain the resting membrane potential. In addition, this ion exchange also regulates cell volume through osmolarity and can play a role in secondary regulation of other ions, like calcium through the Sodium-Calcium Exchanger (NCX). The exchange of ions is an active transport process, as it requires energy provided by ATP hydrolysis. Inside the cell, the pump has a higher affinity for sodium ions. Upon binding of sodium, ATP binds to the pump leading to the addition of a phosphate group which subsequently causes a conformational change releasing the bound sodium at the external side of the bilayer **(Fig 1.10).** Upon this conformational change, two K^+ from outside the cell bind to the conformationally altered pump, causing the pump to return to its original shape. The pump then releases the phosphate and two K^+ inside the cell. The process requires energy, as both sodium and potassium are moving against their concentration gradients.

Figure 1.10: Ion exchange through the Sodium-Potassium pump.
The Sodium-Potassium ATPase is a pump that facilitates exchange of sodium and potassium ions across cells to maintain ionic homeostasis using ATP as an energy source. In step 1 (unbound ATP), the pump has a high affinity for sodium, in which three sodium ions bind to the pump (step 2), followed by phosphorylation of the pump from ATP hydrolysis (step 3). Once the pump is phosphorylated, the pump undergoes a conformational change to release the sodium ions outside the cell (step 4). At this stage, the pump now has a high affinity for potassium, which causes the binding of two potassium ions from outside the cell (step 5). Upon potassium binding, the pump gets dephosphorylated and potassium is released inside the cell (step 6).

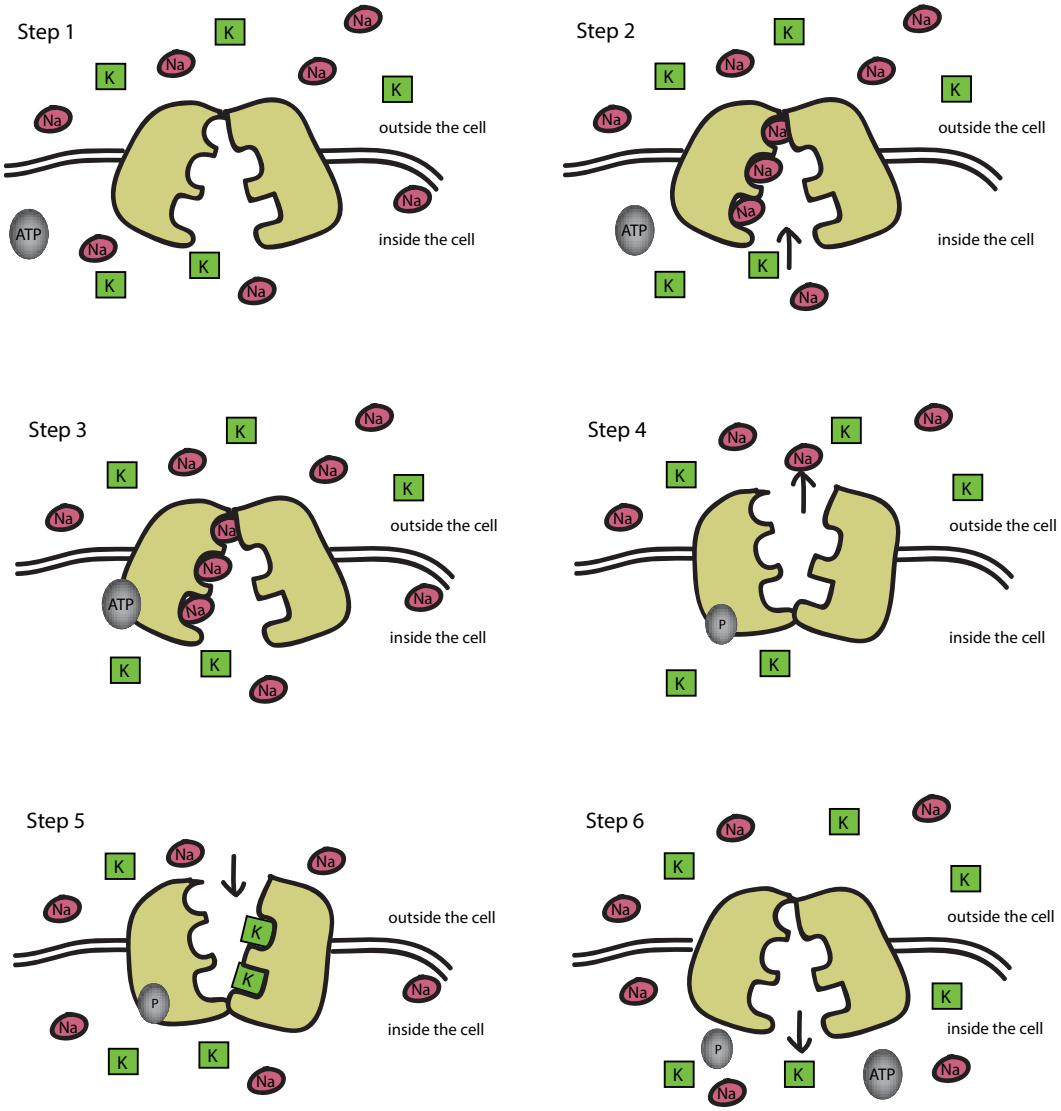

The Na^+/K^+ pump is present on neurons and is used for signal transduction. The role of the pump in the pre-axonal area is for depolarization by creating an electrotonic stream. This would suggest that an increase in the pump, more depolarization would be needed as the stream is getting inhibited. In the axon, where the signal is regenerative, the pump works with other voltage-gated channels to produce an action potential. Once the signal arrives at the axon terminal, it can be spread to the dendrite of the next neuron in the same way. An increase in the pump would cause fewer action potentials and therefore cause less depolarization at the nerve terminals demonstrating the importance of this pump in signal transduction.

As stated previously, the beta subunit of Na^+/K^+ ATPase in *Drosophila* is called Nervana. Although this section will not focus too much on this protein, it is important to note that Nervana is a 38 kDa HRP-epitope carrying protein. Not much is known about this protein except that it regulates the heterodimerization of the pump and therefore controls the number of pump complexes that get to the plasma membrane.

Other roles of ATPalpha

The results from the next chapter indicate that ATPα is a substrate of an ubiquitin ligase and alters glycosylation and organelle function. This section will focus on some of the previously known functions of ATPα, as this is the specific subunit that is investigated in the next chapter. Aside from its ion pumping function, ATPα has been implicated in other signaling, trafficking and neurological roles. It also acts as a signal transducer to regulate intracellular calcium and maintains other secondary processes.

In *Drosophila,* mutations in ATPα expression led to a neural behavioral phenotype, called bang-sensitive paralysis (Schubiger et al., 1994). In *C. elegans*, the pump is found at the NMJ and controls synaptic efficiency (Doi and Iwasaki, 2008). A mutation in the worm of the alpha subunit of a specific Na^+/K^+ ATPase caused the accumulation of the pump at post-synaptic densities. Since the pumps surround

receptors, these ultimately do not rigidly cluster at the NMJ, which is a requirement for the subunits of the PSD receptors. Upon further investigations, the pump was observed to be involved in localization and expression of the post-synaptic receptors, as the pump is extremely concentrated in the muscles, in very close proximity to the acetylcholine receptors in *C. elegans*. It was ultimately suggested that in the absence of the pump, inhibition of the receptors on the membrane or an increase in internalization of the receptors takes place. However this activity seemed to vary by receptor type, but nevertheless represents the first example of the non-ion pumping role of ATPα at the NMJ and synapse. Additionally, there are other non-ion pumping functions of ATPα in septate junction function in combination with other proteins like Neuroglian, Gliotactin and Neurexin (Genova and Fehon, 2003). The pump is concentrated at the septate junctions and is responsible for formation of paracellular barrier, which is needed for regulating solute flow in epithelial cells to maintain proper nutrient absorption and secretion. Failure of proper septate junction leads to problems in the blood-brain barrier, ultimately leading to neurological diseases such as Alzheimer's and multiple sclerosis (Huber et al., 2001).

Furthermore, the Na^+/K^+ ATPase has been implicated in other neural specific functions as well. Disruption of the pump causes neural degeneration and disorders including seizures (Palladino et al., 2003). It also induces neural cell death leading to diseases such as rapid-onset dystonia (Ashmore et al., 2009; de Carvalho Aguiar et al., 2004). Other studies in *Drosophila* revealed that mutations in ATPα lead to behavioral abnormalities, excessive neuronal hyperexcitability, paralysis and reduced life span (Palladino et al., 2003).

ATPα is also associated with signaling; it interacts directly with Src kinase at the plasma membrane (Tian et al., 2006) and inhibits its function as it remains bound to it, thereby keeping it inactive. Studies using ouabain, an inhibitor of ATPα by disabling

conformational changes in the protein required for proper function, describes that upon ouabain binding, the pump releases Src kinase. The released Src kinase is then active and able to phosphorylate many respective targets demonstrating an essential role of this pump in controlling the activity of kinases and phosphorylation of proteins and perhaps ubiquitination. Similarly, ATPα directly interacts with ankyrin (Jordan et al., 1995), an adaptor protein linking membrane proteins to the cytoskeleton. Ankyrin connects spectrin related membrane proteins and is also required for synaptic stability. The association of ankyrin and spectrin helps in proper distribution of the pump in epithelial cells.

Based on the numerous examples, the Na^+/K^+ pump plays a crucial role in several cell and protein functions, all of which highlight the importance of this protein. However, given the number of associations with this particular protein, there are presumably still a variety of roles that are yet to be discovered. For example, an area not studied to date is the vital ion-pumping role of ATPα in the secretory pathway. A study carried out by Jan and Jan's group emphasizes the importance of controlled ionic environments for organelle structure and function, specifically in the Golgi. In this study, they found that under depolarizing conditions caused by increased extracellular potassium, Golgi fragmentation was observed, which in turn can lead to many dysfunctions in protein processing and trafficking and ultimately in neuronal signaling (Thayer et al., 2013). Considering the amount of unknowns in this particular field, ATPα may exhibit additional roles, which are tremendously fundamental in understanding trafficking through the secretory pathway and glycosylation.

Golgi complex, structure and function

The Golgi complex is central of the secretory pathway and the main center for post-translational modifications, processing and sorting. In mammals, the Golgi forms stacks composed of cisternae, which are characterized as cis (located closest to ER exit

site), medial, and trans (closest to the plasma membrane) compartments. Together the cisternae form one organelle called the Golgi stack. In vertebrate cells these stacks are linked together to form ribbons. In *Drosophila*, the Golgi is punctate because individual stacks are not connected to each other but are dispersed throughout the cytoplasm (Ripoche et al., 1994). However, cisternal-specific functions are conserved in both *Drosophila* and mammals, as each of these cisternae has specific enzymes and functions. Previous studies have confirmed that the *Drosophila* Golgi is compartmentalized and each of these compartments are distinct in function and localization of enzymes (Yano et al., 2005).

After processing and modification, cargo is transported from the Golgi to their respective destinations and this highly regulated process uses tethers, coat proteins and vesicles (Kondylis and Rabouille, 2009). There are also other proteins involved in the machinery including kinases, and the importance of these kinases in regulating Golgi vesicle tethering and trafficking is a subject that has been extensively studied in the past. For example, in the absence of these kinases there is an accumulation of vesicles containing resident Golgi proteins (Nakamura et al., 1997). Previous studies also underscore the importance of proper Golgi trafficking and regulation in glycan expression through kinases. *Sff*/SAD kinase alters presynaptic vesicle tethering and in the mutants, improper trafficking occurs leading to neuron specific glycan expression defects. This led to the hypothesis that *sff* is required for Golgi dynamics (Baas et al., 2011), highlighting not only the requirement of proper Golgi machinery but also the relevance of kinases for its function.

Another major task of the Golgi is protein glycosylation. Glycoproteins are modified in the Golgi from high-mannose into complex or hybrid type N-glycans. The diversity of glycoprotein glycosylation is so great that understanding the specificity of the glycosyltransferases involved becomes imperative. As mentioned earlier, proper

glycosylation is highly organized, and localization as well as timing of these enzymes is key to perform the modifications in the correct biosynthetic order (Kornfeld and Kornfeld, 1985). For example, GnT1 is present in the *medial* Golgi, because this is the first step in N-glycan synthesis that will drive the fate of glycans towards greater complexity in later compartments in the Golgi (Varki et al., 2009; Rabouille et al., 1995). Similarly, Mannosidase I (ManI) and ManII are found in the *medial-trans* Golgi (Velasco et al., 1993); in the *trans*-Golgi, the resident enzymes are α2,6 sialyltransferase (ST6Gal) and β4Gal-T1 (Colley, 1997; Gleeson, 1998) (**Fig 1.11**). Studies have shown that proper localization might depend on the domain structure, as this is the only common factor between the hundreds of glycosyltransferases present, but this has yet to be determined. The precise localization of the enzymes provides efficiency for glycan biosynthesis, which also requires appropriate availability of nucleotide sugar donor (e.g., UDP-GlcNAc) as well as glycoprotein substrate for proper enzyme function. Segregation of these enzymes decreases competition, which further enhances sequential modification.

Glycosylation has to be organized due to its complexity and due to the different pathways involved. For example, GnT-1 creates a $GlcNAcMan_5GlcNAc_2$ substrate for Fucosyltranferase A (FucTA), placing FucTA and production of the HPR-epitope immediately downstream of GnT-1. However, if GnTII (which also lies downstream of GnT-1) acts before FucTA, the HRP-epitope cannot be synthesized and the glycoprotein would be diverted down a completely different modification pathway. Upon the addition of a second GlcNAc by GnTII, the glycan can no longer serve as substrate for FucTA to get difucosylated. Therefore, addition of two antennal GlcNAcs drives the glycan towards greater complexity, while difucosylated glycans go through a parallel pathway. In *Drosophila*, there is a hexosaminidase, called Fdl, that competes for the same

substrates as FucTA, creating a third pathway that the glycoprotein could be modified through the Golgi.

In conclusion, mislocalization of enzymes, or the mislocalization and/or lack of a donor (e.g., GDP-Fuc) for one of these enzymes, influences the synthesis of glycans based on the way they are presented and on the enzymes it passes along resulting in a completely different glycan structure. This organization emphasizes the sophistication through which Golgi compartmentalization orchestrates proper glycosylation, and further demonstrates the importance of this organelle in cellular function.

Figure 1.11: Golgi compartmentalization and localization of glycosyltransferases. The Golgi stacks are important in compartmentalizing glycosyltransferases; this aids in keeping the glycosylation process and machinery organized. In the cis Golgi, high mannose structures are trimmed to Man_5, and in the medial Golgi the same glycan can have two different paths, based on the enzyme present at the time. In the figure below the glycan gets either modified with an α1,3 linked fucose by FucTA, or with a second GlcNAc in case of GnTII. In the trans Golgi unit, depending on the route the glycan took, the presence of galactosyltransferases and sialyltransferases can then modify the glycan further.

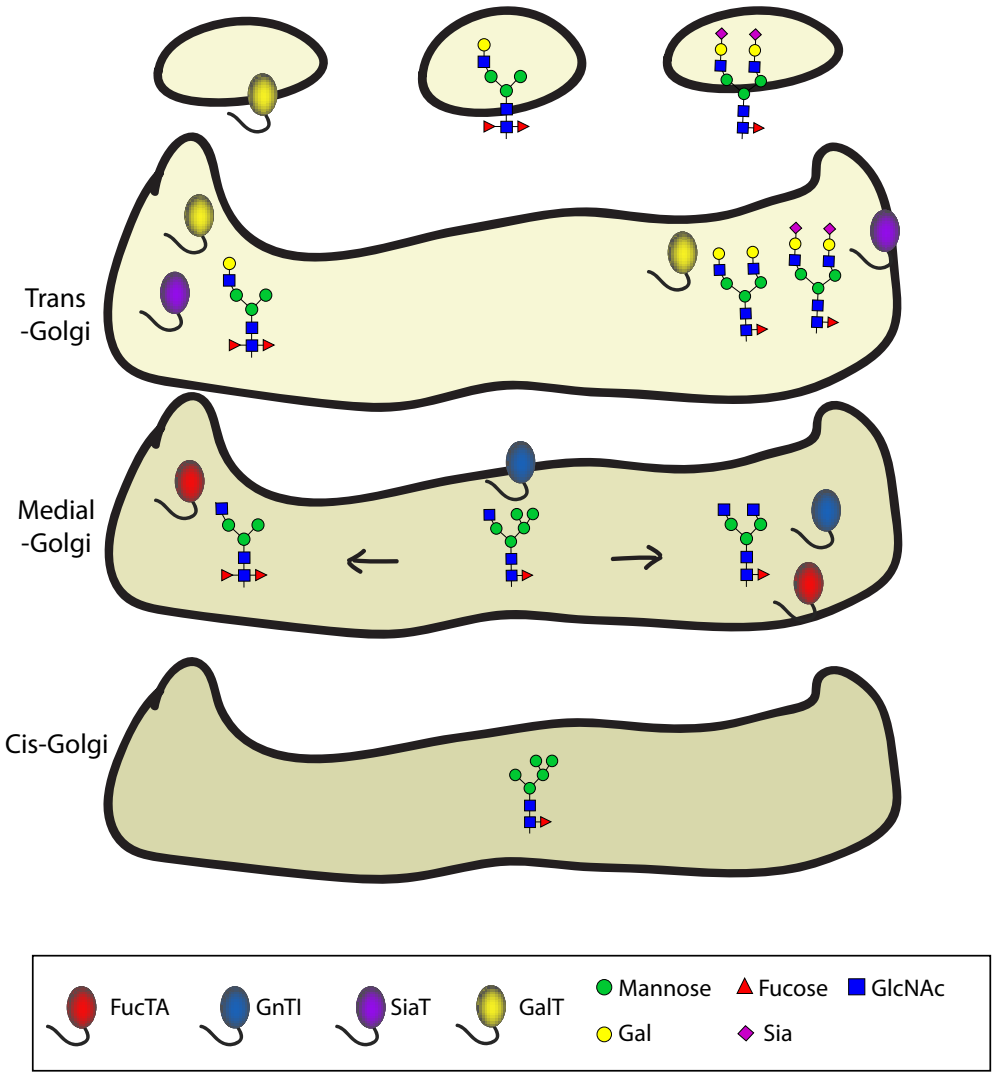

Summary and scope of Dissertation

This chapter is an overview of topics that are the fundamentals of this thesis. An understanding of glycosylation and its biosynthesis, specifically N-glycosylation in *Drosophila* is a field in which a lot is still unknown. Since we are interested in understanding the regulation of tissue-specific glycosylation, in particular in the development of the nervous system, a brief understanding of neural fate and development was discussed. In addition, some previously known glycosylation defects in neural development were presented as well as the role of neuromuscular junctions. Since we use HRP-epitopes as reporters to study neural development, a brief overview of its biosynthesis as well as previously studied mutants were introduced. Ubiquitination, ubiquitin ligases and the Sodium-Potassium ATPase were also reviewed with respect to their previously known functions.

The next chapter reports for the first time that a mutation in an ubiquitin ligase alters neural-specific glycosylation. The mutant has behavioral defects and a changed N-glycan profile. Since ubiquitin ligases are broadly and ubiquitously expressed, we sought to find a direct substrate to elucidate this mechanism. A neural-specific ion pump, Sodium-Potassium ATPase is altered in the mutant and mechanisitic possibilities that link ATPase function to glycosylation will be discussed.

Chapter three of this thesis presents an advance in analytical techniques for glycan analysis. Using mass spectrometry as a tool, small amounts of glycans can be analyzed in a limited amount of sample. This technique is now being widely used and improving the methods is beneficial. This chapter demonstrates a new quantification method by using an external standard, thereby not only gaining the intensities of each individual glycan structure but also to quantify the exact amount of each glycan present in the sample. Furthermore, it is a great tool to compare total glycan densities. The final chapter of this dissertation is a short summary of chapter three and four, along with the

big picture of the thesis. It also lists future directions to add significance and put the results into context.

References

Acheson, A., Sunshine, J. L. & Rutishauser, U. 1991. NCAM polysialic acid can regulate both cell-cell and cell-substrate interactions. *J Cell Biol,* 114(1)**,** pp 143-53.

Aoki, K., Perlman, M., Lim, J. M., Cantu, R., Wells, L. & Tiemeyer, M. 2007. Dynamic developmental elaboration of N-linked glycan complexity in the Drosophila melanogaster embryo. *J Biol Chem,* 282(12)**,** pp 9127-42.

Ashmore, L. J., Hrizo, S. L., Paul, S. M., Van Voorhies, W. A., Beitel, G. J. & Palladino, M. J. 2009. Novel mutations affecting the Na, K ATPase alpha model complex neurological diseases and implicate the sodium pump in increased longevity. *Hum Genet,* 126(3)**,** pp 431-47.

Baas, S., Sharrow, M., Kotu, V., Middleton, M., Nguyen, K., Flanagan-Steet, H., Aoki, K. & Tiemeyer, M. 2011. Sugar-free frosting, a homolog of SAD kinase, drives neural-specific glycan expression in the Drosophila embryo. *Development,* 138(3)**,** pp 553-63.

Barr, F. A., Puype, M., Vandekerckhove, J. & Warren, G. 1997. GRASP65, a protein involved in the stacking of Golgi cisternae. *Cell,* 91(2)**,** pp 253-62.

Baumann, K. 2014. Post-translational modifications: Lys33-linked ubiquitin in post-Golgi transport. *Nat Rev Mol Cell Biol,* 15(6)**,** pp 365.

Belvin, M. P. & Anderson, K. V. 1996. A conserved signaling pathway: the Drosophila toll-dorsal pathway. *Annu Rev Cell Dev Biol,* 12(393-416.

Beumer, K., Matthies, H. J., Bradshaw, A. & Broadie, K. 2002. Integrins regulate DLG/FAS2 via a CaM kinase II-dependent pathway to mediate synapse elaboration and stabilization during postembryonic development. *Development,* 129(14)**,** pp 3381-91.

Bilak, H., Tauszig-Delamasure, S. & Imler, J. L. 2003. Toll and Toll-like receptors in Drosophila. *Biochem Soc Trans,* 31(Pt 3)**,** pp 648-51.

Blunk, A. D., Akbergenova, Y., Cho, R. W., Lee, J., Walldorf, U., Xu, K., Zhong, G., Zhuang, X. & Littleton, J. T. 2014. Postsynaptic actin regulates active zone spacing and glutamate receptor apposition at the Drosophila neuromuscular junction. *Mol Cell Neurosci,* 61(241-54.

Broadie, K., Baumgartner, S. & Prokop, A. 2011. Extracellular matrix and its receptors in Drosophila neural development. *Dev Neurobiol,* 71(11)**,** pp 1102-30.

Campos-Ortega, J. A. 1988. Cellular interactions during early neurogenesis of Drosophila melanogaster. *Trends Neurosci,* 11(9)**,** pp 400-5.

Campos-Ortega, J. A. 1994. Genetic mechanisms of early neurogenesis in Drosophila melanogaster. *J Physiol Paris,* 88(2)**,** pp 111-22.

Colley, K. J. 1997. Golgi localization of glycosyltransferases: more questions than answers. *Glycobiology,* 7(1)**,** pp 1-13.

Crump, J. G., Zhen, M., Jin, Y. & Bargmann, C. I. 2001. The SAD-1 kinase regulates presynaptic vesicle clustering and axon termination. *Neuron,* 29(1)**,** pp 115-29.

de Carvalho Aguiar, P., Sweadner, K. J., Penniston, J. T., Zaremba, J., Liu, L., Caton, M., Linazasoro, G., Borg, M., Tijssen, M. A., Bressman, S. B., Dobyns, W. B., Brashear, A. & Ozelius, L. J. 2004. Mutations in the Na+/K+ -ATPase alpha3 gene ATP1A3 are associated with rapid-onset dystonia parkinsonism. *Neuron,* 43(2)**,** pp 169-75.

de la Pompa, J. L., Wakeham, A., Correia, K. M., Samper, E., Brown, S., Aguilera, R. J., Nakano, T., Honjo, T., Mak, T. W., Rossant, J. & Conlon, R. A. 1997. Conservation of the Notch signalling pathway in mammalian neurogenesis. *Development,* 124(6)**,** pp 1139-48.

Desai, C. J., Popova, E. & Zinn, K. 1994. A Drosophila receptor tyrosine phosphatase expressed in the embryonic CNS and larval optic lobes is a member of the set of proteins bearing the "HRP" carbohydrate epitope. *J Neurosci,* 14(12)**,** pp 7272-83.

DiAntonio, A., Petersen, S. A., Heckmann, M. & Goodman, C. S. 1999. Glutamate receptor expression regulates quantal size and quantal content at the Drosophila neuromuscular junction. *J Neurosci,* 19(8)**,** pp 3023-32.

Doe, C. Q. & Goodman, C. S. 1985. Early events in insect neurogenesis. I. Development and segmental differences in the pattern of neuronal precursor cells. *Dev Biol,* 111(1)**,** pp 193-205.

Doi, M. & Iwasaki, K. 2008. Na+/K+ ATPase regulates the expression and localization of acetylcholine receptors in a pump activity-independent manner. *Mol Cell Neurosci,* 38(4)**,** pp 548-58.

Donaldson, T. D., Noureddine, M. A., Reynolds, P. J., Bradford, W. & Duronio, R. J. 2004. Targeted disruption of Drosophila Roc1b reveals functional differences in the Roc subunit of Cullin-dependent E3 ubiquitin ligases. *Mol Biol Cell,* 15(11)**,** pp 4892-903.

Ellgaard, L. & Helenius, A. 2003. Quality control in the endoplasmic reticulum. *Nat Rev Mol Cell Biol,* 4(3)**,** pp 181-91.

Featherstone, D. E., Davis, W. S., Dubreuil, R. R. & Broadie, K. 2001. Drosophila alpha- and beta-spectrin mutations disrupt presynaptic neurotransmitter release. *J Neurosci,* 21(12)**,** pp 4215-24.

Fortini, M. E. 2009. Notch signaling: the core pathway and its posttranslational regulation. *Dev Cell,* 16(5)**,** pp 633-47.

Fortini, M. E. 2012. Introduction--Notch in development and disease. *Semin Cell Dev Biol,* 23(4)**,** pp 419-20.

Fouquet, W., Owald, D., Wichmann, C., Mertel, S., Depner, H., Dyba, M., Hallermann, S., Kittel, R. J., Eimer, S. & Sigrist, S. J. 2009. Maturation of active zone assembly by Drosophila Bruchpilot. *J Cell Biol,* 186(1)**,** pp 129-45.

Freeze, H. H. 2002. Human disorders in N-glycosylation and animal models. *Biochim Biophys Acta,* 1573(3)**,** pp 388-93.

Fuerstenberg, S., Broadus, J. & Doe, C. Q. 1998. Asymmetry and cell fate in the Drosophila embryonic CNS. *Int J Dev Biol,* 42(3)**,** pp 379-83.

Geering, K. 1991a. Posttranslational modifications and intracellular transport of sodium pumps: importance of subunit assembly. *Soc Gen Physiol Ser,* 46(31-43.

Geering, K. 1991b. The functional role of the beta-subunit in the maturation and intracellular transport of Na,K-ATPase. *FEBS Lett,* 285(2)**,** pp 189-93.

Geisler, C., Kotu, V., Sharrow, M., Rendić, D., Pöltl, G., Tiemeyer, M., Wilson, I. B. & Jarvis, D. L. 2012. The Drosophila neurally altered carbohydrate mutant has a defective Golgi GDP-fucose transporter. *J Biol Chem,* 287(35)**,** pp 29599-609.

Genova, J. L. & Fehon, R. G. 2003. Neuroglian, Gliotactin, and the Na+/K+ ATPase are essential for septate junction function in Drosophila. *J Cell Biol,* 161(5)**,** pp 979-89.

Gleeson, P. A. 1998. Targeting of proteins to the Golgi apparatus. *Histochem Cell Biol,* 109(5-6)**,** pp 517-32.

Grewal, P. K. & Hewitt, J. E. 2003. Glycosylation defects: a new mechanism for muscular dystrophy? *Hum Mol Genet,* 12 Spec No 2(R259-64.

Gu, Q., Bowden, G. T., Normolle, D. & Sun, Y. 2007a. SAG/ROC2 E3 ligase regulates skin carcinogenesis by stage-dependent targeting of c-Jun/AP1 and IkappaB-alpha/NF-kappaB. *J Cell Biol,* 178(6)**,** pp 1009-23.

Gu, Q., Tan, M. & Sun, Y. 2007b. SAG/ROC2/Rbx2 is a novel activator protein-1 target that promotes c-Jun degradation and inhibits 12-O-tetradecanoylphorbol-13-acetate-induced neoplastic transformation. *Cancer Res,* 67(8)**,** pp 3616-25.

Guerriero, C. J., Weiberth, K. F. & Brodsky, J. L. 2013. Hsp70 targets a cytoplasmic quality control substrate to the San1p ubiquitin ligase. *J Biol Chem,* 288(25)**,** pp 18506-20.

Haltiwanger, R. S. & Lowe, J. B. 2004. Role of glycosylation in development. *Annu Rev Biochem,* 73(491-537.

Hartenstein, V. & Campos-Ortega, J. A. 1985. *The Embryonic Development of Drosophila melanogaster*, 1st.

Hershko, A. & Ciechanover, A. 1998. The ubiquitin system. *Annu Rev Biochem,* 67(425-79.

Hilgenberg, L. G., Su, H., Gu, H., O'Dowd, D. K. & Smith, M. A. 2006. Alpha3Na+/K+-ATPase is a neuronal receptor for agrin. *Cell,* 125(2)**,** pp 359-69.

Hiramatsu, Y., Kitagawa, K., Suzuki, T., Uchida, C., Hattori, T., Kikuchi, H., Oda, T., Hatakeyama, S., Nakayama, K. I., Yamamoto, T., Konno, H. & Kitagawa, M. 2006. Degradation of Tob1 mediated by SCFSkp2-dependent ubiquitination. *Cancer Res,* 66(17)**,** pp 8477-83.

Horisberger, J., -D. 1994. The Na,K-ATPase: Structure-Function Relationship. Austin, TX: R. G. Landes Co.

Huang, Y., Duan, H. & Sun, Y. 2001. Elevated expression of SAG/ROC2/Rbx2/Hrt2 in human colon carcinomas: SAG does not induce neoplastic transformation, but antisense SAG transfection inhibits tumor cell growth. *Mol Carcinog,* 30(1)**,** pp 62-70.

Huber, J. D., Egleton, R. D. & Davis, T. P. 2001. Molecular physiology and pathophysiology of tight junctions in the blood-brain barrier. *Trends Neurosci,* 24(12)**,** pp 719-25.

Imler, J. L. & Zheng, L. 2004. Biology of Toll receptors: lessons from insects and mammals. *J Leukoc Biol,* 75(1)**,** pp 18-26.

Jackson, P. K., Eldridge, A. G., Freed, E., Furstenthal, L., Hsu, J. Y., Kaiser, B. K. & Reimann, J. D. 2000. The lore of the RINGs: substrate recognition and catalysis by ubiquitin ligases. *Trends Cell Biol,* 10(10)**,** pp 429-39.

Jan, L. Y. & Jan, Y. N. 1982. Antibodies to horseradish peroxidase as specific neuronal markers in Drosophila and in grasshopper embryos. *Proc Natl Acad Sci U S A,* 79(8)**,** pp 2700-4.

Jiang, J. & Struhl, G. 1998. Regulation of the Hedgehog and Wingless signalling pathways by the F-box/WD40-repeat protein Slimb. *Nature,* 391(6666)**,** pp 493-6.

Jin, J. & Harper, J. W. 2002. RING finger specificity in SCF-driven protein destruction. *Dev Cell,* 2(6)**,** pp 685-7.

Jordan, C., Püschel, B., Koob, R. & Drenckhahn, D. 1995. Identification of a binding motif for ankyrin on the alpha-subunit of Na+,K(+)-ATPase. *J Biol Chem,* 270(50)**,** pp 29971-5.

Kamimura, K., Ueno, K., Nakagawa, J., Hamada, R., Saitoe, M. & Maeda, N. 2013. Perlecan regulates bidirectional Wnt signaling at the Drosophila neuromuscular junction. *J Cell Biol,* 200(2)**,** pp 219-33.

Katz, F., Moats, W. & Jan, Y. N. 1988. A carbohydrate epitope expressed uniquely on the cell surface of Drosophila neurons is altered in the mutant nac (neurally altered carbohydrate). *EMBO J,* 7(11)**,** pp 3471-7.
Keshishian, H., Broadie, K., Chiba, A. & Bate, M. 1996. The drosophila neuromuscular junction: a model system for studying synaptic development and function. *Annu Rev Neurosci,* 19(545-75.

Kishi, M., Pan, Y. A., Crump, J. G. & Sanes, J. R. 2005. Mammalian SAD kinases are required for neuronal polarization. *Science,* 307(5711)**,** pp 929-32.

Kittel, R. J., Wichmann, C., Rasse, T. M., Fouquet, W., Schmidt, M., Schmid, A., Wagh, D. A., Pawlu, C., Kellner, R. R., Willig, K. I., Hell, S. W., Buchner, E., Heckmann, M. & Sigrist, S. J. 2006. Bruchpilot promotes active zone assembly, Ca2+ channel clustering, and vesicle release. *Science,* 312(5776)**,** pp 1051-4.

Kondylis, V. & Rabouille, C. 2009. The Golgi apparatus: lessons from Drosophila. *FEBS Lett,* 583(23)**,** pp 3827-38.

Kornfeld, R. & Kornfeld, S. 1985. Assembly of asparagine-linked oligosaccharides. *Annu Rev Biochem,* 54(631-64.

Landgraf, M., Bossing, T., Technau, G. M. & Bate, M. 1997. The origin, location, and projections of the embryonic abdominal motorneurons of Drosophila. *J Neurosci,* 17(24)**,** pp 9642-55.

Landgraf, M. & Thor, S. 2006. Development of Drosophila motoneurons: specification and morphology. *Semin Cell Dev Biol,* 17(1)**,** pp 3-11.

Lebovitz, R. M., Takeyasu, K. & Fambrough, D. M. 1989. Molecular characterization and expression of the (Na+ + K+)-ATPase alpha-subunit in Drosophila melanogaster. *EMBO J,* 8(1)**,** pp 193-202.

Litterman, N., Ikeuchi, Y., Gallardo, G., O'Connell, B. C., Sowa, M. E., Gygi, S. P., Harper, J. W. & Bonni, A. 2011. An OBSL1-Cul7Fbxw8 ubiquitin ligase signaling mechanism regulates Golgi morphology and dendrite patterning. *PLoS Biol,* 9(5)**,** pp e1001060.

Léonard, R., Rendic, D., Rabouille, C., Wilson, I. B., Préat, T. & Altmann, F. 2006. The Drosophila fused lobes gene encodes an N-acetylglucosaminidase involved in N-glycan processing. *J Biol Chem,* 281(8)**,** pp 4867-75.

Marrus, S. B., Portman, S. L., Allen, M. J., Moffat, K. G. & DiAntonio, A. 2004. Differential localization of glutamate receptor subunits at the Drosophila neuromuscular junction. *J Neurosci,* 24(6)**,** pp 1406-15.

Matkovic, T., Siebert, M., Knoche, E., Depner, H., Mertel, S., Owald, D., Schmidt, M., Thomas, U., Sickmann, A., Kamin, D., Hell, S. W., Bürger, J., Hollmann, C., Mielke, T., Wichmann, C. & Sigrist, S. J. 2013. The Bruchpilot cytomatrix determines the size of the readily releasable pool of synaptic vesicles. *J Cell Biol,* 202(4)**,** pp 667-83.

Medzhitov, R., Preston-Hurlburt, P. & Janeway, C. A., Jr. 1997. A human homologue of the Drosophila Toll protein signals activation of adaptive immunity. *Nature,* 388(6640)**,** pp 394-7.

Menon, K. P., Carrillo, R. A. & Zinn, K. 2013. Development and plasticity of the Drosophila larval neuromuscular junction. *Wiley Interdiscip Rev Dev Biol,* 2(5)**,** pp 647-70.

Mobasheri, A., Avila, J., Cózar-Castellano, I., Brownleader, M. D., Trevan, M., Francis, M. J., Lamb, J. F. & Martín-Vasallo, P. 2000. Na+, K+-ATPase isozyme diversity; comparative biochemistry and physiological implications of novel functional interactions. *Biosci Rep,* 20(2)**,** pp 51-91.

Moremen, K. W., Tiemeyer, M. & Nairn, A. V. 2012. Vertebrate protein glycosylation: diversity, synthesis and function. *Nat Rev Mol Cell Biol,* 13(7)**,** pp 448-62.

Nakamura, N., Lowe, M., Levine, T. P., Rabouille, C. & Warren, G. 1997. The vesicle docking protein p115 binds GM130, a cis-Golgi matrix protein, in a mitotically regulated manner. *Cell,* 89(3)**,** pp 445-55.

Noureddine, M. A., Donaldson, T. D., Thacker, S. A. & Duronio, R. J. 2002. Drosophila Roc1a encodes a RING-H2 protein with a unique function in processing the Hh signal transducer Ci by the SCF E3 ubiquitin ligase. *Dev Cell,* 2(6)**,** pp 757-70.

Palladino, M. J., Bower, J. E., Kreber, R. & Ganetzky, B. 2003. Neural dysfunction and neurodegeneration in Drosophila Na+/K+ ATPase alpha subunit mutants. *J Neurosci,* 23(4)**,** pp 1276-86.

Parkinson, W., Dear, M. L., Rushton, E. & Broadie, K. 2013. N-glycosylation requirements in neuromuscular synaptogenesis. *Development,* 140(24)**,** pp 4970-81.

Paschinger, K., Rendic, D. & Wilson, I. B. 2009. Revealing the anti-HRP epitope in Drosophila and Caenorhabditis. *Glycoconj J,* 26(3)**,** pp 385-95.

Pickart, C. M. 2001. Ubiquitin enters the new millennium. *Mol Cell,* 8(3)**,** pp 499-504.

Rabouille, C., Hui, N., Hunte, F., Kieckbusch, R., Berger, E. G., Warren, G. & Nilsson, T. 1995. Mapping the distribution of Golgi enzymes involved in the construction of complex oligosaccharides. *J Cell Sci,* 108 (Pt 4)(1617-27.

Rendic, D., Sharrow, M., Katoh, T., Overcarsh, B., Nguyen, K., Kapurch, J., Aoki, K., Wilson, I. B. & Tiemeyer, M. 2010. Neural-specific alpha3-fucosylation of N-linked glycans in the Drosophila embryo requires fucosyltransferase A and influences developmental signaling associated with O-glycosylation. *Glycobiology,* 20(11)**,** pp 1353-65.

Repnikova, E., Koles, K., Nakamura, M., Pitts, J., Li, H., Ambavane, A., Zoran, M. J. & Panin, V. M. 2010. Sialyltransferase regulates nervous system function in Drosophila. *J Neurosci,* 30(18)**,** pp 6466-76.
Reynolds, P. J., Simms, J. R. & Duronio, R. J. 2008. Identifying determinants of cullin binding specificity among the three functionally different Drosophila melanogaster Roc proteins via domain swapping. *PLoS One,* 3(8)**,** pp e2918.

Ripoche, J., Link, B., Yucel, J. K., Tokuyasu, K. & Malhotra, V. 1994. Location of Golgi membranes with reference to dividing nuclei in syncytial Drosophila embryos. *Proc Natl Acad Sci U S A,* 91(5)**,** pp 1878-82.

Risinger, A. L. & Kaiser, C. A. 2008. Different ubiquitin signals act at the Golgi and plasma membrane to direct GAP1 trafficking. *Mol Biol Cell,* 19(7)**,** pp 2962-72.

Ruiz-Cañada, C. & Budnik, V. 2006. Introduction on the use of the Drosophila embryonic/larval neuromuscular junction as a model system to study synapse development and function, and a brief summary of pathfinding and target recognition. *Int Rev Neurobiol,* 75(1-31.

Sarkar, M., Leventis, P. A., Silvescu, C. I., Reinhold, V. N., Schachter, H. & Boulianne, G. L. 2006. Null mutations in Drosophila N-acetylglucosaminyltransferase I produce defects in locomotion and a reduced life span. *J Biol Chem,* 281(18)**,** pp 12776-85.

Schachter, H. 2014. Complex N-glycans: the story of the "yellow brick road". *Glycoconj J,* 31(1)**,** pp 1-5.

Schmid, A., Chiba, A. & Doe, C. Q. 1999. Clonal analysis of Drosophila embryonic neuroblasts: neural cell types, axon projections and muscle targets. *Development,* 126(21)**,** pp 4653-89.

Schubiger, M., Feng, Y., Fambrough, D. M. & Palka, J. 1994. A mutation of the Drosophila sodium pump alpha subunit gene results in bang-sensitive paralysis. *Neuron,* 12(2)**,** pp 373-81.

Schuster, C. M., Ultsch, A., Schloss, P., Cox, J. A., Schmitt, B. & Betz, H. 1991. Molecular cloning of an invertebrate glutamate receptor subunit expressed in Drosophila muscle. *Science,* 254(5028)**,** pp 112-4.

Seppo, A., Matani, P., Sharrow, M. & Tiemeyer, M. 2003. Induction of neuron-specific glycosylation by Tollo/Toll-8, a Drosophila Toll-like receptor expressed in non-neural cells. *Development,* 130(7)**,** pp 1439-48.

Seppo, A. & Tiemeyer, M. 2000. Function and structure of Drosophila glycans. *Glycobiology,* 10(8)**,** pp 751-60.

Skeath, J. B. & Thor, S. 2003. Genetic control of Drosophila nerve cord development. *Curr Opin Neurobiol,* 13(1)**,** pp 8-15.

Stanley, P. & Okajima, T. 2010. Roles of glycosylation in Notch signaling. *Curr Top Dev Biol,* 92(131-64.

Storan, M. J., Magnaldo, T., Biol-N'Garagba, M. C., Zick, Y. & Key, B. 2004. Expression and putative role of lactoseries carbohydrates present on NCAM in the rat primary olfactory pathway. *J Comp Neurol,* 475(3)**,** pp 289-302.

Sun, Y., Tan, M., Duan, H. & Swaroop, M. 2001. SAG/ROC/Rbx/Hrt, a zinc RING finger gene family: molecular cloning, biochemical properties, and biological functions. *Antioxid Redox Signal,* 3(4)**,** pp 635-50.

Swaroop, M., Gosink, M. & Sun, Y. 2001. SAG/ROC2/Rbx2/Hrt2, a component of SCF E3 ubiquitin ligase: genomic structure, a splicing variant, and two family pseudogenes. *DNA Cell Biol,* 20(7)**,** pp 425-34.

Swiatek, P. J., Lindsell, C. E., del Amo, F. F., Weinmaster, G. & Gridley, T. 1994. Notch1 is essential for postimplantation development in mice. *Genes Dev,* 8(6)**,** pp 707-19.

Takeda, K. & Akira, S. 2004. TLR signaling pathways. *Semin Immunol,* 16(1)**,** pp 3-9.

Takeuchi, H. & Haltiwanger, R. S. 2010. Role of glycosylation of Notch in development. *Semin Cell Dev Biol,* 21(6)**,** pp 638-45.

Tan, M., Li, H. & Sun, Y. 2015. Inactivation of Sag/Rbx2/Roc2 e3 ubiquitin ligase triggers senescence and inhibits kras-induced immortalization. *Neoplasia,* 17(1)**,** pp 114-23.

Tan, M., Zhao, Y., Kim, S. J., Liu, M., Jia, L., Saunders, T. L., Zhu, Y. & Sun, Y. 2011. SAG/RBX2/ROC2 E3 ubiquitin ligase is essential for vascular and neural development by targeting NF1 for degradation. *Dev Cell,* 21(6)**,** pp 1062-76.

Tang, D., Xiang, Y., De Renzis, S., Rink, J., Zheng, G., Zerial, M. & Wang, Y. 2011. The ubiquitin ligase HACE1 regulates Golgi membrane dynamics during the cell cycle. *Nat Commun,* 2(501.

Thayer, D. A., Jan, Y. N. & Jan, L. Y. 2013. Increased neuronal activity fragments the Golgi complex. *Proc Natl Acad Sci U S A,* 110(4)**,** pp 1482-7.

Tian, J., Cai, T., Yuan, Z., Wang, H., Liu, L., Haas, M., Maksimova, E., Huang, X. Y. & Xie, Z. J. 2006. Binding of Src to Na+/K+-ATPase forms a functional signaling complex. *Mol Biol Cell,* 17(1)**,** pp 317-26.

Tiemeyer, M., Selleck, S. B. & Esko, J. D. 2009. Arthropoda.

Varki, A. 1993. Biological roles of oligosaccharides: all of the theories are correct. *Glycobiology,* 3(2)**,** pp 97-130.

Varki, A., Cummings, R. D., Esko, J. D., Freeze, H. H., Stanley, P., Bertozzi, C. R., Hart, G. W. & Etzler, M. E. 2009. Essentials of Glycobiology. Second Edition ed. Cold Spring Harbor, New York: Cold Spring Harbor Laboratory Press.

Velasco, A., Hendricks, L., Moremen, K. W., Tulsiani, D. R., Touster, O. & Farquhar, M. G. 1993. Cell type-dependent variations in the subcellular distribution of alpha-mannosidase I and II. *J Cell Biol,* 122(1)**,** pp 39-51.

Viquez, N. M., Füger, P., Valakh, V., Daniels, R. W., Rasse, T. M. & DiAntonio, A. 2009. PP2A and GSK-3beta act antagonistically to regulate active zone development. *J Neurosci,* 29(37)**,** pp 11484-94.

Vèolkner, M., B, L.-B., H, B. & B, S. 2000. Novel CNS glutamate receptor genes of *Drosophila* melanogaster. J Neurochem.

Wagh, D. A., Rasse, T. M., Asan, E., Hofbauer, A., Schwenkert, I., Durrbeck, H., Buchner, S., Dabauvalle, M. C., Schmidt, M., Qin, G., Wichmann, C., Kittel, R., Sigrist, S. J. & Buchner, E. 2006. Bruchpilot, a protein with homology to ELKS/CAST, is required for structural integrity and function of synaptic active zones in Drosophila. *Neuron,* 49(6)**,** pp 833-44.

Xu, C. & Ng, D. T. 2015. Glycosylation-directed quality control of protein folding. *Nat Rev Mol Cell Biol,* 16(12)**,** pp 742-52.

Yano, H., Yamamoto-Hino, M., Abe, M., Kuwahara, R., Haraguchi, S., Kusaka, I., Awano, W., Kinoshita-Toyoda, A., Toyoda, H. & Goto, S. 2005. Distinct functional units of the Golgi complex in Drosophila cells. *Proc Natl Acad Sci U S A,* 102(38)**,** pp 13467-72.

Yuan, W. C., Lee, Y. R., Lin, S. Y., Chang, L. Y., Tan, Y. P., Hung, C. C., Kuo, J. C., Liu, C. H., Lin, M. Y., Xu, M., Chen, Z. J. & Chen, R. H. 2014. K33-Linked Polyubiquitination of Coronin 7 by Cul3-KLHL20 Ubiquitin E3 Ligase Regulates Protein Trafficking. *Mol Cell,* 54(4)**,** pp 586-600.

Zhang, H., Miller, R. H. & Rutishauser, U. 1992. Polysialic acid is required for optimal growth of axons on a neuronal substrate. *J Neurosci,* 12(8)**,** pp 3107-14.

CHAPTER 2

REDUCTION OF A SINGLE E3 UBIQUITIN LIGASE ALTERS NEURAL-SPECIFIC GLYCOSYLATION IN *DROSOPHILA MELANOGASTER*[1]

---

[1]Nickita Mehta, Peng Zhao, Mary Sharrow, Katie Tiemeyer, Lance Wells and Michael Tiemeyer. To be submitted to J.Neuroscience.

Abstract

The regulatory pathways that control tissue-specific glycan expression are not well understood. A mutagenesis screen was undertaken in Drosophila to identify mutants that are deficient in the expression of a family of structurally related, neural-specific N-linked glycans known as HRP-epitopes. These epitopes are detectable by anti-HRP antibody staining. To date, three mutants have been identified, each in different genes. Each mutant lacks HRP-epitope expression during embryonic stages and, as a group, the mutants exhibit genetic interactions with each other in regards to the loss of HRP-epitope. Additionally, all three mutants exhibit a similar neuromotor defect as adults. While mutant adults are motile and can right themselves when flipped over, they all fail to exhibit spontaneous climbing activity, which is a robust behavior in wildtype adults. One of these mutants, originally designated ms16, affects the expression level of an E3 ubiquitin ligase known as roc2, which has previously been demonstrated to be essential for neural development. In addition to altered HRP-epitope expression, the total glycan profile of *roc2*^{ms16} embryos was shifted toward increased abundance of complex glycans in comparision to wildtype embryos. In addition, Golgi compartmentation was also shifted such that the overlap between markers for early and late Golgi was increased, suggesting that augmented glycan complexity may arise from altered access of processing enzymes and substrates. Differential proteomic analysis, by LC-MS/MS and validated subsequently by orthogonal approaches, detected significantly increased expression of ATPα (alpha subunit of the Na^+/K^+ pump) in *roc2*^{ms16} mutants compared to wildtype. Conversely, quantification of HRP-epitope expression by ELISA detected increased expression of the neural-specific glycan class in a deficiency line that partially reduced ATPα expression. Therefore, increased ATPα expression (*roc2*^{ms16}) reduced HRP-epitope abundance while decreased ATPα expression (ATPα deficiency line)

increased HRP-epitiope abundance, indicating a role for ATPα in the regulation of glycoprotein glycosylation. Other components of the membrane excitability machinery were also impacted in *roc2*^{ms16}. Notably, expression of the excitatory glutamate receptor at the neuromuscular junction, dGluRIII, was increased in *roc2*^{ms16} larvae, perhaps in response to altered ionic fluxes induced by increased ATPα activity. Thus, altered roc2 activity impacts neural-specific glycosylation and key functions of excitable cells.

KEY WORDS HRP-epitope, glycosylation, neural development, ubiquitination, ion homeostasis, glutamate receptor, Na^+/K^+ ATPase

Introduction

Protein and lipid glycosylation are essential for development in all multicellular organisms because these post-translational and post-synthetic modifications mediate cell-cell interactions, cell migration, cell differentiation, and cell survival across all maturing tissues. As cells differentiate, the glycans they synthesize and present to their environment change, leading to the generation of tissue-specific glycan profiles. While some of these glycosylation changes can be studied in cultured cells, in vitro conditions rarely replicate the complicated and intricate webs of cell-cell interactions, hormonal influences, and receptor activation that are necessary for cells to achieve their mature glycophenotype in vivo. Therefore, to understand this process in its entirety, it is essential to study glycosylation in whole organisms where intrinsic regulatory and modulatory influences are maintained.

The embryonic, larval, pupal, and adult nervous systems of Drosophila melanogaster (as well as other arthropods) express a family of structurally related N-linked glycans known collectively as HRP-epitopes, so named because they can be

visualized by antibodies raised against horseradish peroxidase (REF Jan, Snow). The antigenic determinant shared by all HRP-epitopes in Drosophila consists of a fucose residue (Fuc) linked α3 to the core N-acetylglucosamine (GlcNAc) at the reducing terminal of the N-linked chitobiose core (Jan and Jan, 1982; Katz et al., 1988; Snow et al., 1987; Paschinger et al., 2009; Kurosaka et al., 1991). A single Drosophila fucosyltransferase, FucTA, is capable of core α3 fucosylation and the neural-restricted expression of this enzyme underlies the neural-specific appearance of HRP-epitopes (Rendic et al., 2010; Paschinger et al., 2009). However, the processing and modification of glycoprotein glycans is modulated by many factors in addition to enzyme expression. For example, donor availability (nucleotide sugars), production of appropriate acceptor structures (glycan substrates), placement of enzymes within appropriate Golgi compartments, and directed trafficking of cargo through the secretory pathway, as well as other cellular and molecular factors together provide additional regulatory points that shape the total cellular glycan profile and thereby modulate protein and cell functions (Moremen et al., 2012). The restricted expression of the HRP-epitope in Drosophila provides a platform to identify and interrogate the breadth of molecular mechanisms that regulate tissue-specific glycosylation by generating and characterizing mutants that affect HRP-epitope expression.

Previous reports have characterized a handful of mutations that affect HRP-epitope expression in Drosophila, some are in components of the biosynthetic machinery essential for synthesizing the epitopes and some highlight the existence of novel glycoregulatory pathways. In terms of biosynthetic pathways, mutations in the *nac* gene, which encodes for a GDP-Fuc transporter, or in the *mgat1* gene, which encodes for GlcNAc Transferase-1 (an enzyme that generates the substrate for FucTA), eliminate HRP-epitope expression as expected based on their molecular function (Geisler et al.,

2012; Ioffe and Stanley, 1994). Mutations in two non-biosynthetic genes that affect HRP-epitope expression include tollo/toll-8, a Toll-like receptor family member, and sff/SAD, a neural-specific Ser/Thr Kinase. Both tollo/toll-8 and sff/SAD dramatically reduce neural expression of the HRP-epitope and both share adult behavioral phenotypes associated with geotaxis (Baas et al., 2011; Seppo et al., 2003), Golgi structural disruptions were also detected in sff/SAD mutants, providing a cellular basis for altered glycosylation in the mutant, and expression of sff/SAD mRNA was reduced in tollo/toll-8 mutants, indicating that these two genes function in the same glycoregulatory pathay (Baas et al., 2011).

The sff/SAD mutant was recovered from a chemical mutagenesis screen (EMS) for mutations that affect HRP-epitope production, a Golgi processing step, without interfering with glycoprotein glycosylation, an endoplasmic reticulum (ER) function (Baas et al., 2011). In this screen, mutagenized males were bred to generate stocks that were assessed in the F2 generation for loss of anti-HRP antibody binding but retention of concanavalin A binding in embryo collections. Stocks that produced ConA+/HRP- embryos retained the ability to glycosylate proteins with high-mannose precursors (recognized by ConA) in the ER but lost their ability to process glycans in the Golgi. Here, we report the characterization of another mutant recovered from the same EMS screen that generated the sff/SAD mutant. Based on genetic interactions and shared phenotypes, this new mutant, designated ms16, also functions in the tollo-sff glycoregulatory pathway. Characterization of the ms16 mutant, which we map to the gene encoding for Roc2, an E3 ubiquitin ligase, demonstrates that a small change in the activity of an E3 ligase can generate large changes in the expression of proteins subject to regulation by ubiquitination. Furthermore, one of these proteins, whose expression is exquisitely sensitive to Roc2 activity, is an essential component of the molecular machinery that regulates membrane potential in excitable cells. We demonstrate that

altered expression of this protein, the alpha subunit of the Na+/K+ ATPase (ATPα), is sufficient to modulate HRP-epitope expression. Based on our results, we propose a model in which excitable cells, whose functions are integrally related to membrane potential, leverage this machinery to generate signals that tune protein glycosylation to achieve neural-specific glycophenotypes.

Experimental Proceedure

Reagents.

Antibodies for immunohistochemistry and immunofluorescence used were: rabbit anti-HRP (1:5000 for embryos, 1:1000 for larvae), HRP-conjugated goat anti-rabbit (1:2000), and goat anti-mouse (1:2000) antibodies from Jackson Laboratories; monoclonal antibodies nC82 (anti-Brp; 1:100 for larvae) and mouse anti-En (1:50) from the Developmental Studies Hybridoma Bank (DHSB, University of Iowa, IA, USA); rabbit anti-GM130 (1:1000) monoclonal antibody obtained from Abcam; Alexa-conjugated secondary antibodies (Alexa 488, 568 and 633; 1:500), rabbit anti-GFP (1:1000) and PROLONG anti-fade obtained from Molecular Probes; TRITC-Phalloidin (1:100) obtained from Invitrogen. TGN antibody (1:2000) was a gift Sean Munro (Cambridge, UK). Rabbit anti-ATPalpha (1:1000 for embryos and 1:2000 for larvae was obtained from Thermo Fisher Scientific and DGluRIII (1:2000) was a gift from Dr. DiAntonnio (Marrus et al., 2004). Antibodies used for westerns were Rabbit anti-ATPalpha from Thermo; mouse anti-nrv, mouse anti-a5 from the Developmental Studies Hybridoma Bank (DHSB, University of Iowa, IA, USA); mouse anti-Actin C4 (1:5000) from Molecular probes and rabbit anti-Tubulin from Abcam. For glycan analysis PNGaseF (N-glycanase) was obtained from Prozyme (San Leandro, CA); trypsin and chymotrypsin were from Sigma.

Immunohistochemistry.

Embryos were collected overnight at room temperature and then dechorionated using 50% bleach for 4 minutes. Following dechorionation, embryos were fixed in 4% formaldehyde and heptane and then devitallinized using methanol. Embryos were then stained using blocking and washing solutions as previously described (Patel, 1994; Seppo et al., 2003; Baas et al., 2011). Neuromuscular junction was assessed on third instar wandering larvae and were dissected and stained using protocols described previously (Baas et al., 2011; Kaufmann et al., 2002; Brent et al., 2009).

Quantitative PCR.

Overnight collection of embryos were RNA extracted using RNAeasy kit (Qiagen). cDNA was made from 5 ug of RNA using superscript III (Invitrogen) and different regions within the *Roc2* gene were assessed by qRT using primers from Operon as described previously (Nairn et al., 2007).

Drosophila mutagenesis, fly stocks and generation of rescue crosses.

Wildtype or +;D,ry/TM3lacZ males were treated with 25 mM ethyl methanesulfonate. Surviving mutagenized males were then mated to w;Kr/CyO; +/+ females *en masse*. F1 males w; */CyO; *D,ry/+ were individually mated to w;Kr/CyO; +/+ females and w; */CyO;+ lines that survived were screened for HRP epitope expression. Lines that showed HRP epitope mutation were then scrubbed to ensure there was only one mutation.

All P-elements, deficiencies and UAS/Gal4 lines were obtained from Bloomington Stock Center (Bloomington, Indiana). UAS-*Roc2* (34049) and En-Gal4 (30730) were inserted into an ms16 homozygous background through recombination. These lines were used to drive specific expression of *Roc2* in engrailed positive cells for rescue. The Golgi-YFP line was used to get the YFP transgene into a ms16 background and this was used to asses the Golgi phenotype as compared to wildtype (w1118; +; EYFP).

Dissected and stained embryos were then analyzed on confocal microscope Olympus FV1000 LSC microscope with a 60× (N.A. 1.42) oil objective and analyzed as described (Baas et al., 2011)

***In-situ* hybridization.**

Roc2 cDNA (clone RE61847) in a pFLC-I vector was obtained from *Berkeley Drosophila Genome Project* and sense and anti-sense Digoxigene-11-UTP labeled RNA probes were made using the DIG labeling kit (Roche) (Kopczynski et al., 1996). After hybridization, anti-sense and sense probes were detected using alkaline phosphatase and NBT/BCIP (nitro blue tetrazolium/5-bromo-4-chloro-3-indolyl-phosphate) color reaction.

Proteomic analysis of Roc2 peptide and potential substrates.

Wildtype and mutant protein extracts were run on a 4-20% polyacrylamide SDS-page gel and were separated by electrophoresis. For *Roc2* peptide analysis bands between 10-15kDa were cut and reduced, alkylated and digested with sequence grade Trypsin. To look for potential substrates for *Roc2*, whole protein extract as well as gel pieces were cut and analyzed using the protocol (Lim et al., 2008). External AQUA peptide for *Roc2* and Actin (Thermo Fisher) were used as an external standard to verify protein amounts between samples. Samples were run off a C18 column and analyzed by LC/MS-MS on a LTQ orbitrap mass spectrometer (Discover, Thermo Fisher) with a MS pump. For ubiquitin-targeted proteomics, whole lysates were run and global peptide changes were analyzed. The protein samples were denatured by incubating with 10 mM of dithiothreitol at 56 °C for an hour and alkylated by 55 mM of iodoacetamide for 45 minutes in dark prior to digestion with trypsin overnight at 37 °C. The resulting peptides were cleaned-up over C18 spin columns (The Nest Group), dried in Speed Vac, and reconstituted in 0.1% formic acid. The peptides were separated on a 75 µm (I.D.) x 15 cm C18 capillary column (packed in house, YMC GEL ODS-AQ120ÅS-5, Waters) and

eluted into the nano-electrospray ion source of an Orbitrap Fusion™ Tribrid™ mass spectrometer (Thermo Fisher Scientific) with a 180-min linear gradient consisting of 0.5-100% solvent B over 150 min at a flow rate of 200 nL/min. The spray voltage was set to 2.2 kV and the temperature of the heated capillary was set to 280 °C. Full MS scans were acquired from m/z 300 to 2000 at 120k resolution, and MS2 scans following collision-induced fragmentation were collected in the ion trap for the most intense ions in the Top-Speed mode within a 3-sec cycle using Fusion instrument software (v1.1, Thermo Fisher Scientific). The raw spectra were searched against the *Drosophila Melanogaster* protein database (UniProt, Oct. 2014) using SEQUEST (Proteome Discoverer 1.4, Thermo Fisher Scientific) with full MS peptide tolerance of 20 ppm and MS2 peptide fragment tolerance of 0.5 Da, and filtered using ProteoIQ (v2.7, Premier Biosoft) at the protein level to generate a 1% false discovery rate for protein assignments. Quantification was performed by normalizing spectral counts generated in ProteoIQ (v2.7, Premier Biosoft). The peptides found were verified against previous literature on proteins associated with ubqituins (Franco et al., 2011)

Preparation of Glycopeptides and release of N-linked Glycans.

N-linked glycans were released and collected from wildtype and ms16 total fly powder (Aoki et al., 2007). In short, 3 mg of total protein (dry weight) was resuspended and digested with trypsin and chymotrypsin. Glycopeptides were enriched and cleaned by Sep-Pak C18 cartridge chromatography and then digested with PNGase F for 18 h at 37 °C. Released glycans were separated from residual peptide by Sep-Pak C18 clean-up and permethylated before mass spectrometric analysis. Permethylated N-linked glycans were then analyzed by nanospray ionization mass spectrometry using an ion trap instrument (NSI-LTQ Orbi Discoverer, Thermo-Fisher) by dissolving glycans in 1mM NaOH in 50% methanol. Direct infusion method was used and a syringe flow rate of 0.4 uL/min.

Geotaxis and viability.

Seven-day old males raised at 25 degrees were starved and placed in the dark for one hour at 18 degrees before testing. These males were then tapped to the bottom and individually tested for the amount of time it took to reach the top of a 3 cm vial at 18 degrees, visualized with a red light. A maximum of 120 seconds was given to all the males, and the number of flies that did not reach the designated height in 120 sections was recorded.

Immunoblotting and western analysis.

Embryos were collected overnight and extract was made using lysis buffer (5mM Tris-HCl, NaCl, protease inhibitors (Roche), 5% NP-40 and dTT). Proteins were then separated using a 4-20% SDS-Polyacrylamide gel and transferred to a PVDF membrane. The blots were then probed with rabbit anti-ATPalpha (1:5000), mouse anti-a5 antibody (1:2000), mouse anti-Nrv (1:00), rabbit anti-Tubulin (1:2000) and mouse anti-actin (1:5000) to compare steady state levels between wildtype and mutant.

Neuromuscular junction.

Wandering third instar larvae were dissected in larval dissection buffer (128mM NaCl, 2nM KCl, 4mM $MgCl_2$, 35.5mM sucrose, 5mM HEPES, 1mM EGTA). Dissected pelts were fixed in 4% formaldehyde in 1x PBS for 15 minutes. The pelts were then placed in a 24 well plate and washed three times for 10 minutes in 1x PBS-T (.3% Triton X-100). The pelts were blocked for four hours in 0.1% BSA diluted in wash with an added 10% normal goat serum. Primary antibody diluted in blocking buffer was added and allowed to incubate overnight at 4° Celsius (DGluRIII 1:2000, NC82 1:100, KDEL 1:100 ATPα 1:1000*). The pelts were washed again three times for 10 minutes before being re-blocked for 30 minutes. Secondary antibody diluted in blocking buffer was added and allowed to incubate for two hours (Goat anti-Rabbit 568 1:500, Goat anti-

mouse 488 1:1000, Phalloidin 1:100). The pelts were then mounted and analyzed with confocal microscopy. Junctions between muscle 6 and 7 were analyzed.

Elisa.

Embryo lysates were prepared with lysis buffer (0.1M tris-HCl, .087g NaCl, protease inhibitor, and 1% Tween 20). Additionally, 2X Coating Buffer (.795g Na_2CO_3, 1.465g $NaHCO_3$, .5 mL 20% NaN_3) and PBS-T (.05% Tween 20, .02% NaN_3) were prepared. Lysates were boiled for 5 minutes. The samples were then diluted in 1X coating buffer to a concentration of 0.003ug/ul. Equal amounts of protein were aliquoted into the wells of a Thermo Scientific Nunc . The plate was covered in parafilm and left to incubate at 4 degrees Celsius overnight. Plates were then rinsed three times with 1X PBS-T and then filled with 0.5% BSA in PBS-T and blocked for 30 minutes. 100 µl of rabbit anti-HRP primary antibody was added at a 1:500 dilution and allowed to incubate at room temperature for 2 hours. After rinsing again, 100µl of rabbit alkaline-phosphatase secondary antibody was added at a 1:500 dilution and allowed to incubate at room temperature for 2 hours. The wells were then rinsed and 200ul of Sigma PNPP substrate was added to each well to initiate the color reaction. The plate was then read on a plate reader for 1 hour and 15 minutes before 50µl of 3M NaOH was added to each well to stop the reaction and the absorbance was checked again.

Drug treatment.

Wildtype and mutant embryos were collected for 6 hours and then dechorionated as normal. The embryos were then permeabilized using EPS/MBIM and treated with 50µM Ouabain in PBS overnight at 20 degrees. Untreated embryos were left overnight in PBS alone. After 16 hours embryos were lysed in lysis buffer ((0.1M tris-HCl, .087g NaCl, protease inhibitor, and 1% Tween 20). 0.3 ug of extract was loaded and analyzed by Elisa as mentioned above.

Results

HRP epitopes in drosophila are decreased in ms16 mutants

A mutation on the second chromosome, designated ms16, was identified in a random EMS screen for mutations that altered HRP-epitope expression but did not affect core glycoprotein glycosylation, as assessed by the ability of concanavalin A to recognize high-mannose glycans (**Fig 2.1**). The ms16 mutant embryos, stained with anti-HRP antibodies, show an absence of HRP-epitope expression in the peripheral nervous system (pns), the hindgut (hg) and anal pads (ap). The residual staining in the ventral nerve cord (vnc) can be detected throughout development as can be seen in Figure 2.1. As the embryos age, HRP-epitope expression in the vnc continues to increase but never fully rescues to wildtype (**Fig 2.1**).

Figure 2.1: HRP epitopes in Drosophila are decreased in m16.
Anti-HRP antibody staining of WT (A) and ms16 (C) embryos showing HRP epitope expression at stage 14 and ConA staining (B,D). In the WT embryo, HRP epitope expression can be seen in the ventral nerve cord (vnc), peripheral nervous system (pns), hind gut (hg) and garland gland (gg). In the mutant (C) this staining is decreased in the vnc and completely absent from other tissues. As embryos stage, HRP-epitope expression increases in the mutant, but never fully rescues (E-H).

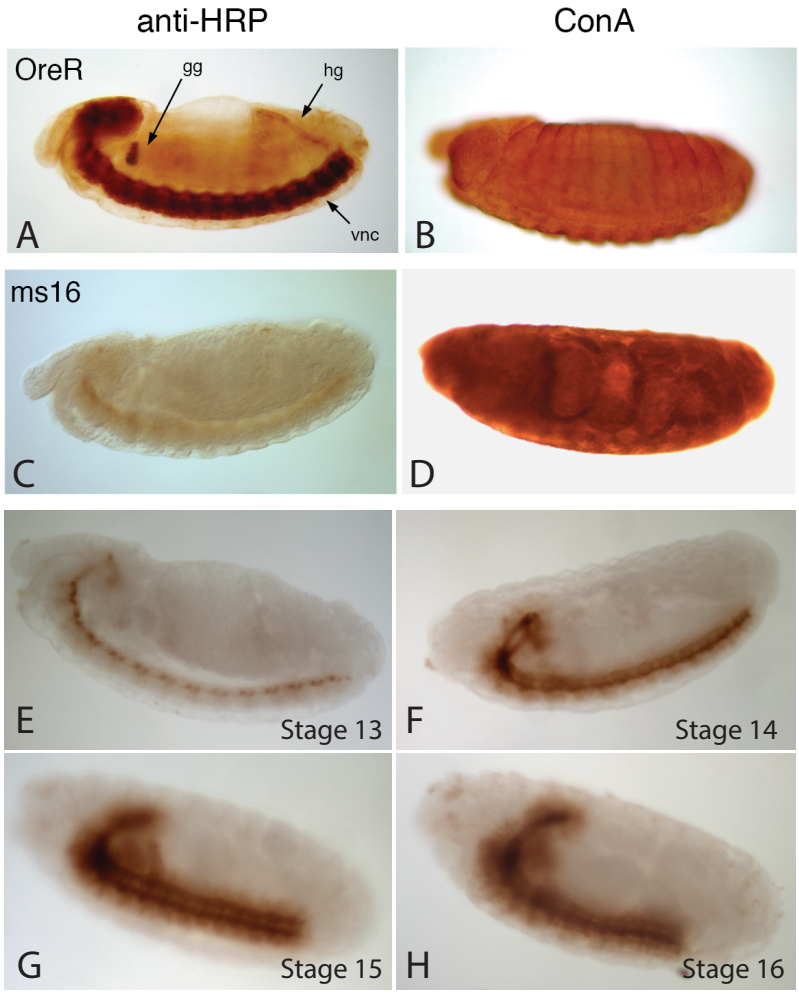

ms16 maps to Roc2, an E3 ubiquitin ligase

The mutagenesis screen targeted the 2nd chromosome; after initial scrubbing, recombination mapping was undertaken using P-element insertion lines which mapped to positions across the entire 2nd chromosome. After the first round of recombination, we then obtained more P-elements on the right arm of the 2nd chromosome and repeated the recombination mapping (**Table 2.1**). Following recombination, we used deletion lines to narrow the interval down; non-complementation was seen in stock 8912 (48A3-48D5) when crossed to ms16 and this region contained approximately 10 genes. P-elements and deletion lines within this interval were then crossed to our mutant and using this technique, we were able to narrow down to a single gene, Roc2.

The mutation in *Roc2*^{ms16} is a single nucleotide change from cytosine to adenine in the 2nd intron of the *Roc2* gene (**Fig 2.2A**). This intronic base change blocks the ability to sequence in the mutant, so we propose a change in the secondary structure as predicted by secondary structure prediction software, GeneBee. No change in message level was seen within the exon before the intronic nucleotide change (exon 2) thorugh qRT-PCR, however there was a 9 fold increase in the amount of message produced by the mutant between the exon 2 and intron 2, in the region spanning over the nucleotide change (**Fig 2.2B**). The presence of intron suggests that this nucleotide change does affect splicing ability in the mutant. Due to the ineffectiveness of splicing we see a decrease in message level. The abundance of Roc2 protein in the ms16 mutant was quantified by LC-MS/MS based proteomics. A tryptic Roc2 peptide detected in both wildtype and ms16 mutant was decreased by 21% in the mutant (n=3 biological replicates) (**Fig 2.2C,D**) (Lim et al., 2008). The base-peak filtered chromatogram presents a representative analysis for a Roc2 peptide fragment. In the chromatograms and in the summary quantification, Roc2 peptide signal intensities are normalized to the intensity detected for a control peptide from the ribosomal protein RPL30.

Table 2.1: P-element recombination mapping suggested that the mutation was between nucleotide 6141579 and 9637727.

Nucleotide	Cytological location of P-element	% Recombination
6141579	46F9	10.45
7836754	48D3	0.68
9637727	50C3	3.14
11707464	52C7	9.88
13521416	54D3	6.10
15221312	56D1	10.00

Figure 2.2: A mutation in Roc2, an E3 ubiquitin ligase is responsible for the ms16 phenotype.
(A) By sanger sequencing, we identified a C to A_{583} change in the second intron.
(B) Results from qRT-PCR suggests an inability of splicing in the mutant due to the change in secondary structure causing part of the intron to get retained in the mutant.
(C) Proteomic analysis reveals Roc2 protein levels are also decreased in the mutant. External *Roc2* standard (Thermo) was used to quantify endogenous levels of Roc2 in Wild type and mutants. There is a 21% decrease of *Roc2* in the mutant.

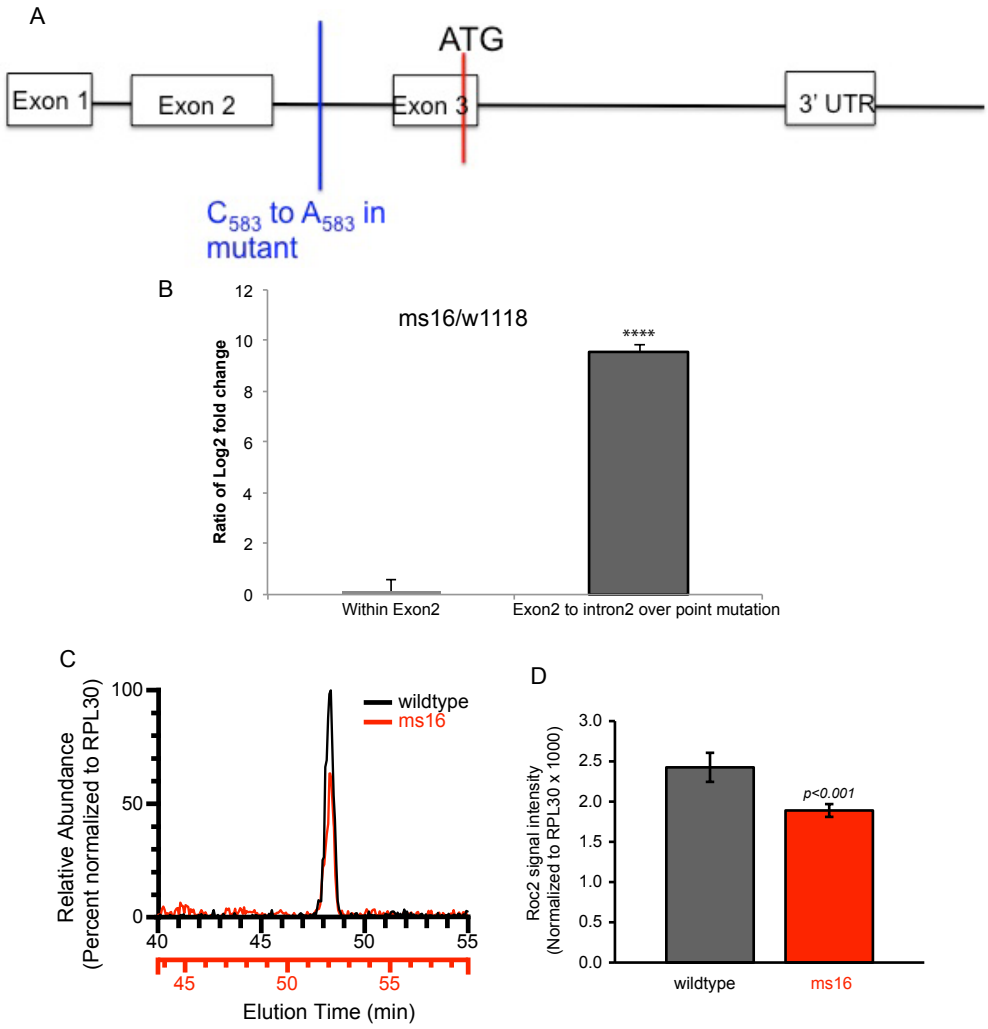

Insertion of Roc2 in an ms16 background, rescues HRP expression

To test directly whether *Roc2* is required for HRP-epitope expression, *we* reintroduced *roc2* into the ms16 mutant background. In *Drosophila*, transcription factors drive neural cell fate (Blagburn, 2008), so we took advantage of this genetically, to manipulate rescue of HRP in specific cells. Roc2 expression was driven in cells that normally express the HRP epitope (en-Gal4), which includes a subset of neurons in the central nervous system. en-Gal4 driven expression of *Roc2* (UAS-*Roc2*) resulted in reappearance of the HRP epitope in the embryonic nervous system of the ms16 mutant (**Fig 2.3C-F**), indicating that decreased *Roc2* expression is responsible for the HRP deficiency in ms16.

Roc2^{ms16} interacts with Tollo and Sff

Roc2^{ms16} interacts genetically with both tollo and sff, other HRP mutants we previously identified and together are part of the non-cannonical Tollo transcellular pathway. Embryos that are heterozygous for tollo, *Roc2*^{ms16}, or sff behave like wildtype (**Fig 2.4A**) and display normal HRP-epitope expression; which means that one copy of any single mutant gene over a wild-type chromosome is normal with respect to HRP-epitope expression. However, when homozygous *Roc2*^{ms16} (**Fig 2.4B,I**) parents are crossed with homozygous Tollo (**Fig 2.4F,H**) or homozygous sff parents (**Fig 2.4C,E**), the resulting embryos show non-complementation for HRP-epitope expression; one wild-type copy of either gene is now insufficient to rescue the phenotype, indicating genetic interaction, placing roc2 in the neuronal side of the tollo pathway.

Figure 2.3: Insertion of Roc2 in ms16 background rescues HRP-epitope expression in specific cells.
(A-D) Expression of engrailed (red) and HRP (green) positive cells in en-Gal4, ms16;+ (A,B) and UAS-*Roc2*,ms16/en-Gal4,ms16;+ (C,D) dissected embryos. Control driver line shows no HRP in the absence of UAS-*Roc2* in a homozygous mutant background however we see rescue of HRP (C,D) epitope expression in cells that don't already express the epitope, confirming that *Roc2* is the molecular lesion responsible for the ms16 phenotype. (B, D) magnified view of the cross-section of one cell showing HRP expression in a en positive cell.

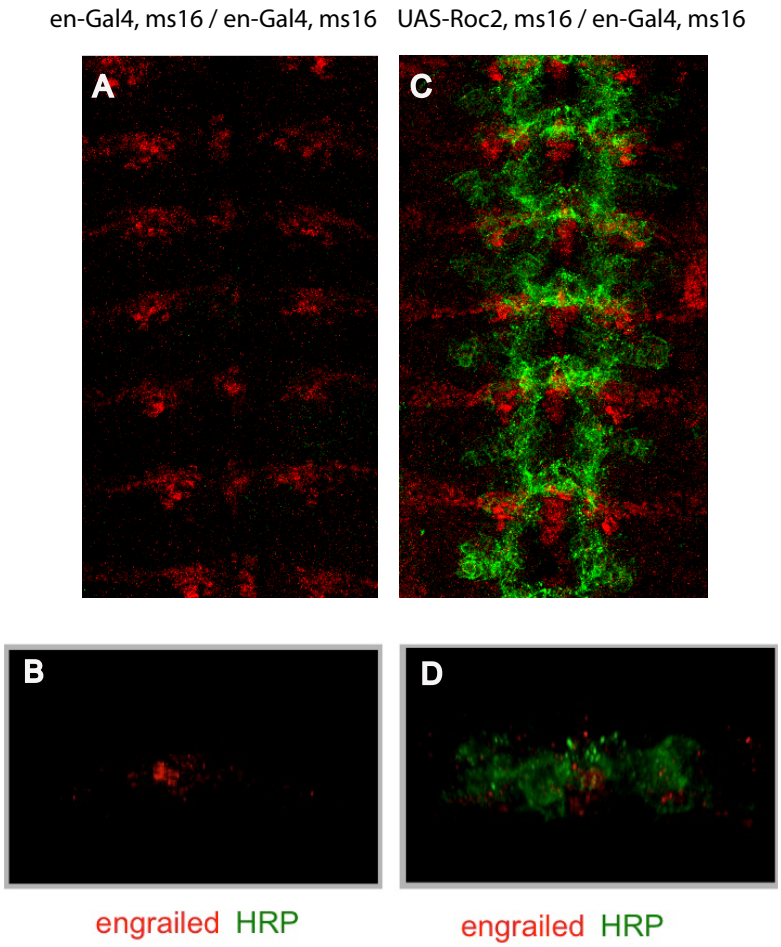

Figure 2.4: *Roc2*^{ms16} interacts with other players of the pathway, Tollo and sff.
(A) Wild type or heterozygous mutant embryos show normal HRP epitope expression. Embryos homozygous for the *Roc2*^{ms16} mutation (B, I) only show partial vnc staining, homozygous sff mutants (C, E) show axonal scaffold vnc and some gg and Tollo homozygous mutants (F,H) only express HRP in non-neural tissues like gg and hg. (B-D) Upon crossing *Roc2*^{ms16} homozygote mutants (B) to sff homozygote mutants (C) the transheterozygote (D) containing only one copy of each of the mutations now phenocopies both mutants individually and fails to rescue showing genetic interactions. The same effect is seen when sff homozygotes (E) are crossed to tollo homozygotes (F) and Tollo to *Roc2*^{ms16} mutants (I). All heterozygotes (D, G, J) show intermaediate staining that fails to rescue.

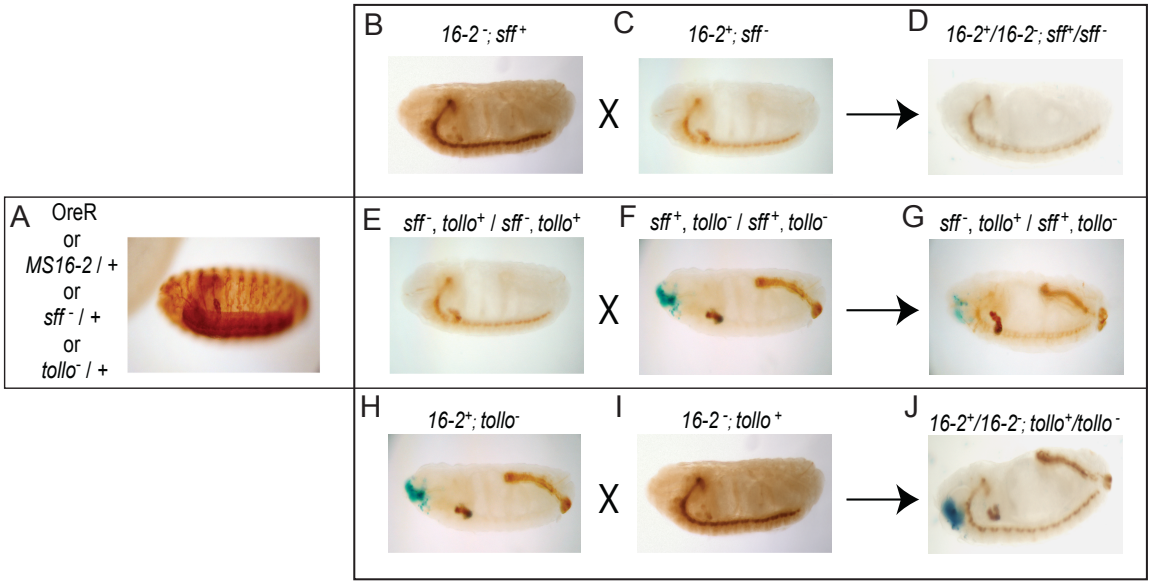

N-glycans are shifted to greater complexity in Roc2^{ms16}

HRP epitopes comprise less than 1% of the glycome (Aoki et al., 2007). To assess whether reduction in Roc2 impacts protein glycosylation more broadly, the N-linked glycome of wildtype and *Roc2*^{ms16} embryos was analyzed by mass spectrometry, following release by PNGaseF digestion. HRP-epitopes are resistant to PNGaseF due to the presence of a3-linked Fuc at the chitobiose core. Therefore, analysis of PNGaseF-released glycans highlights changes in other classes of structures. The population of N-glycans released by PNGaseF exhibited enrichments in complex glycans **(Fig 2.5)**, usually minor components of the total profile. A significant decrease in M3N2F, normally a major contributor to the total profile, likely reflects enhanced channeling of M5N2 toward complex processing and away from degradative pathways that produce paucimannose endpoints. Consistent with the hypothesis that the *Roc2*^{ms16} mutant skews glycosylation to greater complexity, there is an increase in complex glycosylation and a decrease in the major paucimannose glycan (6.1% for M3N2F). To ensure that these glycan changes weren't the cause of changed glycosyltransferase expression in the mutant, transcript levels of glycosyltransferases was assessed through qRT-PCR and found unchanged (data not shown).

Figure 2.5: Overall N-glycosylation is altered in the mutant and shifted to an increase of a subset of complex sialylated glycans using PNGaseF.
In *Roc2*^{ms16}, dominant high mannose structure are unchanged, paucimannose structures are decreased and glycosylation is driven toward a subset of complex glycans.

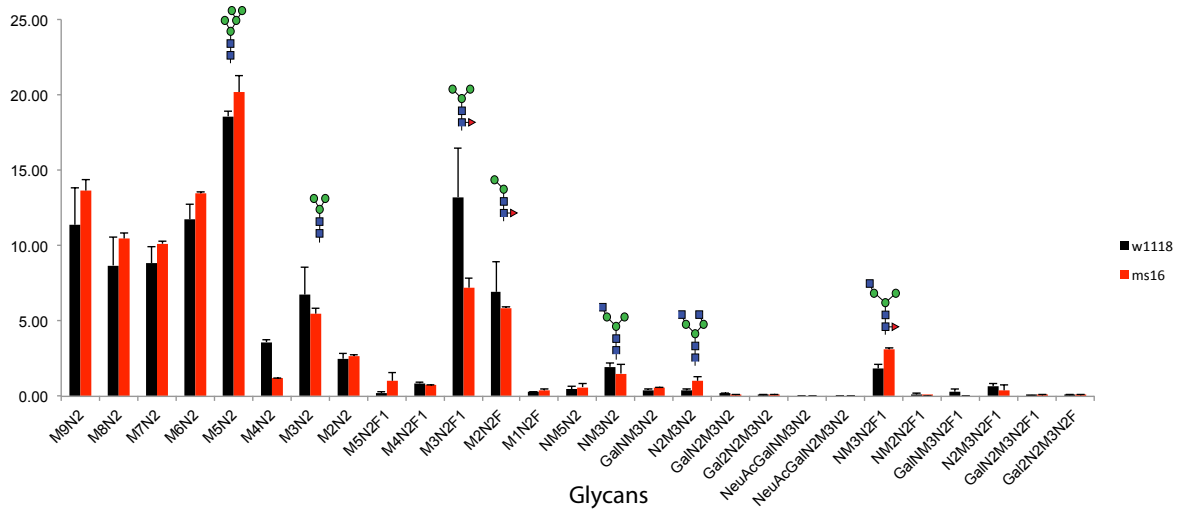

Golgi architecture is altered in the mutant

The shift in the N-glycan profile observed in *Roc2*^{ms16} embryos suggests that Golgi processing has been altered. Using previously established markers for the Golgi (Nakamura et al., 1995) we assessed the Golgi compartmentation and architecture. Using these markers we were able to assess colocalization, intensity as well as size for each of the Golgi units. The region of interest was in the neural region, and the section analyzed contained Golgi units within 15-20 neurons. We localized an early and later Golgi marker (GM130 and Golgi Mannosidase II, respectively) by confocal microscopy and observed two changes in the distribution of Golgi compartments. First, the cis-Golgi compartment (GM130) was substantially expanded in the *Roc2*^{ms16} mutant (**Fig 2.6B**) compared to wild type (**Fig 2.6A**), while the medial/trans marker (Golgi Mannosidase II) was unchanged in size. Second, the colocalization of cis and medial/trans markers was also expanded in *Roc2*^{ms16} (**Fig 2.6C**). In particular, the expansion in the pool of complex glycans is consistent with the hypothesis that later-acting processing enzymes (GlcNAcT's, GalT's, and SiaT) have gained increased access to substrates and may now more efficiently compete with early processing enzymes (Fdl, Golgi mannosidases) that normally drive glycans toward the production of paucimannose structures. These observations indicate a breakdown in Golgi compartmentation and are also consistent with the dilution of early processing steps and increased access of later processing enzymes to appropriate substrates, leading to increased glycan complexity.

Figure 2.6: Golgi architecture and integrity is altered in the mutant.
(A-B) 3D reconstructions of wild-type (A) and mutant (B) ventral nerve cord with Golgi markers for cis, medial and trans Golgi. We used GM130 staining as a cis-Golgi marker (blue), Golgi mannosidase II for medial (red) and TGN for trans. In the mutant, we see a stark increase in GM130 staining which suggests an increase in overall Cis-Golgi . This change is consistent with an increase in colocalization of the Cis golgi with both medial and trans Golgi in mutant embryo's (C).

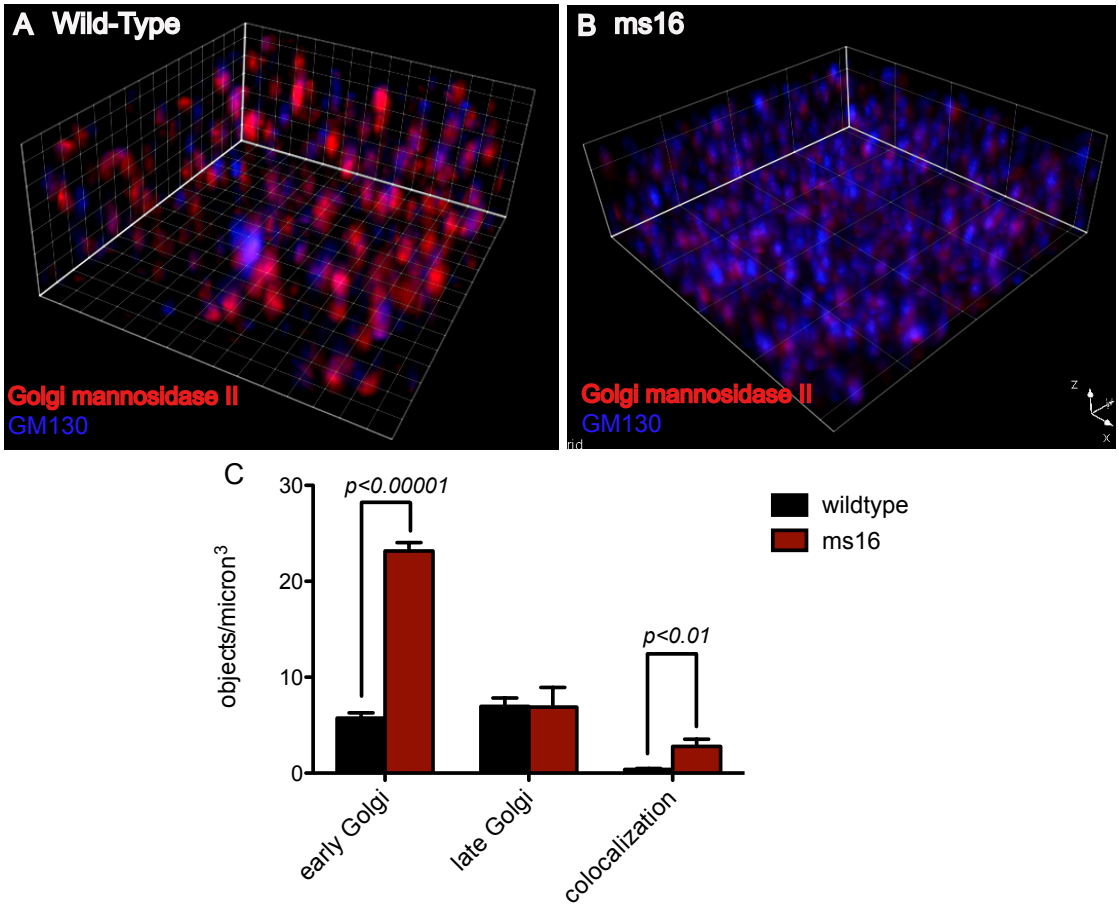

Na^+/K^+ ATPase is a substrate of Roc2^{ms16}

We performed LC-MS/MS proteomic analysis of wild type and *Roc2*^{ms16} embryos to investigate whether decreased expression of Roc2 resulted in increased abundance of proteins normally targeted for degradation by this E3 ubiquitin ligase. These proteins were cross-referenced to previously established proteins found through ubiqtuin pull downs (Franco et al., 2011). Proteins increased in *Roc2*^{ms16} were classified as candidate substrates for Roc2. Among these identified proteins, the Na+/K+-ATPase a-subunit (ATPα) was increased almost 2-fold by spectral counts (**Fig 2.7A**, green arrow). Anti-ATPα antibody staining of embryos also exhibited substantially increased accumulation of the protein within the ventral nerve cord (**Fig 2.7B**). These images show expression on axon bundles (arrows) and on neuronal and glial cell bodies that lie ventral to the axon scaffolds (arrowheads). In many areas of the nerve cord, ATPα appears localized within vesicular structures.

By western blot of whole fly extracts, ATPα was increased in *Roc2*^{ms16}. Whole adult collections from a deletion line (DATPα, collected over a balancer chromosome, ie: 25% homozygous deletion, 50% heterozygous for deletion, 25% wildtype) were significantly reduced in ATPα abundance (**Fig 2.7C**). We also tested other Roc2 deficiency lines and found enhanced ATPα expression (data not shown). Since ubiquitin ligases have multiple substrates, the increased ATPα abundance we detected in *Roc2*^{ms16} might be unrelated to HRP-epitope expression. Therefore, we compared expression of the HRP-epitope by ELISA of extracts prepared from wildtype adults, from *Roc2*^{ms16} homozygous adults, and from a balanced deletion line heterozygous for complete loss of ATPα (DATPα). While *Roc2*^{ms16} adults were greatly reduced in HRP-epitope expression compared to wildtype, adults from the deletion line exhibited enhanced total HRP-epitope expression (**Fig 2.7D**). For a final experiment to tie ATPα directly to HRP, we used a cardiac glycoside, Ouabain, that is known to inhibit the

function of ATPα (Cherniavsky-Lev et al., 2014; Kulikov et al., 2007). We used this drug to show that a change in ATPα corresponds directly to a change in HRP. Using this drug at a fixed concentration, we show that both wildtype and mutant HRP epitope expression changes 1.5-fold in treated vs. untreated embryos (**Fig 2.7E**). Therefore, we hypothesize that the ionic environment regulated by the activity of the Na+/K+-ATPase influences protein glycosylation in addition to its well understood role in maintaining membrane potentials in excitable cells (Palladino et al., 2003).

Figure 2.7: Several proteins are affected by the absence of a ubqituin ligase including Na+/K+-ATPase*, which alters HRP-epitope expression.*
In order to investigate the role a ubiquitin ligase can play in altering golgi trafficking and cause neuromuscular junction defects to ultimately affecting cell surface glycosylation, proteomics was performed to look for possible substrates and players in the pathway. We looked for substrates that were ubiquitinated in WT or mutant, or both wild type and mutant. (A) Graph shows substrates that were changed by 2-fold or more. (B,C) Wildtype (B) and mutant (C) stage 14 embryos, dissected showing an increase in ATPalpha in the nerve cord. (D) Western blot confirms an increase in ATPα in the mutant, and is almost completely absent in the ATPα deficiency. (E) An increase in HRP-epitope expression is associated with a decrease in ATPalpha as seen by Elisa.
(F) Wildtype and mutant embryos were treated with a cardiac glycoside, Ouabain that is a known inhibitor of ATPalpha. Results from this Elisa experiment are shown as fold change of treated embryos over untreated embryos. In both genotypes we see a 1.5 fold increase in total HRP-expression in treated embryos.

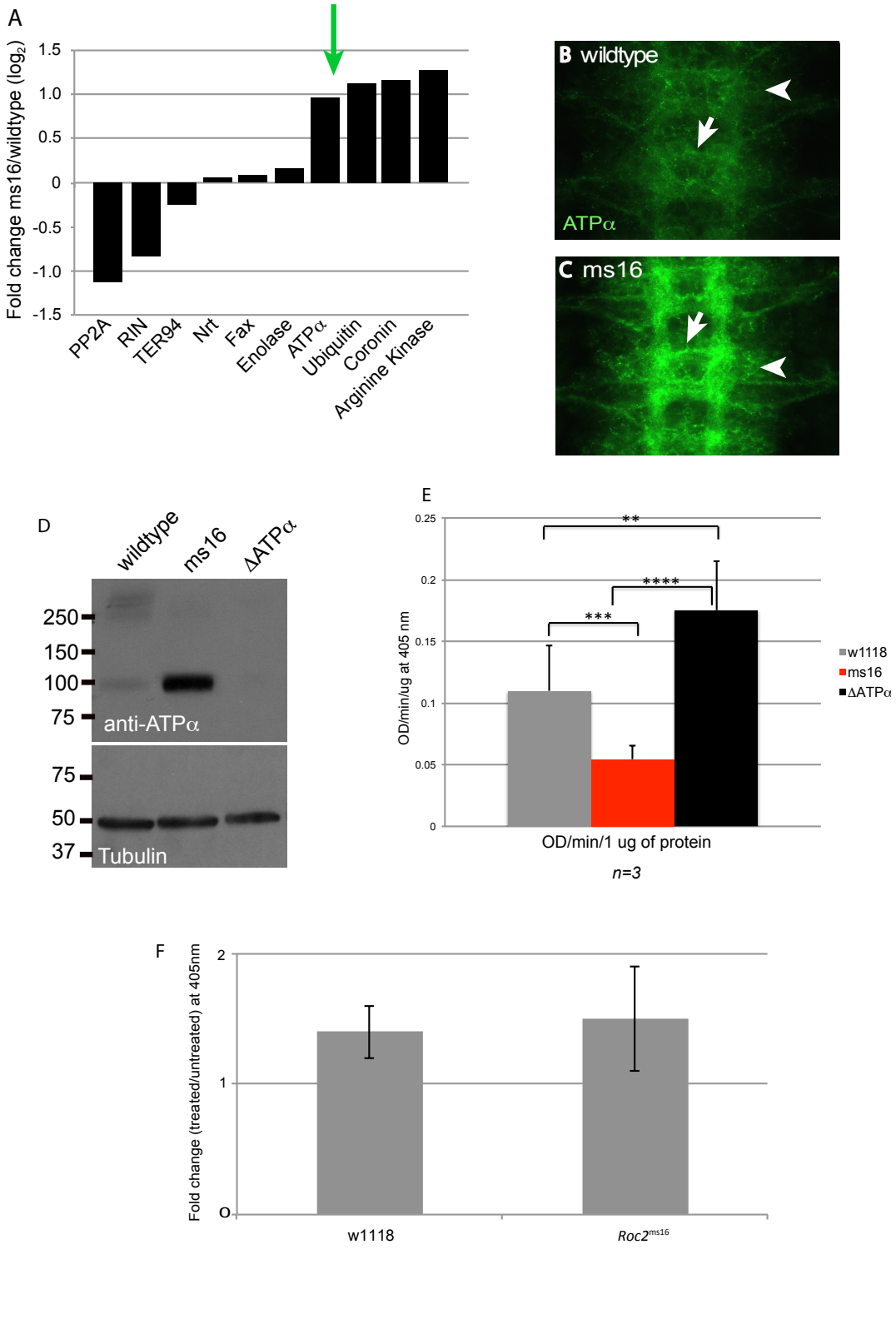
A
Fold change ms16/wildtype (log2)
1.5
1.0
0.5
0
-0.5
-1.0
-1.5
PP2A
RIN
TER94
Nrt
Fax
Enolase
ATPα
Ubiquitin
Coronin
Arginine Kinase
B wildtype
ATPα
C ms16
D
wildtype
ms16
ΔATPα
250
150
100
75
anti-ATPα
75
50
37
Tubulin
E
OD/min/ug at 405 nm
0.25
0.2
0.15
0.1
0.05
0
**
****
***
w1118
ms16
ΔATPα
OD/min/1 ug of protein
n=3
F
Fold change (treated/untreated) at 405nm
2
1
0
w1118
Roc2ms16

HRP- mutants are deficient in negative geotaxis

Tollo/Toll-8, Sff, and *Roc2*^{ms16} mutants are all deficient in negative geotaxis (Baas et al., 2011; Seppo et al., 2003); they are hesitant to climb up the side of their culture vials. This behavior has been quantified by measuring how long an adult mutant takes to climb a pre-designated height. Mutant adults were tested as homozygotes, heterozygotes (over a wild-type chromosome), and transheterozygotes. Adults that carry one copy of the mutation and a single copy of wild type chromosome act as wild type while transheterozygotes that have a single copy of *Roc2*^{ms16} in combination with sff are partially rescued. These effects are influenced by temperature. At 25 degrees, 90% of the wild type flies and heterozygotes in combination with wild type take less than 15 seconds to reach the top as compared to both homozygous *Roc2*^{ms16} and transheterozygotes in combination with sff **(Fig 2.8A)**. The median number (shown by arrows) of homozygous *Roc2*^{ms16} adults take approximately double (~30 seconds) the amount of time with about 50% of the flies still not reaching the top within the maximum time limit (2 minutes). Since sff and *Roc2*^{ms16} both have this defect, transheterozygotes were tested and as seen by the purple dots, these adults are partially rescued with the median amount of adults being able to reach the top within 15 seconds. The distribution of climbing times is also broader in the transheterozygotes. The incomplete rescue is consistent with an interaction between sff and the *Roc2*^{ms16} mutation. Just like in geotaxis, *Roc2*^{ms16} flies do have a decrease in viability as temperature increases (**Fig 2.8B**). We noticed that the mutants arrest at embryonic stages and do not develop into larvae as efficiently as wildtype. At 25 degrees, only about 60% of the embryos mature into adults, a phenotype which is exacerbated at 28 degrees when only 10% survive.

To assess the integrity of neuromuscular communication that might contribute to the locomotor defect, we visualized the glutamate receptor at the neuromuscular junction (GluRIII at the NMJ) of late 3rd instar larvae. We detected a continuum of GluRIII

expression that paralled the expression of ATPα but inversely mirrored expression of the HRP-epitope. Thus, NMJs of *Roc2*^{ms16} larvae exhibited the highest GluRIII expression, while NMJs of DATPα larvae exhibited reduced GluRIII expression (**Fig 2.8C**). This complements the known functions of ATPα in behavioral phenotypes (Schubiger et al., 1994).

In our previously described HRP mutant, *sff,* we found a significant decrease in bouton number and branching (Baas et al., 2011) of the NMJ however the structural integrity of the presynaptic neuron was unaffected in m16. This was done using Bruchpilot protein (Brp), which is a pre-synaptic protein needed for active zone development at the T-bars (Fouquet et al., 2009; Kittel et al., 2006; Wagh et al., 2006).

Figure 2.8: *Roc2*^{ms16} mutants are deficient in negative geotaxis, have reduced viability at increased temperatures and have altered neural muscular junctions (NMJ).
(A) Graph presenting the amount of time flies from each genotype take to climb up a predesigned vial. Each dot in this graph represents a single fly and the dashed arrows represent the mean amount of time taken for each genotype. For the mutants about 50% of the flies do not even make it to the top in the given time and the bracketed asterisk represents these. Populations and temperature at which flies were raised are indicated below. As seen by interaction data, transheterozygotes begin to get better but never fully rescue and heterozygote mutants behave like wildtype. (B) *Roc2*^{ms16} mutants show embryonic lethality at higher temperature (C&D) Magnified view of the neuromuscular junction between muscles 6 and 7, showing wildtype, homozygous mutant and heterozygous ATPα deletion dissected NMJs stained with DGluRIII showing an increase of the glutamate receptor when ATPα is increased and, conversely, a decrease of glutamate receptor when ATPα is decreased, as compared to wildtype third instar larvae.

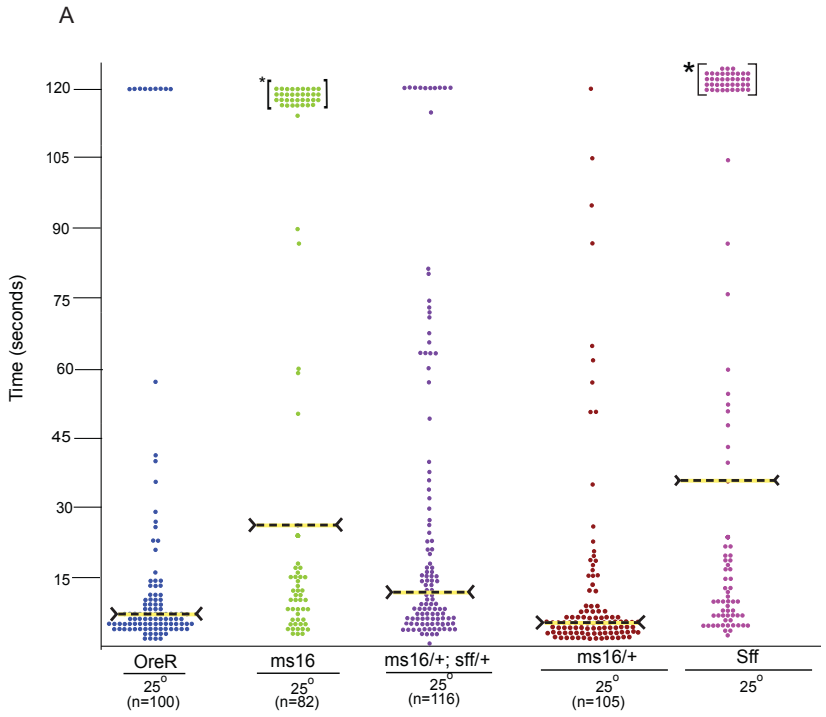

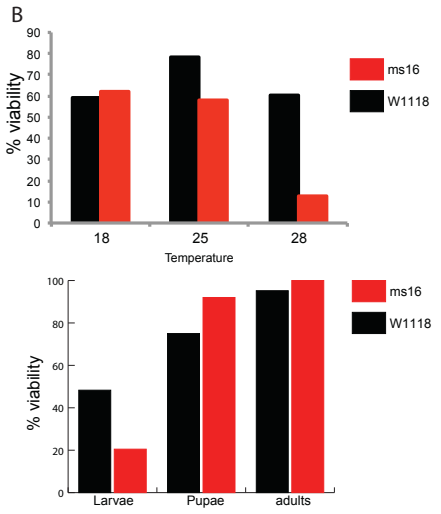
B
% viability
Temperature
18
25
28
ms16
W1118
% viability
Larvae
Pupae
adults
ms16
W1118

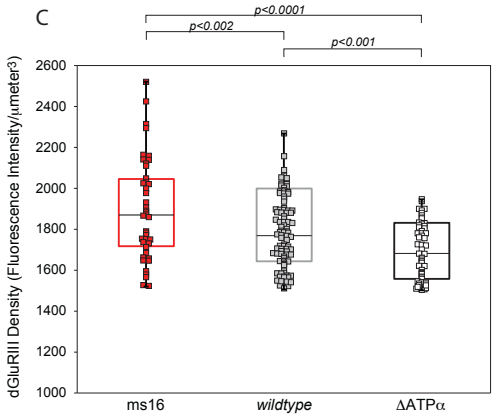
C
p<0.0001
p<0.002
p<0.001
dGluRIII Density (Fluorescence Intensity/µmeter³)
ms16
wildtype
ΔATPα

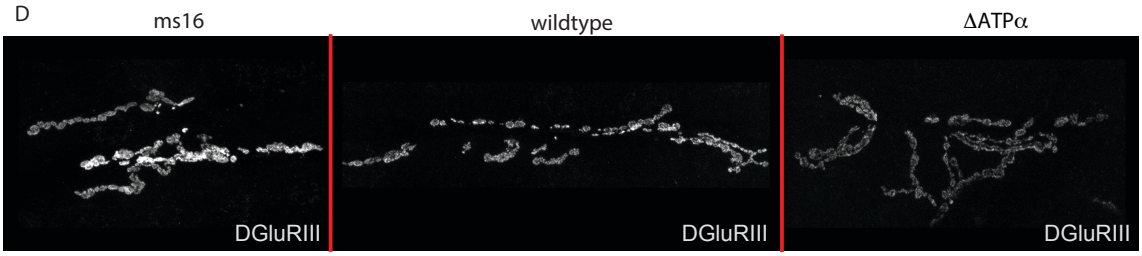
D
ms16
wildtype
ΔATPα
DGluRIII
DGluRIII
DGluRIII

Discussion

Tissue-specific protein glycosylation is a hallmark of developing and mature organisms and aberrant glycosylation in humans underlies a broad range of disorders, including muscular dystrophies, congenital disorders of glycosylation (human CDGs), immunodeficiency, and disorders associated with defects in protein maturation (α1-anti-trypsin deficiency); many of these glycophenotypes have been informatively modeled in mice and other model organisms (Moremen et al., 2012; Haltiwanger and Lowe, 2004; Varki, 1993; Freeze, 2002; Stowell et al., 2015; Parkinson et al., 2013; Bammens et al., 2015). To understand the molecular mechanisms that generate tissue-specific glycosylation, we have undertaken a long-term effort to screen for genes that impact neural-specific glycosylation in Drosophila. With this report, we have now identified three interacting genes that are essential for expression of neural-specific glycans, known as HRP-epitopes, in the Drosophila embryonic nervous system. Although HRP-epitopes have not been described in vertebrate species, the genes that we have recovered from our mutagenesis screens do have very clear functional homologues in vertebrates. We expect that the function of these genes in regulating neural-specific glycosylation will be conserved, although the specific glycan structures whose expression they regulate may differ across species.

Almost all of the human CDGs identified so far result from hypomorphic mutations in essential glycan biosynthetic or glycosylation regulatory genes (Freeze, 2002). Complete loss-of-function of these genes is generally incompatible with human and mouse embryonic development. This observation guided us in our choice to pursue an EMS-mutagenesis screen, since point mutations might yield hypomorphic alleles that support viability but reveal unknown functions of target proteins for regulating tissue-specific glycosylation. This supposition has been borne out in the case of the three mutations we have recovered; our characterized mutants in tollo/toll-8, sff/SAD, and roc2

are all hypomorphic alleles. Complete loss-of-function mutants in each of these genes results in severely compromised viability. Combined with the understanding of human CDG pathophysiology, it is increasingly clear that proteins responsible for regulating tissue-specific glycosylation may subserve other functions which impinge on organismal viability. Therefore, dissecting protein functions that modulate protein glycosylation from functions that underlie cellular viability can only be accomplished in the context of analyzing partial loss-of-function mutants, such as the *roc2*^{ms16} allele described here.

A striking result of these studies is the magnitude of the increase in ATPα expression compared to the relatively modest decrease in roc2 expression. This disparity indicates that ATPα protein stability must be a major target of roc2 activity in the wildtype nervous system. Decreased Roc2 abundance is associated with increased abundance of the Na+/K+-ATPase α-subunit (ATPα) in *Roc2*^{ms16} embryos. We also observed altered neural distribution in the axon, suggesting that the excess ATPα produced as a result of decreased ubiquitin ligase is mislocalized, which could result in altered membrane potential and Golgi dynamics. Decreased ATPα abundance is associated with increased HRP-epitope expression. Considered in conjunction with the decreased HRP-epitope expression observed when ATPα is increased (*Roc2*^{ms16}), we hypothesize that membrane depolarization and repolarization impacts glycoprotein glycosylation in excitable cells. This has been demonstrated before as changes in the ionic environment and activity regulates Golgi dynamics (Thayer et al., 2013). A corollary of this hypothesis is that excitable cells may utilize membrane depolarization as a controlling signal that maintains or modifies neural glycosylation.

Another consequence of altered homeostasis was seen at the NMJ. These results can be understood as a compensatory response of the muscle cell; overexpression of ATPα should dampen the duration of muscle cell depolarization in response to presynaptic glutamate release, perhaps triggering increased GluRIII

expression to compensate for decreased muscle cell depolarization. Conversely, decreased ATPα should result in enhanced muscle depolarization, driving the muscle cell to downregulate GluRIII. The specific molecular relationship between neurotransmitter receptor dynamics and HRP-epitope expression, if any, remains to be determined.

The sodium-potassium pump is a well-studied protein that is seen to play a role in not only ion pumping but is associated with several signaling proteins and is responsible for several known neurological defects (Palladino et al., 2003; Ashmore et al., 2009). The pump consists of two subunits, however most known functions involve the alpha subunit. Through western blot analysis, we also saw a small increase (~11%) of the beta-subunit, Nervana, which could be compensation for the increase in the alpha subunit. The beta subunit, Nervana is a HRP epitope carrying protein. While the main role of ATPα remains to maintain high K^+ levels and low Na^+ levels intracellularly, studies have indicated that multiple pathways control ATPα activity including PKA, PKC and Src tyrosine kinase protein phosphorylation (Borghini et al., 1994; Beguin et al., 1994; Wang and Yu, 2005); these kinases have also been implicated in Golgi dynamics. An example of this is that increased activity of Src Kinases causes Golgi fragmentation (Bard et al., 2003). The opposite effect could be seen in our mutant where the presence of too much ATPα gives rise to inactivated Src and the lack of proper Golgi polarization (**Fig 2.9**).

Accordingly, another requirement for proper ATPα function is hydrolysis of ATP. With an increase of ATPα in our mutants, the amount of ATP expenditure in the neuron also increases, which may lead to an increase of AMP and thereby affecting ATP homeostasis. The constant shift from ATP to AMP can be stressful on cells, especially the Golgi of excitable cells; an impact of this would be on protein trafficking and ultimately glycosylation. An increase in AMP levels could also have downstream consequences on the activity of kinases like AMP-activated Kinases (AMPK), which

further regulates the action of several different proteins and enzymes as well as Golgi assembly (**Fig 2.9**). Sugar free frosting (*sff*), one of the other HRP epitope mutants that came out of our screen, is a Ser/Thr kinase previously shown to affect neuromuscular junction morphology (NMJ) and neural polarity in *C.elegans* (Baas et al., 2011) and resembles most closely the family of AMP-kinases. This would suggest that in the presence of increased ATPα, the increase in AMP could accelerate the activity of sff in the mutant as well. Additionally, *sff* is also activated and inhibited by the activity of other kinases including, Akt/Protein Kinase B which could potentially be affected by the activity of ATPα.

A change in a single ubiquitin ligase can alter levels of several different proteins. Our proteomics results indicate that a change in Roc2 leads to modifications in proteins involving a multitude of pathways including kinases, actin binding proteins, phosphatases, etc. This study focuses on a single target found through our results but doesn't explain the entirety of phenotypes we see in our mutants, so we do not rule out that other proteins could be contributing to the phenotypes. These additional targets will also be investigated to assess their role in glycosylation.

The mechanisms that control tissue specific glycosylation are largely unknown and our studies reveal a new role for an E3 ubiquitin ligase as well as a sodium potassium ATPase in trafficking, especially in the secretory pathway and, ultimately in glycosylation. Investigating the ionic environment required for the secretory pathway is an area that is not well studied and its importance is highlighted in this report. As our model demonstrates, a modest decrease in Roc2, an E3 ubiquitin ligase significantly increases the levels of Na+/K+ ATPase in the mutant. Membrane depolarization is a consequence of this increase, which ultimately alters Golgi architecture and therefore trafficking through the Golgi by altering enzyme distribution and accessibility of glycosyltransferases like FucTA, Fdl and GnT's, essential for keeping glycan balance.

Another hypothesis is that with the expansion of the cis-Golgi, its possible to change access to substrate as now the enzymes and donors (like GDP-fuc) are more diluted as compared to wildtype (**Fig 2.9**). This leads to an increased amount of cargo that shifts toward complexity, however don't get α1,3 linked-fucosylated. At the synapse, an increase of ATPα causes a shorter membrane transient time, which consequently requires the post-synaptic muscle cells to make more glutamate receptor. Ultimately, this has led us to try to understand how the function of a pump might regulate glycan processing and add a broader function in Golgi regulation and glycosylation to the already known functions.

Figure 2.9: Golgi architecture and overall glycosylation is altered in the mutant. (A) Our model suggests a change in Golgi architecture is the consequence of altered kinase functions that associate with ATPα at the membrane as well as a possible decrease of Roc2. (B) The outcome of altered Golgi architecture is a shift in glycosylation due to changes in enzyme accessibility.

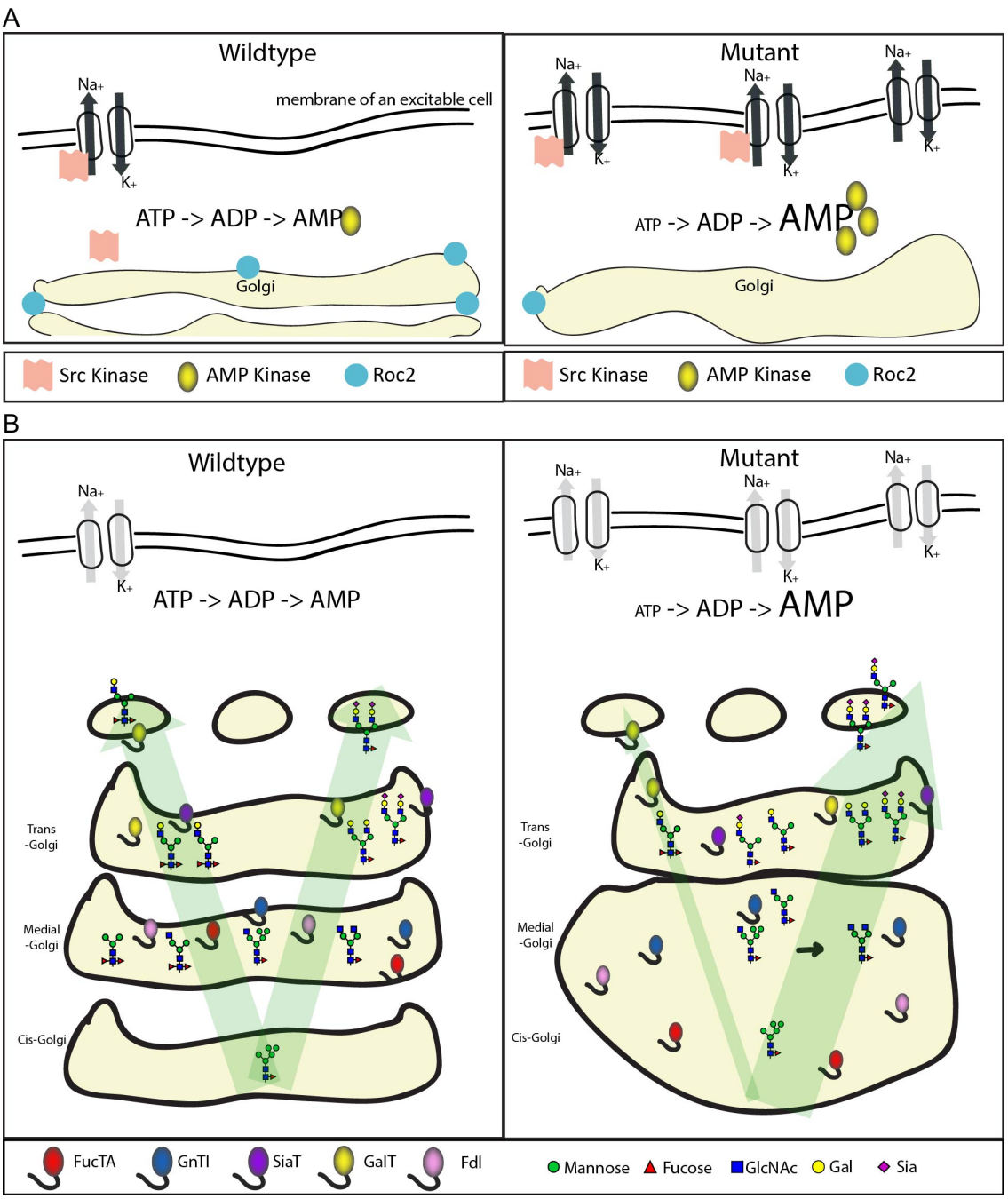

References

Aoki, K., Perlman, M., Lim, J. M., Cantu, R., Wells, L. & Tiemeyer, M. 2007. Dynamic developmental elaboration of N-linked glycan complexity in the Drosophila melanogaster embryo. *J Biol Chem,* 282(12)**,** pp 9127-42.

Ashmore, L. J., Hrizo, S. L., Paul, S. M., Van Voorhies, W. A., Beitel, G. J. & Palladino, M. J. 2009. Novel mutations affecting the Na, K ATPase alpha model complex neurological diseases and implicate the sodium pump in increased longevity. *Hum Genet,* 126(3)**,** pp 431-47.

Baas, S., Sharrow, M., Kotu, V., Middleton, M., Nguyen, K., Flanagan-Steet, H., Aoki, K. & Tiemeyer, M. 2011. Sugar-free frosting, a homolog of SAD kinase, drives neural-specific glycan expression in the Drosophila embryo. *Development,* 138(3)**,** pp 553-63.

Bammens, R., Mehta, N., Race, V., Foulquier, F., Jaeken, J., Tiemeyer, M., Steet, R., Matthijs, G. & Flanagan-Steet, H. 2015. Abnormal cartilage development and altered N-glycosylation in Tmem165-deficient zebrafish mirrors the phenotypes associated with TMEM165-CDG. *Glycobiology,* 25(6)**,** pp 669-82.

Bard, F., Mazelin, L., Péchoux-Longin, C., Malhotra, V. & Jurdic, P. 2003. Src regulates Golgi structure and KDEL receptor-dependent retrograde transport to the endoplasmic reticulum. *J Biol Chem,* 278(47)**,** pp 46601-6.

Beguin, P., Beggah, A. T., Chibalin, A. V., Burgener-Kairuz, P., Jaisser, F., Mathews, P. M., Rossier, B. C., Cotecchia, S. & Geering, K. 1994. Phosphorylation of the Na,K-ATPase alpha-subunit by protein kinase A and C in vitro and in intact cells. Identification of a novel motif for PKC-mediated phosphorylation. *J Biol Chem,* 269(39)**,** pp 24437-45.

Blagburn, J. M. 2008. Engrailed expression in subsets of adult Drosophila sensory neurons: an enhancer-trap study. *Invert Neurosci,* 8(3)**,** pp 133-46.

Borghini, I., Geering, K., Gjinovci, A., Wollheim, C. B. & Pralong, W. F. 1994. In vivo phosphorylation of the Na,K-ATPase alpha subunit in sciatic nerves of control and diabetic rats: effects of protein kinase modulators. *Proc Natl Acad Sci U S A,* 91(13)**,** pp 6211-5.

Brent, J., Werner, K. & McCabe, B. D. 2009. Drosophila larval NMJ immunohistochemistry. *J Vis Exp,* 25)**,** pp.

Cherniavsky-Lev, M., Golani, O., Karlish, S. J. & Garty, H. 2014. Ouabain-induced internalization and lysosomal degradation of the Na+/K+-ATPase. *J Biol Chem,* 289(2)**,** pp 1049-59.

Fouquet, W., Owald, D., Wichmann, C., Mertel, S., Depner, H., Dyba, M., Hallermann, S., Kittel, R. J., Eimer, S. & Sigrist, S. J. 2009. Maturation of active zone assembly by Drosophila Bruchpilot. *J Cell Biol,* 186(1)**,** pp 129-45.

Franco, M., Seyfried, N. T., Brand, A. H., Peng, J. & Mayor, U. 2011. A novel strategy to isolate ubiquitin conjugates reveals wide role for ubiquitination during neural development. *Mol Cell Proteomics,* 10(5)**,** pp M110.002188.

Freeze, H. H. 2002. Human disorders in N-glycosylation and animal models. *Biochim Biophys Acta,* 1573(3)**,** pp 388-93.

Geisler, C., Kotu, V., Sharrow, M., Rendić, D., Pöltl, G., Tiemeyer, M., Wilson, I. B. & Jarvis, D. L. 2012. The Drosophila neurally altered carbohydrate mutant has a defective Golgi GDP-fucose transporter. *J Biol Chem,* 287(35)**,** pp 29599-609.

Haltiwanger, R. S. & Lowe, J. B. 2004. Role of glycosylation in development. *Annu Rev Biochem,* 73(491-537.

Ioffe, E. & Stanley, P. 1994. Mice lacking N-acetylglucosaminyltransferase I activity die at mid-gestation, revealing an essential role for complex or hybrid N-linked carbohydrates. *Proc Natl Acad Sci U S A,* 91(2)**,** pp 728-32.

Jan, L. Y. & Jan, Y. N. 1982. Antibodies to horseradish peroxidase as specific neuronal markers in Drosophila and in grasshopper embryos. *Proc Natl Acad Sci U S A,* 79(8)**,** pp 2700-4.

Katz, F., Moats, W. & Jan, Y. N. 1988. A carbohydrate epitope expressed uniquely on the cell surface of Drosophila neurons is altered in the mutant nac (neurally altered carbohydrate). *EMBO J,* 7(11)**,** pp 3471-7.

Kaufmann, N., DeProto, J., Ranjan, R., Wan, H. & Van Vactor, D. 2002. Drosophila liprin-alpha and the receptor phosphatase Dlar control synapse morphogenesis. *Neuron,* 34(1)**,** pp 27-38.

Kittel, R. J., Wichmann, C., Rasse, T. M., Fouquet, W., Schmidt, M., Schmid, A., Wagh, D. A., Pawlu, C., Kellner, R. R., Willig, K. I., Hell, S. W., Buchner, E., Heckmann, M. & Sigrist, S. J. 2006. Bruchpilot promotes active zone assembly, Ca2+ channel clustering, and vesicle release. *Science,* 312(5776)**,** pp 1051-4.

Kopczynski, C. C., Davis, G. W. & Goodman, C. S. 1996. A neural tetraspanin, encoded by late bloomer, that facilitates synapse formation. *Science,* 271(5257)**,** pp 1867-70.

Kulikov, A., Eva, A., Kirch, U., Boldyrev, A. & Scheiner-Bobis, G. 2007. Ouabain activates signaling pathways associated with cell death in human neuroblastoma. *Biochim Biophys Acta,* 1768(7)**,** pp 1691-702.

Lim, J. M., Sherling, D., Teo, C. F., Hausman, D. B., Lin, D. & Wells, L. 2008. Defining the regulated secreted proteome of rodent adipocytes upon the induction of insulin resistance. *J Proteome Res,* 7(3)**,** pp 1251-63.

Marrus, S. B., Portman, S. L., Allen, M. J., Moffat, K. G. & DiAntonio, A. 2004. Differential localization of glutamate receptor subunits at the Drosophila neuromuscular junction. *J Neurosci,* 24(6)**,** pp 1406-15.

Moremen, K. W., Tiemeyer, M. & Nairn, A. V. 2012. Vertebrate protein glycosylation: diversity, synthesis and function. *Nat Rev Mol Cell Biol,* 13(7)**,** pp 448-62.

Nairn, A. V., Kinoshita-Toyoda, A., Toyoda, H., Xie, J., Harris, K., Dalton, S., Kulik, M., Pierce, J. M., Toida, T., Moremen, K. W. & Linhardt, R. J. 2007. Glycomics of

proteoglycan biosynthesis in murine embryonic stem cell differentiation. *J Proteome Res,* 6(11)**,** pp 4374-87.

Nakamura, N., Rabouille, C., Watson, R., Nilsson, T., Hui, N., Slusarewicz, P., Kreis, T. E. & Warren, G. 1995. Characterization of a cis-Golgi matrix protein, GM130. *J Cell Biol,* 131(6 Pt 2)**,** pp 1715-26.

Palladino, M. J., Bower, J. E., Kreber, R. & Ganetzky, B. 2003. Neural dysfunction and neurodegeneration in Drosophila Na+/K+ ATPase alpha subunit mutants. *J Neurosci,* 23(4)**,** pp 1276-86.

Parkinson, W., Dear, M. L., Rushton, E. & Broadie, K. 2013. N-glycosylation requirements in neuromuscular synaptogenesis. *Development,* 140(24)**,** pp 4970-81.

Paschinger, K., Rendic, D. & Wilson, I. B. 2009. Revealing the anti-HRP epitope in Drosophila and Caenorhabditis. *Glycoconj J,* 26(3)**,** pp 385-95.

Patel, N. H. 1994. Imaging neuronal subsets and other cell types in whole-mount Drosophila embryos and larvae using antibody probes. *Methods Cell Biol,* 44(445-87.

Rendic, D., Sharrow, M., Katoh, T., Overcarsh, B., Nguyen, K., Kapurch, J., Aoki, K., Wilson, I. B. & Tiemeyer, M. 2010. Neural-specific alpha3-fucosylation of N-linked glycans in the Drosophila embryo requires fucosyltransferase A and influences developmental signaling associated with O-glycosylation. *Glycobiology,* 20(11)**,** pp 1353-65.

Schubiger, M., Feng, Y., Fambrough, D. M. & Palka, J. 1994. A mutation of the Drosophila sodium pump alpha subunit gene results in bang-sensitive paralysis. *Neuron,* 12(2)**,** pp 373-81.

Seppo, A., Matani, P., Sharrow, M. & Tiemeyer, M. 2003. Induction of neuron-specific glycosylation by Tollo/Toll-8, a Drosophila Toll-like receptor expressed in non-neural cells. *Development,* 130(7)**,** pp 1439-48.

Snow, P. M., Patel, N. H., Harrelson, A. L. & Goodman, C. S. 1987. Neural-specific carbohydrate moiety shared by many surface glycoproteins in Drosophila and grasshopper embryos. *J Neurosci,* 7(12)**,** pp 4137-44.

Stowell, S. R., Ju, T. & Cummings, R. D. 2015. Protein glycosylation in cancer. *Annu Rev Pathol,* 10(473-510.

Thayer, D. A., Jan, Y. N. & Jan, L. Y. 2013. Increased neuronal activity fragments the Golgi complex. *Proc Natl Acad Sci U S A,* 110(4)**,** pp 1482-7.

Varki, A. 1993. Biological roles of oligosaccharides: all of the theories are correct. *Glycobiology,* 3(2)**,** pp 97-130.

Wagh, D. A., Rasse, T. M., Asan, E., Hofbauer, A., Schwenkert, I., Durrbeck, H., Buchner, S., Dabauvalle, M. C., Schmidt, M., Qin, G., Wichmann, C., Kittel, R., Sigrist, S. J. & Buchner, E. 2006. Bruchpilot, a protein with homology to ELKS/CAST, is required

for structural integrity and function of synaptic active zones in Drosophila. *Neuron,* 49(6)**,** pp 833-44.

Wang, X. Q. & Yu, S. P. 2005. Novel regulation of Na, K-ATPase by Src tyrosine kinases in cortical neurons. *J Neurochem,* 93(6)**,** pp 1515-23.

CHAPTER 3

MASS SPECTROMETRIC QUANTIFICATION OF N-LINKED GLYCANS BY REFERENCE TO EXTERNAL STANDARDS[1]

[1]Nickita Mehta, Mindy Porterfield, Weston Struwe, Christian Heiss, Parastoo Azadi, Pauline Rudd, Michael Tiemeyer, and Kazuhiro Aoki. Submitted to *JPR*, 02/14/2016.

Abstract

Environmental, signaling, and metabolic processes shape the profile of glycoprotein glycans expressed by cells, whether in culture, in developing tissues, or in mature organisms. Quantitative characterization of the glycomic changes associated with these conditions has been achieved historically and most effectively by reductive coupling of oligosaccharides to various fluorophores following release from glycoprotein and subsequent HPLC or capillary electrophoretic separation with fluorescence detection. These labeling/HPLC-based approaches provide a robust means of quantifying absolute glycan amount based on fluorescence yield. Mass spectrometry, on the other hand, has generally been limited to relative quantification, in which the contribution of the detected signal intensity for an individual glycan is expressed as a percent of the signal intensity summed over the total glycan profile. Relative quantification by MS has been valuable for highlighting changes in glycan expression between samples because sensitivity is very high and structural information for unknown glycans can be derived by systematic fragmentation. We have investigated whether MS-based glycomics is amenable to absolute quantification by referencing signal intensities of full MS profiles to well-characterized oligosaccharide standards. Here, we report the qualification of a select group of N-linked oligosaccharide standards by NMR, HPLC, and MS. We also demonstrate the dynamic range, sensitivity, and recovery from complex sample matrices for these standards in their permethylated form. Our results indicate that absolute quantification of permethylated glycans is achievable for MS-based glycomic analysis.

KEYWORDS: quantification, N-glycan, permethylation, standard, mass spectrometry

Introduction

The complete characterization of glycans isolated from biological materials requires multiple, complementary analytical approaches. The techniques available currently each possess their own characteristic benefits and limitations. The most structurally informative technique, NMR, requires amounts of material that are frequently not available from biological samples. Other more sensitive methods, such as HPLC (with amperometric or fluorescence detection), gel electrophoresis, capillary electrophoresis (CE), and mass spectrometry (MS), are frequently coupled with orthogonal techniques, such as methylation/linkage analysis, exoglycosidase digestion, or affinity chromatography to characterize glycan structures released from samples at the scale usually encountered in glycomics experiments (Cummings and Pierce, 2014; Geyer and Geyer, 2006; Ito et al., 2015). Among these approaches, HPLC or CE coupled to fluorescence detection of tagged glycans possesses the significant advantage that glycan quantification can be achieved by referencing unknown peak heights to a known amount of a tagged standard (Bigge et al., 1995; Guile et al., 1996; Huffman et al., 2014; Knezevic et al., 2011; Nagels et al., 2011; Novotny and Sudor, 1993; Takahashi et al., 1995; Wada et al., 2007). Since fluorescence yield is independent of the glycan structure, a single standard compound is sufficient to quantify all detectable glycans in a sample profile. For tagged glycans, structural characteristics can be further assigned based on exoglycosidase sequencing and on chromatographic retention relative to known standards (Royle et al., 2006).

Due to its sensitivity and speed, as well as to the rich structural data obtained by tandem approaches (MS/MS and MSn), mass spectrometry is becoming one of the most broadly employed technologies for glycomic analysis of biological materials (Ashline et al., 2005; Dell and Morris, 2001; Hamouda et al., 2014; Hu and Mechref, 2012; Jang-Lee et al., 2006; Lapadula et al., 2005; Leymarie et al., 2013; Parker et al., 2013; Walther et

al., 2013; Yamada et al., 2010; Zhang et al., 2005; Aoki et al., 2007; Aoki et al., 2008). However, quantification of glycans by MS remains largely underdeveloped. Significant questions remain unanswered regarding whether and under what conditions mass spectral signals can be used to quantify absolute amounts of glycan structures. Currently, the predominant practice is for individual components of glycan profiles generated by MS to be quantified relative to each other. This calculation describes each glycan as a percent of the total signal summed across the whole spectrum. While this normalized parameter has been broadly useful for comparing major changes in profiles across samples or biological conditions, its value for characterizing minor glycans is frequently subject to the undue influence of the major components; teasing apart the impact of variability in numerator and denominator quantification can be difficult for low abundance (but biologically significant) glycans. Generating methods for absolute quantification by MS would allow profile changes to be assessed glycan-by-glycan, independent of variations in the whole profile. A set of well-characterized oligosaccharide standards with demonstrated robustness for quantification of glycans in biological materials is essential to realize this potential.

Underivatized glycans are hydrophilic; their chemistries are dominated by the spatial distribution of hydroxyl, acetamido, and carboxyl moieties. Therefore, the response factors for native glycans in mass spectrometers, which are driven largely by ionization efficiency, vary in proportion to the content of these polar determinants. Permethylation neutralizes these differences, enhancing desolvation and ionization efficiency. Although never rigorously tested, published data has suggested that molar responses for permethylated glycans may be relatively uniform (Aoki et al., 2007; Mechref et al., 2009; Yu et al., 2009). If true, quantification of MS signals derived from permethylated glycans could be achieved by reference to a single standard or a small set of standards. The aim of this study was to assess the validity of the proposition that

permethylation makes it possible to quantify the profile of N-linked glycans in biological materials by reference to a permethylated standard or set of standards. To that end, we have investigated linearity of quantification and recovery from biological matrix using permethylated glycan standards. We also compare quantification across analytic platforms (^{1}H-NMR, nanospray-iontrap/MS, MALDI-TOF/MS, HPLC with fluorescence detection) in order to qualify glycan standards for use as quantification standards.

Experimental Procedure

Materials and Reagents.

PNGaseF (N-glycanase) was obtained from Prozyme (San Leandro, CA). N-glycan standards were obtained from the Consortium for Functional Glycomics (CFG) and from The Scripps Research Institute (Jim Paulson). Sodium hydroxide (50%) was purchased from Fisher Scientific. Sep-Pak C18 disposable extraction columns were obtained from Waters Corporation (Milford, MA, USA). Malto-series oligosaccharides, trypsin, bovine pancreatic ribonuclease B (RNaseB) and all other chemicals reagents were purchased from Sigma-Aldrich (St Louis, MO, USA). Malto-series oligosaccharides were also obtained from Wako Chemicals (Richmond, VA) and Cosmo Bio USA (Carlsbad, CA).

Analytical platforms.

Analytic platforms representative of the major instrumentations currently in use for glycomic analysis were used to analyze glycan standards. Mass spectra were obtained by MALDI-TOF using a Bruker Microflex LRP operating in reflectron mode and by nanospray ionization using a Thermo Fisher LTQ/Orbitrap. Tandem mass spectrometry (MSn) was also performed by NSI-LTQ/Orbitrap. HPLC analysis of fluorescent labeled glycan standards was performed as previously described, using normal phase separations on a TSK-amide-80 column with a 2695 Alliance separations

module and 2475 fluorescence detector (Waters, Milford, MA) (Olajos et al., 2008; Royle et al., 2006). ^{1}H-NMR spectra were acquired on a Varian Inova 600 MHz spectrometer.

Permethylation

All glycan standards and samples were permethylated prior to MS analysis according to the method of Anumula and Taylor (Anumula and Taylor, 1992). Malto-series oligosaccharide standards were permethylated with ^{12}C-, ^{13}C- or deuterated methyliodide (^{12}C-MeI, ^{13}C-MeI, or $^{12}CD_3I$).

Glycan Mass Spectrometry.

Permethylated glycan samples and standards were analyzed on MALDI-TOF/MS and NSI-MS platforms. For MALDI analysis, permethylated glycans were analyzed in positive ion mode using α-dihyroxybenzoic acid (DHBA, 20mg/mL solution in 50% methanol:water) as matrix (Aoki et al., 2007). For nanospray ion trap analysis, infusion and ionization conditions were optimized across three isotopic variants (^{12}C-MeI, ^{13}C-MeI, or $^{12}CD_3I$) of permethylated, equimolar mixtures of malto-series oligosaccharides (maltotetraose, maltopentaose, maltohexaose and maltoheptaose) by comparing the signal intensities achieved in three different infusion buffers: 1mM NaOH in 50% methanol, in 50% 2-propanol, and in a mixture of 50% 2-propanol and 50% methanol (1:1, v/v). Maximum signal intensities were achieved by reconstitution and infusion of glycans in 50% methanol containing 1 mM NaOH using a nanospray source at a syringe flow rate of 0.40 µL/min and capillary temperature set to 210°C (Aoki et al., 2007). The instrument was tuned with permethylated oligosaccharide standards in positive ion mode. For fragmentation by collision-induced dissociation (CID) in MS/MS, normalized collision energy of 30% was applied. Most permethylated glycan components were identified as singly, doubly, and triply charged, sodiated species [M+Na] in positive mode. Peaks for all charge states were deconvoluted by charge state and summed for

quantification using the Xtract functionality of the Xcalibur software package version 2.0 (Thermo Fisher Scientific) as previously described (Porterfield et al., 2014).

Analysis of glycan standards

Two N-linked glycan standards (standard 107 and 108) were received from the Consortium for Functional Glycomics (CFG) and an additional N-linked glycan standard (standard 121) was received as a gift from Jim Paulson, The Scripps Research Institute (**Table 3.1**). Standards 107, 108, and 121 were resuspended in water, dispensed nominally into 2.5 nmol aliquots based on the previous characterization of the supplier. Following drying by vacuum centrifugation, the N-glycan standard aliquots were stored frozen at -80 ^{o}C. Aliquots of the N-linked standards were subjected to reductive labeling with 2-aminobenzamide (2-AB) and subsequently analyzed by HPLC coupled to fluorescence detection as previously described (Olajos et al., 2008; Royle et al., 2006). The structures of the labeled N-linked standards were validated by exoglycosidase sequencing with HPLC and fluorescence detection (Royle et al., 2006) and by NMR (Lu and van Halbeek, 1996). For NMR analysis N-linked glycan standards were deuterium exchanged by dissolving in D_2O and lyophilization. Dried samples were resuspended in 80 ml D_2O and 5 ml of 1% acetone in D_2O was added as internal reference. The samples were placed in 3 mm Shigemi NMR tubes and 1-D Proton, TOCSY and NOESY NMR spectra, run with water presaturation, and gradient enhanced COSY and HSQC spectra were acquired on a Varian Inova-600 MHz spectrometer at 25 ^{o}C. Chemical shifts were measured relative to internal acetone (d_H=2.218 ppm, d_C=33.00 ppm). Standard Varian acquisition parameters were used (**Appendix Table S1**). Malto-series oligosaccharide standards were dessicated under vacuum, quantitatively weighed, and dissolved in water to produce stock solutions at 1 mM. The stock solutions were distributed into 10 mmol aliquots and re-dried by vacuum centrifugation before being stored at -80 ^{o}C. Mixures of malto-series oligosaccharide standards containing various

combinations of maltotri-, tetra, penta, hexa, and hepta-oligosaccharide (dp3, dp4, dp5, dp6, and dp7, respectively) were permethylated and analyzed by NSI-LTQ/Orbitrap MS and MALDI-TOF MS. The malto-series mixtures were also analyzed by fluorescence detection as 2-AB derivatives following HPLC separation.

Quantification of glycans released from a well-characterized glycoprotein, RNaseB.

N-linked glycans were released from 1 mg of RNaseB glycoprotein (80% purity) by two approaches: 1) glycopeptides were enriched following tryptic digestion of RNaseB by Sep-Pak C18 cartridge chromatography and the glycans were then released by PNGaseF treatment (18 h at 37 °C), or 2) N-glycans were released by PNGaseF treatment (18 h at 37 °C) of denatured but undigested RNaseB (Aoki et al., 2007; Tarentino and Plummer, 1994). For both approaches, released N-glycans were cleaned-up by passage over Sep-Pak C18 and permethylated prior to MS analysis. Permethylated RNaseB glycans were analyzed by NSI-LTQ/Orbitrap MS and quantified relative to a known amount of maltotetraose (10 pmol of dp4) that was permethylated with heavy methyliodine (^{13}C-MeI) and spiked into the sample prior to infusion.

Recovery of glycan standards from biological matices.

To assess the effect of biological matrices on detection and quantification, permethylated standards were spiked into two different biological samples. First, a mixture of N-glycan standards permethylated with ^{12}C-MeI was added to N-glycans prepared from glycoproteins harvested from Drosophila melanogaster embryos (Aoki et al., 2007). The mixture of N-glycan standards and the Drosophila glycans were each analyzed separately and as a mixture. The N-glycan standards were prepared as an equimolar mixture at a known concentration and were added to the Drosophila glycans to yield standard peak heights comparable in magnitude to the major Drosophila structures. Matrix interference was assessed by calculating standard recovery. Second,

a similar experiment was performed using mouse brain N-glycans. Glycoproteins were extracted from the frontal cortex of a single wildtype mouse by the same method used to prepare Drosophila embryo glycoproteins (Aoki et al., 2007). Using this procedure, 51 mg of protein-enriched solids were harvested from 286 mg wet weight of brain and 3 mg aliquots of the solids were used for N-glycan preparation and analysis. For quantification of mouse brain N-glycans, N-glycan standards and malto-series glycans were permethylated with ^{13}C-MeI and mixed together at known concentrations before being spiked into mouse brain glycans that had been permethylated with ^{12}C-MeI prior to analysis. Matrix interference was assessed by calculating standard recovery and endogenous mouse brain glycans were quantified relative to each of the spiked standards.

Results and Discussion

Availability of glycan standards.

Ideally, a set of well-characterized N-linked glycan standards, obtainable in reasonable amounts and representative of the full range of biologically relevant glycan complexities, would be available for use as quantification standards. Additionally, candidate standards would be most useful if they possessed a free, underivatized reducing end. This preference reflects the broad practice in glycomic analysis of using PNGaseF to release N-linked glycans from glycoproteins, an enzyme that removes the glycan *en bloc*, generating a glycan with an intact reducing end. While a growing number of commercial and academic sources offer synthetic or purified N-linked glycans in small quantities (less than 10 mg), full qualification of these glycans would significantly deplete the available material. Therefore, we chose to pursue standards that we could acquire in larger quantities. One useful source was the Consortium for Functional Glycomics (CFG), which maintains a reagent bank of oligosaccharides for use by investigators (http://www.functionalglycomics.org). Most of these oligosaccharides carry linker arms on their reducing end for immobilization on surfaces (Bohorov et al., 2006). Some, however, are available with free reducing ends (**Table 3.1**). CFG standards 107 and 108 were made available to us in 100 mg amounts. Our interaction with the CFG also facilitated the acquisition of 9 mg of standard 121, a sialylated complex glycan (courtesy of James Paulson, The Scripps Research Institute). We also acquired a larger amount (> 100 mg each) of defined maltose oligosaccharide polymers (Sigma, Wako, and Cosmo Bio) comprising a linear series of size standards from 3 hexoses to 7 hexoses in length. We refer to the malto-series oligosaccharides by their degree of polymerization (dp number, dp3-dp7).

Table 3.1: N-glycan and malto-series oligosaccharide standards for glycan modification.

Standard Identifier	Trivial Name	Structure	Amount Obtained	Native Mass	Permethylated Mass $(m+Na)^+$
107	NGA2B or A2(2,2)B	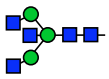	9 mg	1519.56	1906.96[a]
108	NGA3B(1-4) or A3(2,4,2)B	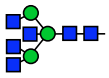	100 mg	1722.64	2152.09
121	A2G2S(6)2	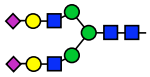	100 mg	2222.78	2792.38
dp3	maltotriose		not limited	504.17	681.33
dp4	maltotetraose		not limited	666.22	885.43
dp5	maltopentaose	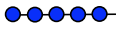	not limited	828.27	1089.53
dp6	maltohexaose	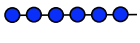	not limited	990.33	1293.63
dp7	maltoheptaose	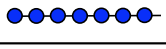	not limited	1152.38	1497.73

[a]Mass of glycan as singly-charged sodium adduct permethylated with ^{12}C-MeI

Qualification of glycan standards.

The N-linked glycan standards 107, 108, and 121 (107-121) were assessed for purity and quantity by several approaches. Each standard was subjected to 1-D and 2-D Proton NMR for verification of linkage and anomericity, mass spectrometry (MALDI-TOF and NSI-LTQ/Orbitrap MS) for confirmation of expected mass, and HPLC with reductive labeling for purity by mass. 1-D and 2-D proton NMR of standards 107-121 yielded carbon glycosylation shifts and NOE contacts in agreement with the structures presented in Table 1 (**Appendix Tables S1-S5**). Sequential exoglycosidase sequencing coupled to HPLC separation of 2-AB labeled standards 107-121 were also consistent with the proposed structures (**Appendix Figures S1-S3**). Each of the N-linked glycan standards exhibited a predominant species (ranging between 74-83% of the total signal intensity by NSI-MS, 68-93% by MALDI-TOF, and 62-93% by HPLC) and an additional minor species corresponding to the absence of one or more non-reducing terminal residues (**Appendix Figures S1 – S5 and Appendix Table S6**). The heterogeneity in the standards was comparable across all platforms (MALDI- and NSI-MS, HPLC, NMR), indicating that it likely reflects the chemical nature of the standard and not an artifact of the analytic approach (**Fig 3.1A**). Disassembly of the N-glycan standards 107, 108, and 121 by NSI-LTQ/Orbitrap MS/MS and MSn yielded fragmentation patterns consistent with the expected structures (**Appendix Figure S6**).

To assess the purity of standards 107-121, known amounts of malto-series oligosaccharides (dp3-dp7) were quantitatively labeled with 2-AB and analyzed by HPLC coupled to fluorescence detection. Molar response factors were generated for each malto-series standard from the resulting data (**Appendix Figure S7**). The 5 malto-series standards gave nearly identical results, from which a mean molar response factor was calculated (**Appendix Table S6**). Fluorescence signals for HPLC-resolved 107-121 were converted to stock concentrations by referencing the detected signal for all glycan

peaks to the average malto-series molar response factor and the mass purity of each N-glycan standard was subsequently calculated relative to the mass of the original stock aliquot. Stock concentrations for 107-121 were also independently calculated from NMR data by referencing standard signals to the known amount of acetone added as internal reference. The two methods, HPLC coupled to fluorescence detection and NMR referenced to internal standard, gave mass purity and stock concentrations in good agreement (**Fig 3.1B and Appendix Table S6**). The consistency of the observed molar response factors for each of the malto-series oligosaccharides and the reproducibility of the stock concentrations measured for standards 107-121 provided a basis for investigating the usefulness of these compounds as mass spectrometry quantification standards.

Linearity of MS and MS/MS responses.

All three N-linked glycan standards gave well-behaved MS responses upon dilution. Linear standard curves were obtained for each structure across 4 orders of magnitude (from 0.5 nM to 6.5 mM at infusion) with regression coefficients (r^2) of 0.9958, 0.9856, and 0.9987 for standards 107, 108, and 121, respectively. Combining the data for all three standards, a linear response curve was also observed, with an overall regression coefficient of 0.9561 **(Fig 3.2).** Linearity of response upon dilution was also observed for the major fragment ions associated with each standard (**Fig 3.3**). MS/MS analysis produced consistent ratios between the two major fragment ions for each standard at dilutions spanning 4 orders of magnitude (**Fig 3.4**). The broadly linear responses detected for the N-linked glycan standards indicate that MS-based quantification by standards possesses a useful dynamic range. The conservation of response linearity at MS2 suggests the possibility, although not directly tested here, that quantification may also be achieved utilizing diagnostic fragments that can distinguish between isobaric species.

Figure 3.1: Heterogeneity and mass purity of N-glycan standards.
Aliquots of N-glycan standards 107, 108, and 121 were analyzed as 2-AB derivatives by HPLC, or as permethylated glycans by MALDI-TOF MS and NSI-LTQ/Orbitrap MS. All three analytic platforms revealed the presence of a major component, corresponding to the expected structure, and minor but structurally related components. **Panel A.** The percent of the total signal contributed by the expected structure across all three platforms is plotted (mean±SD, n=6). The low magnitude of the error indicates that the detected heterogeneity of the standards reflects true structural diversity in the material and was not generated by the analytic technique. **Panel B.** Mass purity for the N-glycan standards was calculated by referencing 2-AB fluorescence of N-glycan peaks to known amounts of 2-AB labeled malto-series standards following HPLC separation or by referencing N-glycan signals to an acetone internal standard by NMR. Mass purity values obtained by fluorescence-coupled HPLC and by NMR were averaged for each of the N-glycan samples (mean±SD, n=10).

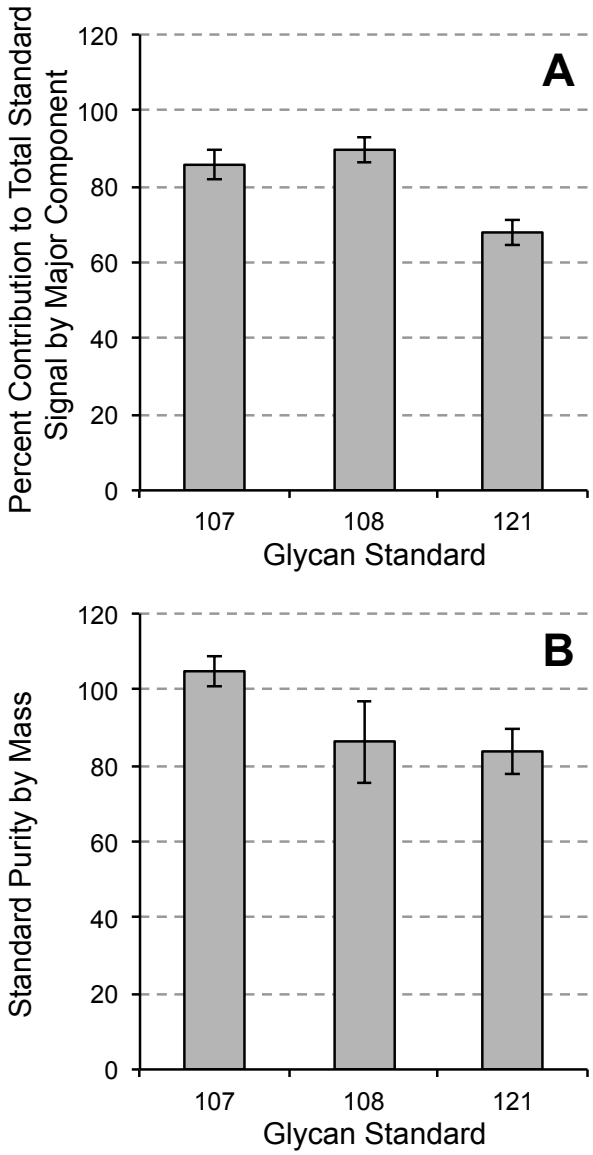

Figure 3.2: Linearity of MS responses for N-glycan standards.
Known amounts of N-glycan standards 107, 108, and 121 were permethylated and analyzed as a dilution series ranging from 0.5 nM to 6.5 mM at infusion. Regression analysis of all datapoints from the three standards yields a high coefficient of correlation (r^2>0.95) and linearity over 4 orders of magnitude. Black square, standard 107; red diamond, standard 108; gray triangle, standard 121.

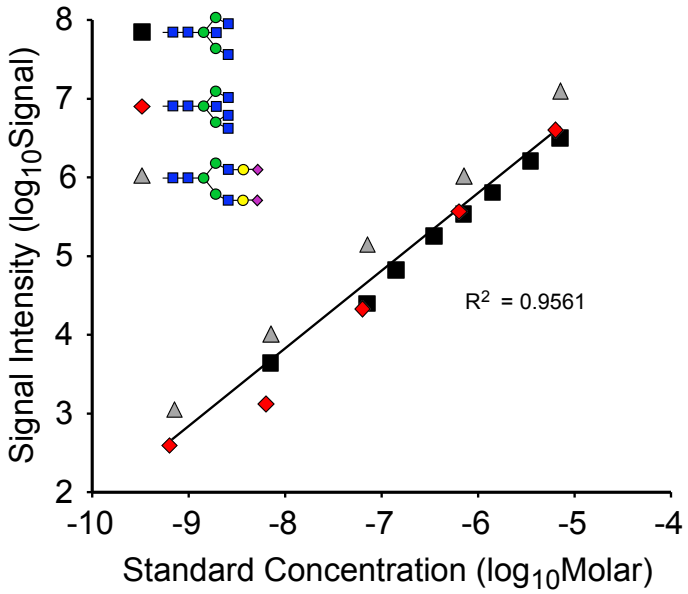

Figure 3.3: Linearity of MS/MS responses for major N-glycan standard fragments. For each of the N-glycan standards 107, 108, and 121, MS/MS spectra were obtained by NSI-LTQ/Orbitrap mass spectrometry. Signal intensities for the two most abundant fragment ions for each standard were quantified at multiple dilutions of the parent compound. **Panel A.** Fragmentation of standard 107 (parent m/z=946.98, doubly charged) yielded major products at m/z=835 (black diamonds, loss of 1 HexNAc) and at m/z=706 (gray circles, loss of 2 HexNAc residues). **Panel B.** Fragmentation of standard 108 (parent m/z=1087.54, triply charged) yielded major products at m/z=958 (black diamonds, loss of 1 HexNAc) and at m/z=828 (gray circles, loss of 2 HexNAc residues). **Panel C.** Fragmentation of standard 121 (parent m/z=1407.68, doubly charged) yielded major products at m/z=1220 (black diamonds, loss of 1 NeuAc, doubly charged) and at m/z=821 (gray circles, loss of 1 NeuAc, triply charged). For all three N-glycan standards, regression analysis of MS/MS fragment signal intensities as a function of standard concentration at infusion were linear, with r^2>0.996.

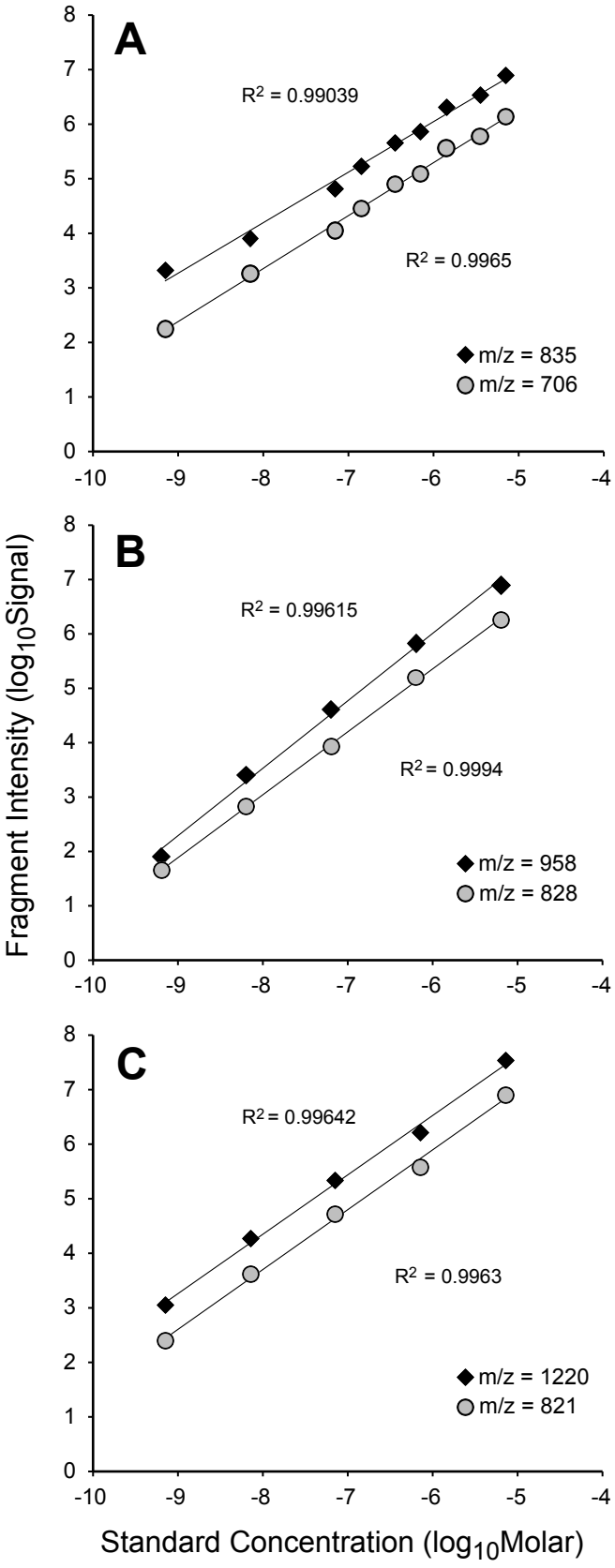
A
R2 = 0.99039
R2 = 0.9965
m/z = 835
m/z = 706
B
R2 = 0.99615
R2 = 0.9994
m/z = 958
m/z = 828
C
R2 = 0.99642
R2 = 0.9963
m/z = 1220
m/z = 821
Fragment Intensity (log10Signal)
Standard Concentration (log10Molar)

Figure 3.4: Constant ratio of major MS/MS fragments for N-glycan standards.
The ratios of the two major MS/MS fragments derived from each of the N-glycan standards (see Figure 3.3) were constant as a function of glycan concentration at infusion over 4 orders of magnitude. The ratio of the major fragment ions for each of the N-glycan standards was calculated at each of the concentrations assayed in Figure 3. The mean±SD (n≥5) of the ratio for each standard is plotted.

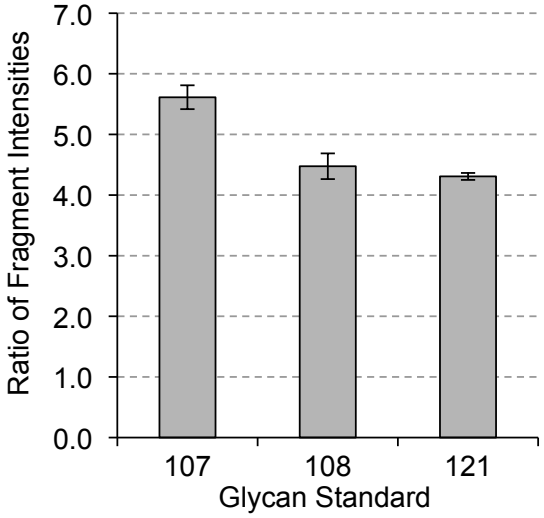

Malto-series oligosaccharides are available in reasonably large amounts at high purity, cover a broad mass range, and can be selected or modified so that they are not isobaric with glycans of interest in the test material. Therefore, malto-series oligosaccharides composed of between 3 and 7 hexose units (dp3-dp7) were tested for suitability as MS quantification standards. While the dp3 maltotriose was easily detectable and gave well-behaved MS responses, its small size presented problems for commercially available signal processing software. Specifically, the Xtract functionality of the Xcalibur software package (Thermo-Fisher) routinely underestimated the amount of dp3 oligosaccharide present compared to manual interpretation of the spectra. This underestimation arises from the software's dependence on using average isotopic distributions characteristic of amino acids for deconvoluting charge states; no currently available commercial deconvolution software has the capacity to use average isotopic distributions of permethylated monosaccharides, which differ from average amino acids with respect to the relative abundance of carbon, nitrogen, hydrogen, and oxygen, for charge state deconvolution. The error imposed by matching glycan isotope envelopes with amino acid isotope distributions becomes less pronounced as the glycan structure increases in size. Accordingly, the malto-series oligosaccharides dp4-dp7 gave well-behaved and consistent MS responses upon dilution. Linear standard curves were obtained for each dp standard across the tested range (from 30 nM – 3 mM at infusion) with regression coefficients of 0.9877, 0.9877, 0.9880, and 0.9869 for dp4, 5, 6, and 7, respectively. Combining the data for all four malto-series standards, a linear response curve was also observed, with an overall regression coefficient of 0.9856 (**Fig 3.5**).

To investigate directly the impact of glycan mass on signal response, the slopes of the standard curves for the three N-glycan standards (107, 108, and 121) and for the 4 malto-series standards (dp4-7) were plotted as a function of their molecular weights (**Fig 3.6**). While a very slight, but nonetheless consistent, trend toward increased

response was observed as the mass of the standard was increased, the maximum difference was only 8% across the tested mass range. The average slope ± standard deviation was 0.98 ± 0.03 $\log_{10}$(MS signal)•$\log_{10}$(pM)$^{-1}$ from 885 – 2831 Daltons, a mass range that encompasses most N-linked glycans released from biologically relevant glycoprotein sources. The minimal size of the incremental increase in signal response associated with increased glycan mass is consistent with the hypothesis that permethylation diminishes the impact of glycan functional groups (hydroxyl, carboxylate, and acetamido) and molecular shape (linear, branched, bisected, terminally sialylated) on ionization efficiency and further supports the usefulness of glycan standards as quantification tools.

Figure 3.5: Linearity of MS responses for malto-series standards.
Known amounts of malto-series oligosaccharide standards dp4, 5, 6, and 7 were permethylated and analyzed as a dilution series ranging from 30 nM to 3 mM at infusion. Regression analysis of all datapoints from the four malto-series standards yields a high coefficient of correlation (r^2>0.98) and linearity over the assayed range. Black square, dp4; red diamond, dp5; gray triangle, dp6; white circle, dp7.

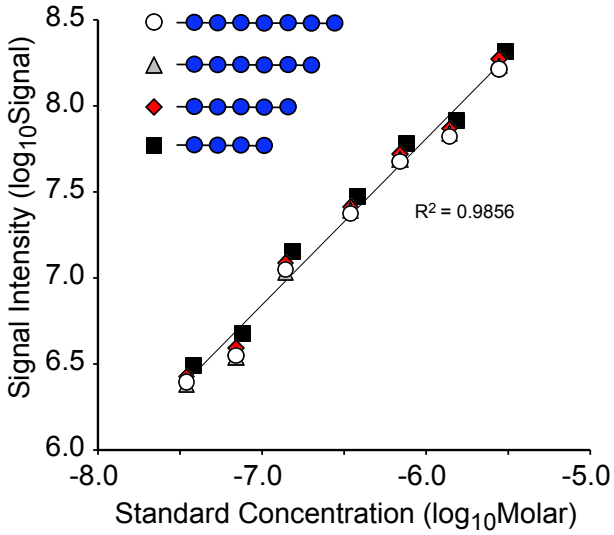

Figure 3.6: Molar responses for permethylated N-glycan and malto-series standards are independent of glycan mass.
The slopes of the standard curves for N-glycan standards 107, 108, 121 and malto-series standards dp4, 5, 6, and 7 were plotted as a function of the mass of the standard. Minimal deviation across the indicated mass range was detected, indicating that permethylation effectively equalizes ionization efficiency across a broad range of glycan structures.

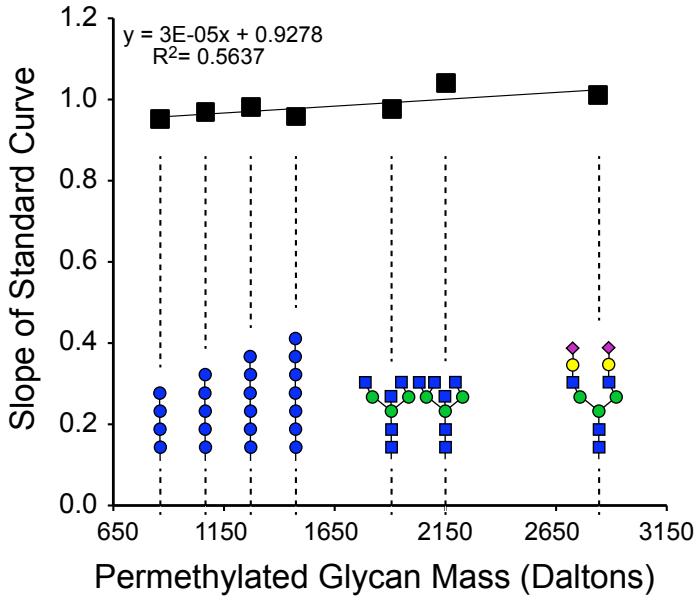

Cross-platform performance and alternative derivatization of malto-series oligosaccharide standards.

The malto-series oligosaccharides dp3-dp7 were analyzed by NSI-LTQ/Orbitrap MS, MALDI-TOF MS and HPLC to assess their performance across commonly used analytic platforms. The five glycans were mixed together at equimolar ratio except for dp4, which was added at 10% molar excess in order to distinguish the dp4 peak from others. Once the NSI-MS data were deconvoluted for charge state using Xtract, the relative signal characteristics for the three analytic platforms were well conserved across the platforms (**Fig 3.7**). Molar response factors were calculated as detector signal response per compound concentration (pM) for 9 HPLC runs and 7 NSI-LTQ/Orbitrap MS runs for each dp (**Fig 3.8**). For dp4-dp7, the molar response factors were 12.9 ± 0.3 and 68.1 ± 2.3 (signal/pM, mean±SD) by HPLC and NSI-MS, respectively (**Appendix Table S6**). As discussed above, Xtracted MS signals for dp3 under-represented its abundance and therefore the molar response factor for dp3 diverged appreciably from the other malto-series glycans. The relatively low and comparable variability of the molar response factors detected by MS and by HPLC support the usefulness of the dp4-dp7 malto-series oligosaccharides as quantification standards.

The lack of HexNAc residues in the dp4-dp7 standards minimizes the likelihood that these compounds would have the same mass/charge ratio as N-linked glycans released from glycoproteins isolated from biological sources. However, many biological samples possess varying amounts of a laddered polyhexose contaminant, probably from glycogen or from a cellulosic source, which would be isobaric with the malto-series standards and would negatively impact quantification. The mass of the dp4-dp7 standards can be shifted away from the endogenous sample hexose ladder by differential permethylation with reagents carrying stable isotopes. To assess the potential impact of alternative permethylation reagents on dp4-dp7 detection, the malto-

Figure 3.7: Comparability of signal responses for malto-series standards across three analytic platforms.
Malto-series oligosaccharide standards dp3, 4, 5, 6, and 7 were analyzed as permethylated derivatives by NSI-LTQ/Orbitrap MS (**Panel A**, full MS; **Panel B**, charge states deconvoluted by Xtract), by MALDI-TOF MS (**Panel C**) or as 2-AB derivatives by HPLC (**Panel D**). The malto-series standard mixture was prepared with 10% more dp4 than the other malto-oligosaccharides in order to readily confirm elution positions and standard identities.

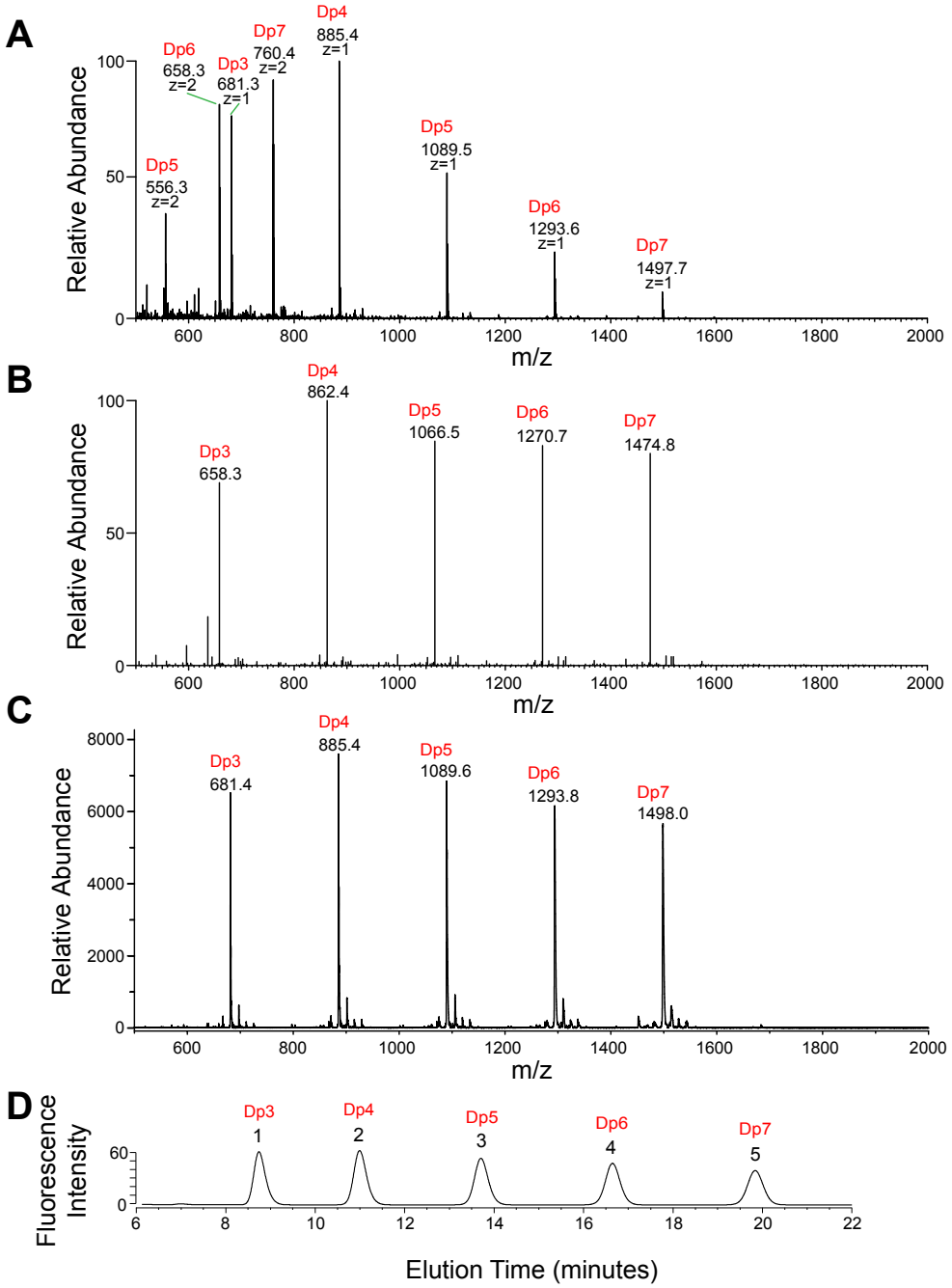

Figure 3.8: Molar response factors for malto-series standards measured by HPLC-fluorescence detection and by mass spectrometry.
Molar response factors, calculated as detector signal per pM concentration of standard, were measured for the malto-series oligosaccharide standards dp3 – dp7 at a range of concentrations (35 nM – 3 mM). The mean±SEM of the molar response factors across the analyzed concentrations for each standard is presented for HPLC coupled to fluorescence detection (black squares, n=9 for each standard) and for NSI-MS (red diamonds, n=7 for each standard). For the malto-series standards dp4 – dp7, the relationship between molar response and standard mass is identical for HPLC and MS.

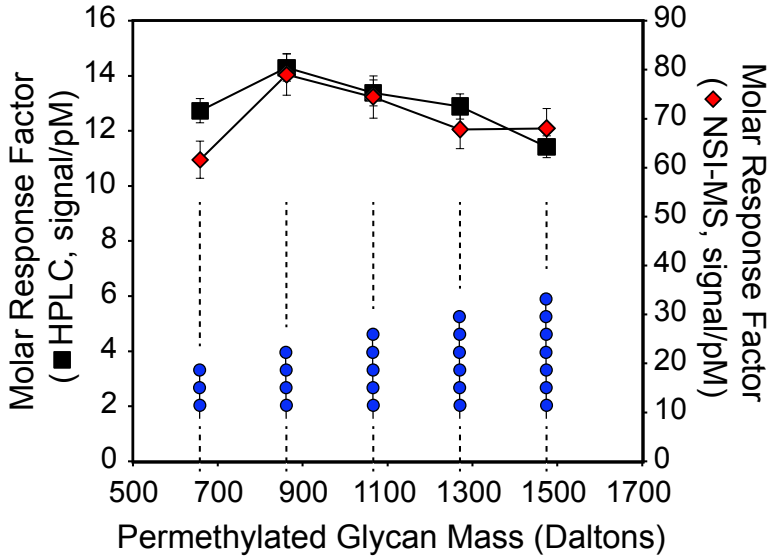

series glycans were permethylated with ^{12}C-, ^{13}C- or deuterated methyliodide (^{12}C-MeI, ^{13}C-MeI, or CD_3I). The signal detected for dp4-dp7 following permethylation with ^{12}C-MeI or with CD_3I was compared to the signal detected for dp4-dp7 following permethylation with ^{13}C-MeI (**Fig 3.9**). Signal intensities did not vary as a result of alternative derivatization, allowing flexibility in positioning the standard peaks in relation to peaks of interest in biological samples.

Quantification of RNaseB N-glycans

RNaseB possesses one high-mannose type N-linked glycan per molecule of protein, providing a simple test of glycan quantification (Liang et al., 1980; Prien et al., 2009; Tarentino et al., 1970). Based on the mass of the non-glycosylated protein backbone (RNaseA) and on the mass of the dominant N-linked glycan shown previously to be attached to RNaseB (M5N2), the expected contribution of glycan mass to the total mass of the protein is 8.7%. N-glycans were prepared from RNaseB by PNGaseF digestion of denatured intact protein or by PNGaseF digestion of tryptic glycopeptides. N-glycans released from RNaseB by both methods were permethylated and spiked with ^{13}C-labeled maltotetraose (dp4) as external quantification standard prior to analysis by NSI-MS. For both glycan preparation methods, quantification by external standard detected 1.37 µg of N-glycan from 16.0 µg of RNaseB, corresponding to 8.6% of the RNaseB mass attributable to glycan, which is 98% of the expected amount.

Figure 3.9. Permethylation of malto-series standards with methyliodide containing stable isotopes of carbon or hydrogen yields equivalent MS responses. The indicated malto-series standards were permethylated with with ^{12}C-, ^{13}C- or deuterated methyliodide (^{12}C-MeI, ^{13}C-MeI, or CD_3I, respectively) and analyzed by NSI-LTQ/Orbitrap MS. Instrument responses for standards permethylated with ^{12}C-MeI or CD_3I were normalized to the responses obtained for standards permethylated with ^{13}C-MeI, which were set to 100. Normalized responses were averaged for all replicates of the standards permethylated with ^{12}C-MeI or CD_3I and are plotted as mean±SD (n=3 for each standard). The minor variation around the mean indicates that standards can be permethylated with reagents that induce mass shifts most suitable for the biological sample being studied.

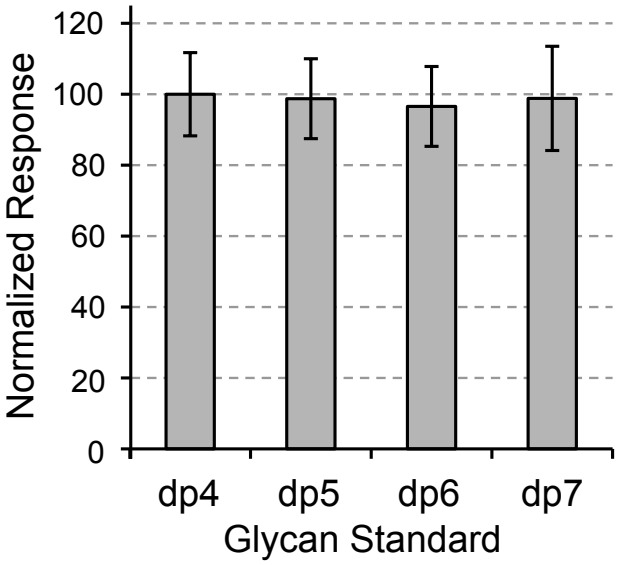

Recovery of external standard from biological matrices.

To assess whether a biological matrix might suppress detection of external standards, the permethylated N-glycan standards 107, 108, and 121 were mixed and spiked into a preparation of permethylated N-linked glycans released from *Drosophila melanogaster* embryo glycoproteins. This matrix was chosen as a first test of recovery because the three N-glycan standard structures (all complex type) have not previously been detected in *Drosophila* preparations, an organism that is characterized by a predominance of high-mannose type glycans (Aoki et al., 2007). The standard mix and the *Drosophila* glycans were analyzed separately and then in combination (**Fig 3.10**). The mean recovery for standard N-glycan signals was 101.6% ± 3.2% relative to the standard mix analyzed alone. To more stringently and comprehensively test for the recovery of spiked standards, the malto-series standards (dp4-dp7) and the N-glycan standards (107, 108, and 121) were mixed and permethylated with ^{13}C-MeI before being spiked into N-glycans released from mouse brain glycoproteins that had been permethylated with ^{12}C-MeI. This biological matrix contains high-mannose and complex glycans, providing a source richer in potentially interfering components than the *Drosophila* material. The mean recovery of all standards together was 90.1% ± 9.3%. The malto-series glycans were recovered at 98.7% ± 6.0% and the N-glycan standards were recovered at 85.0% ± 5.7%. Thus, signal suppression is not a significant concern when using external glycan standards to quantify N-glycans prepared from biological sources.

Figure 3.10: Recovery of MS signal responses for external standards mixed into a biological matrix.

The N-glycan standards 107, 108, and 121 were permethylated with ^{13}C-MeI and analyzed as a standard mix alone (**Panel A**). N-linked glycans prepared from *Drosophila melanogaster* embryos were permethylated with ^{12}C-MeI and analyzed alone (**Panel B**) or after being supplemented with the ^{13}C-MeI permethylated N-glycan standard mix (**Panel C**). Recovery of signal intensities for standards and sample peaks indicates the lack of suppression or matrix interference for quantification by external standard.

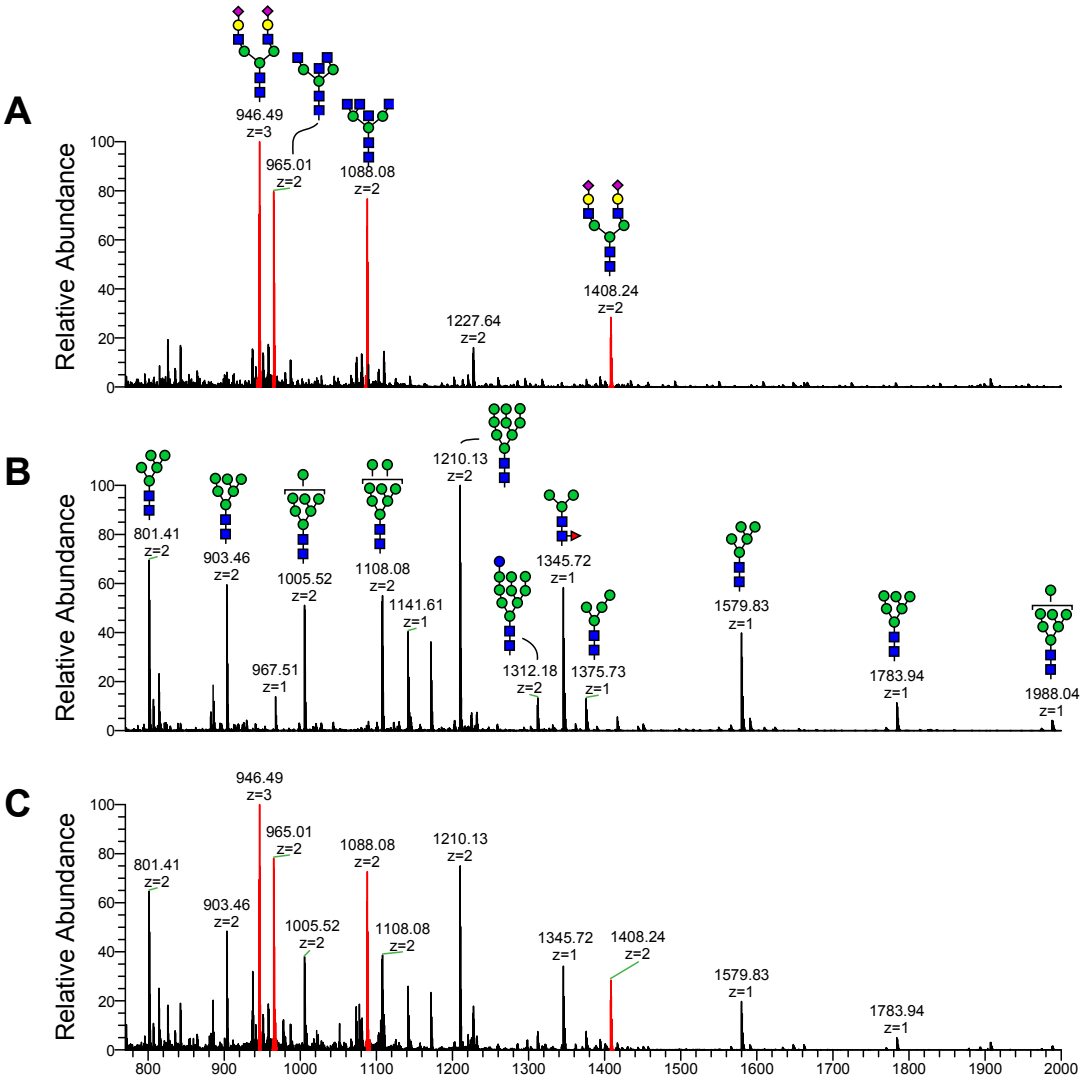

Quantification of mouse brain glycans by N-glycan and malto-series standards.

A subset of the major N-linked glycans in mouse brain was quantified using each of the malto-series and each of the N-glycan standards as external reference standards. The 8 quantified glycans, which individually account for between 4 – 23% of the total glycans, together represent 64% of the total detectable glycan profile in the mouse brain. The resulting values for the amount of N-linked glycan in brain (nmol glycan/gram of tissue wet weight) were compiled to determine if the malto-series or N-glycan standards produced substantially different results (**Fig 3.11**). The average percent deviation from the mean for measured glycan amount was 9.0% ± 4.5% for amounts determined by reference to the malto-series and N-glycan standards. Therefore, regardless of which type of standard or which individual standard is used for quantification, the resulting abundance measurements vary by less than 10%.

Based on quantification relative to external standards, the data presented here indicate that the N-glycan content of the whole mouse brain is 138 ± 11 nmol oligosaccharide/g wet weight. Despite the extensive use of the mouse as an experimental system in glycobiology, it is surprisingly difficult to determine from the literature the absolute amount of N-linked glycan present in mouse brain tissue. All published mass spectrometry-based studies express N-linked glycan abundances in mouse brain as normalized distributions of glycans (quantified as % total profile) for comparison between wild-type and mutant/experimental samples, further emphasizing the importance of developing a method for quantifying absolute glycan amount. (Nakakita et al., 2005; North et al., 2009; North et al., 2010; Shimizu et al., 1993). Nonetheless, assuming that approximately 10% of brain wet weight is protein and that approximately 10-20% of this protein is secreted or membrane bound glycoprotein, and using the average molecular weight of the major N-glycans detected in this analysis (1935 Daltons), the results presented here indicate that between 3 and 6% of the

glycoprotein mass in the mouse brain is attributable to N-linked glycan (Margolis et al., 1976; Schnaar et al., 2014). Considering a typical membrane protein of 100 kD, this estimate indicates that between 3 and 6 kD of its mass is attributable to glycan, or that, on average, a 100 kD protein possesses between 1.6 and 3.2 N-linked glycans. This range is reasonable based on the most comprehensive and recent glycoproteomic analysis of rodent brain, which indicated that, on average, rodent brain glycoproteins carry 1.7 N-linked glycans per molecule (276 unique consensus sites utilized across 161 identified proteins, range 1 – 27 sites per protein) (Parker et al., 2013). Therefore, quantification by external standard, whether using malto-series glycans or actual N-glycan structures, delivers glycan abundances that are within reason for complex biological samples.

Figure 3.11. Quantification of mouse brain N-glycans by reference to external standards. N-linked glycans were released from mouse brain glycoproteins and permethylated with ^{12}C-MeI. N-glycan and malto-series external standards were permethylated with ^{13}C-MeI, combined, and spiked into preparations of mouse brain-derived glycans. The 8 most abundant mouse brain glycans were quantified by reference to each of the external standards (107, 108, 121, and dp 4 – 7). The calculated amount of each of the brain glycans (mean±SD) is presented for quantification by reference to malto-series standards (***All dp***, grey bars, n=4), N-glycan standards (***All N-Gly***, red bars, n=3), or all glycan standards (***All Gly***, white bars, n=7). Quantification of brain glycans yielded similar results regardless of which standard set was used.

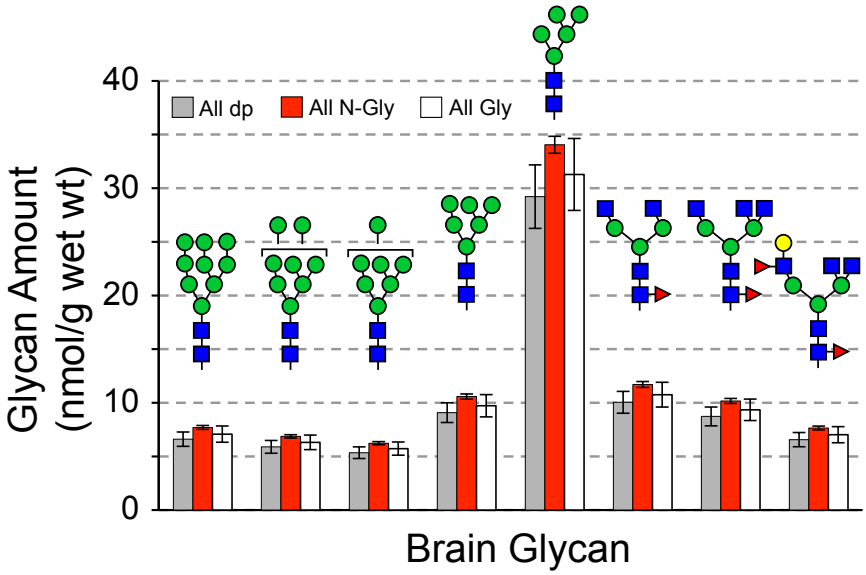

Conclusions

The current use of mass spectrometry for glycomic analysis has been largely limited to the characterization of fold-differences between control and experimental samples. While such studies have been invaluable for appreciating the dynamic nature of glycoprotein glycan structural diversity, they have been unable to discern changes in total glycan amount or in the absolute abundance of individual glycans, especially for minor components in complex mixtures. Two related impediments have limited the adoption of quantification by mass spectrometry: the variability of ionization efficiencies across glycan structures and the lack of availability of standard compounds that reflect the diversity of glycan structures found in biological samples. With regard to the first limitation, permethylation effectively neutralizes any major impact of glycan structural features on ionization. In this study, the slopes of the standard curves were similar for linear, branched, bisected, biantennary, triantennary, sialylated, and non-sialylated glycans. The relatively minor changes in standard curve slope or calculated molar responses that were detected fall within a range of variation (<15%) that is acceptable in light of the benefits to be gained through quantification. With regard to the second limitation, the past few years have seen increasing effort toward the production of glycan standards for use by the research community. As these resources become available, it will be possible to investigate the value of using a broader range of well-characterized glycans as quantification standards. Synthetic glycans will be especially important for establishing quantification protocols for glycans bearing structural moieties, such as sulfation, that impact ionization because they remain charged after permethylation (Kumagai et al., 2013; Kurz et al., 2015). But, for neutral glycans or for charged glycans that become neutral upon permethylation (sialylated, phosphorylated, uronylated), well-characterized materials are currently available that can be useful as quantification standards, including N-glycan structures and simpler glycan polymers.

The method described here makes use of malto-series oligosaccharides from a commercial source as quantification standards. These standards, as well as the N-glycan standards procured from non-commercial sources, performed well, exhibiting broad linearity, a lower limit of quantification in a useful range for glycan abundances in biological materials, and acceptable recovery from a complex biological matrix. While most of the work reported here was performed using nanospray ionization and linear ion or orbital trap mass analyzers, comparable quantification of standards was achieved with MALDI-TOF, NMR, and HPLC, indicating the cross-platform usefulness of the approach. Expanding glycan quantification to mass spectrometry provides another highly sensitive technology platform, along with HPLC and CE coupled to fluorescence detection, for comprehensively exploring glycomic differences in biological samples.

Acknowledgements

This work was supported by grants from the National Institutes of Health (U54 GM62116 and P41 GM103490 from NIGMS and P01 HL107151 from NHLBI). The authors gratefully acknowledge the assistance in acquiring glycan standards provided by Nahid Razi and by the Steering Committee of the Consortium for Functional Glycomics.

Conflict of Interest disclosure

The authors declare no competing financial interest.

References

Cummings, R.D. and J.M. Pierce, The challenge and promise of glycomics. *Chem Biol*, 2014. **21**(1): p. 1-15.

Geyer, H. and R. Geyer, Strategies for analysis of glycoprotein glycosylation. *Biochim Biophys Acta*, 2006. **1764**(12): p. 1853-69.

Ito, H., et al., Comparison of analytical methods for profiling N- and O-linked glycans from cultured cell lines : HUPO Human Disease Glycomics/Proteome Initiative multi-institutional study. *Glycoconj J*, 2015.

Bigge, J.C., et al., Nonselective and efficient fluorescent labeling of glycans using 2-amino benzamide and anthranilic acid. *Anal Biochem*, 1995. **230**(2): p. 229-38.

Guile, G.R., et al., A rapid high-resolution high-performance liquid chromatographic method for separating glycan mixtures and analyzing oligosaccharide profiles. *Anal Biochem*, 1996. **240**(2): p. 210-26.

Huffman, J.E., et al., Comparative performance of four methods for high-throughput glycosylation analysis of immunoglobulin G in genetic and epidemiological research. *Mol Cell Proteomics*, 2014. **13**(6): p. 1598-610.

Knezevic, A., et al., High throughput plasma N-glycome profiling using multiplexed labelling and UPLC with fluorescence detection. Analyst, 2011. **136**(22): p. 4670-3.
Nagels, B., et al., Improved sample preparation for CE-LIF analysis of plant N-glycans. *Electrophoresis*, 2011. **32**(24): p. 3482-90.

Novotny, M.V. and J. Sudor, High-performance capillary electrophoresis of glycoconjugates. *Electrophoresis*, 1993. **14**(5-6): p. 373-89.

Takahashi, N., et al., Three-dimensional elution mapping of pyridylaminated N-linked neutral and sialyl oligosaccharides. *Anal Biochem*, 1995. **226**(1): p. 139-46.

Wada, Y., et al., Comparison of the methods for profiling glycoprotein glycans--HUPO Human Disease Glycomics/Proteome Initiative multi-institutional study. *Glycobiology*, 2007. **17**(4): p. 411-22.

Royle, L., et al., Detailed structural analysis of N-glycans released from glycoproteins in SDS-PAGE gel bands using HPLC combined with exoglycosidase array digestions. *Methods Mol Biol*, 2006. **347**: p. 125-43.

Ashline, D., et al., Congruent strategies for carbohydrate sequencing. 1. Mining structural details by MSn. *Anal Chem*, 2005. **77**(19): p. 6250-62.

Dell, A. and H.R. Morris, Glycoprotein structure determination by mass spectrometry. *Science*, 2001. **291**(5512): p. 2351-6.

Hamouda, H., et al., Rapid analysis of cell surface N-glycosylation from living cells using mass spectrometry. *J Proteome Res*, 2014. **13**(12): p. 6144-51.

Hu, Y. and Y. Mechref, Comparing MALDI-MS, RP-LC-MALDI-MS and RP-LC-ESI-MS glycomic profiles of permethylated N-glycans derived from model glycoproteins and human blood serum. *Electrophoresis*, 2012. **33**(12): p. 1768-77.

Jang-Lee, J., et al., Glycomic profiling of cells and tissues by mass spectrometry: fingerprinting and sequencing methodologies. *Methods Enzymol*, 2006. **415**: p. 59-86.

Lapadula, A.J., et al., Congruent strategies for carbohydrate sequencing. 3. OSCAR: an algorithm for assigning oligosaccharide topology from MSn data. *Anal Chem*, 2005. **77**(19): p. 6271-9.

Leymarie, N., et al., Interlaboratory study on differential analysis of protein glycosylation by mass spectrometry: the ABRF glycoprotein research multi-institutional study 2012. *Mol Cell Proteomics*, 2013. **12**(10): p. 2935-51.

Parker, B.L., et al., Site-specific glycan-peptide analysis for determination of N-glycoproteome heterogeneity. *J Proteome Res*, 2013. **12**(12): p. 5791-800.

Walther, T., et al., Glycomic analysis of human respiratory tract tissues and correlation with influenza virus infection. *PLoS Pathog*, 2013. **9**(3): p. e1003223.

Yamada, K., et al., Hyphenated technique for releasing and MALDI MS analysis of O-glycans in mucin-type glycoprotein samples. *Anal Chem*, 2010. **82**(17): p. 7436-43.

Zhang, H., S. Singh, and V.N. Reinhold, Congruent strategies for carbohydrate sequencing. 2. FragLib: an MSn spectral library. *Anal Chem*, 2005. **77**(19): p. 6263-70.

Aoki, K., et al., Dynamic developmental elaboration of N-linked glycan complexity in the Drosophila melanogaster embryo. *J Biol Chem*, 2007. **282**(12): p. 9127-42.

Aoki, K., et al., The diversity of O-linked glycans expressed during Drosophila melanogaster development reflects stage- and tissue-specific requirements for cell signaling. *J Biol Chem, 2008*. **283**(44): p. 30385-400.

Mechref, Y., P. Kang, and M.V. Novotny, Solid-phase permethylation for glycomic analysis. *Methods Mol Biol*, 2009. **534**: p. 53-64.

Yu, S.Y., et al., Enabling techniques and strategic workflow for sulfoglycomics based on mass spectrometry mapping and sequencing of permethylated sulfated glycans. *Glycobiology*, 2009. **19**(10): p. 1136-49.

Olajos, M., et al., Sample preparation for the analysis of complex carbohydrates by multicapillary gel electrophoresis with light-emitting diode induced fluorescence detection. *Anal Chem*, 2008. **80**(11): p. 4241-6.

Anumula, K.R. and P.B. Taylor, A comprehensive procedure for preparation of partially methylated alditol acetates from glycoprotein carbohydrates. *Anal Biochem*, 1992. **203**(1): p. 101-8.

Porterfield, M., et al., Discrimination between adenocarcinoma and normal pancreatic ductal fluid by proteomic and glycomic analysis. *J Proteome Res*, 2014. **13**(2): p. 395-407.

Lu, J. and H. van Halbeek, ^{1}H and ^{13}C resonance assignments of a 21-amino acid glycopeptide prepared from human serum transferrin. *Carbohydrate Research*, 1996. **296**: p. 1-21.

Tarentino, A.L. and T.H. Plummer, Jr., Enzymatic deglycosylation of asparagine-linked glycans: purification, properties, and specificity of oligosaccharide-cleaving enzymes from Flavobacterium meningosepticum. *Methods Enzymol*, 1994. **230**: p. 44-57.

Bohorov, O., et al., Arraying glycomics: a novel bi-functional spacer for one-step microscale derivatization of free reducing glycans. *Glycobiology*, 2006. **16**(12): p. 21C-27C.

Liang, C.J., K. Yamashita, and A. Kobata, Structural study of the carbohydrate moiety of bovine pancreatic ribonuclease B. *J Biochem*, 1980. **88**(1): p. 51-8.

Prien, J.M., et al., The high mannose glycans from bovine ribonuclease B isomer characterization by ion trap MS. *J Am Soc Mass Spectrom*, 2009. **20**(4): p. 539-56.

Tarentino, A., T.H. Plummer, Jr., and F. Maley, Studies on the oligosaccharide sequence of ribonuclease B. *J Biol Chem*, 1970. **245**(16): p. 4150-7.

Nakakita, S., et al., Alteration of brain type N-glycans in neurological mutant mouse brain. *J Biochem*, 2005. **138**(3): p. 277-83.

North, S.J., et al., Mouse and human glycomes, in Handbook of Glycomics, R.D. Cummings and J.M. Pierce, Editors. 2009, *Academic Press: Amsterdam*. p. 263-328.

North, S.J., et al., Mass spectrometric analysis of mutant mice. *Methods Enzymol*, 2010. **478**: p. 27-77.

Shimizu, H., et al., Structures of N-linked sugar chains expressed mainly in mouse brain. *J Biochem*, 1993. **114**(3): p. 334-8.

Margolis, R.K., et al., Developmental changes in brain glycoproteins. *Brain Res*, 1976. **112**(2): p. 363-9.

Schnaar, R.L., R. Gerardy-Schahn, and H. Hildebrandt, Sialic acids in the brain: gangliosides and polysialic acid in nervous system development, stability, disease, and regeneration. *Physiol Rev*, 2014. **94**(2): p. 461-518.

Kumagai, T., et al., In-gel beta-elimination and aqueous-organic partition for improved O- and sulfoglycomics. *Anal Chem*, 2013. **85**(18): p. 8692-9.

Kurz, S., et al., Targeted release and fractionation reveal glucuronylated and sulphated N- and O-glycans in larvae of dipteran insects. J Proteomics, 2015. **126**: p. 172-88.

CHAPTER 4

CONCLUSIONS AND FUTURE DIRECTIONS

The work described in Chapter 3 validates a method to quantify exact glycan amounts using mass spectrometry. Previous quantitative methods for mass spectrometric based glycomics have been limited to generating relative glycan abundances, in which the abundance of a single glycan is expressed as a percent of the sum of all glycans. Since glycosylation varies based on environment and tissue type, calculating the absolute glycan amount is imperative. We have now demonstrated that, in comparison to other methods, glycan densities of even relatively small sample amounts can be quantified by the use of a known amount of standard. In addition, we used newly developed software tools (GRITS) to extract structural information from MS/MS fragmentation data in a semi-automated workflow. These methods provide a platform for high throughput analysis of exact glycan densities in biological samples.

The results from Chapter 2 demonstrate for the first time that a mutation in an E3 ubiquitin ligase, *Roc2,* alters neural development by affecting tissue-specific glycosylation. This extends the previously known roles of ubiquitination and ubiquitin ligases. In addition, we describe how the Sodium-Potassium ATPase is regulated by this ubiquitin ligase and is involved in several functions aside from its classic role as a pump. Based on our results, we are able to place a broader role of this pump in altering Golgi trafficking by affecting its architecture. These roles are discussed in more detail below.

Roc2 is an ubiquitin ligase involved in neuronal Golgi trafficking

As a result of several different genetic and molecular mapping strategies, we successfully identified a mutation in the *roc2* gene as the molecular lesion responsible for the *roc2*^{ms16} phenotype. We mapped this mutation to a single nucleotide change in

the second intron of the gene, which is predicted to change the secondary structure of the resulting transcript. *In situ* experiments showed that Roc2 mRNA expression is in neurons and is decreased in the mutant. Proteomic analysis revealed a decrease in Roc2 protein of about 22% in the mutant. Subsequent rescue experiments, using the UAS/Gal4 driver system, demonstrated that transgenic expression of *roc2* in the *roc2*^{ms16} background rescued HRP-epitope expression in a cell-autonomous fashion. Using mass spectrometry, the overall glycosylation was assessed, and specifically N-glycans released by PNGase F were altered in *Roc2*^{ms16} mutants with a decrease in *Roc2*. However, the O-linked profile and specific N-linked structures like HRP-epitopes (using PNGase A) through mass spectrometry are experiments that are still in progress. These experiments will be done using methods developed in our laboratory and are described in (Aoki et al., 2008).

Previous studies have shown that ubiquitin ligases play an important role in membrane trafficking (Schwarz and Patrick, 2012). Depletion of CBLC, a RING domain E3 ubiquitin ligase found at the Golgi causes extensive Golgi fragmentation and ultimately disrupts ribbon formation. We hypothesize that Roc2 could have a similar effect although an important aspect of our hypothesis is that roc2 should be localized to the Golgi. The lack of antibodies against Roc2 was a limitation for us to verify this hypothesis. Therefore, we assume that the ubiquitous expression of Roc2 includes its presence in and around the Golgi, but this is yet to be determined and would be useful to directly assign Roc2 in altering Golgi function to strengthen our hypothesis. In addition, our current experiments to assess the Golgi were performed by using antibodies against Golgi resident proteins (Barr et al., 1997; Nakamura et al., 1995). It would be informative to more comprehensively assess the distribution of Golgi markers to provide a higher resolution picture of the integrity of various compartments. To that end, direct

visualization of Golgi structure by electron microscopy could also help to understand how the organelle has been altered.

To expand our hypothesis of how a ubiquitin ligase can alter glycosylation and because of its ubiquitous expression, we did proteomics to identify putative protein changes between wildtype and mutant. As anticipated, this analysis resulted in the identification of a variety of proteins that were either up or down regulated. In general, we are interested in both categories based on the role of ubiquitin as a tag for localization and signaling as well as for proteosomal degradation (Acconcia et al., 2009). Some of these proteins include protein phosphatase A (PP2A) and rasputin which is downregulated and Coronin and Arginine kinase (*Drosophila* specific creatine kinase) are upregulated. We do not rule out the possibility that some of these proteins could be involved in the HRP-epitope expression pathway. Future experiments include detailed investigation of these proteins to assess whether they have a function in regulating glycosylation. Several of these proteins are of particular interest as their previously described roles involve Golgi dynamics as well as trafficking and signaling. For example, PP2A is a key protein in controlling the phosphorylation of the proteins extracellular signal regulated kinase (ERK) by mitogen-activated protein kinase (MAPK) 1 and 2 (Kimura et al., 2011). These proteins are involved in cell proliferation and differentiation and in Golgi disassembly. Similarly, Arginine Kinase found mostly in areas of the nervous system where energy is used, is required for the conversion of ADP to ATP using phosphoarginine as a donor, a process that is important in every cell and a topic which was discussed in Chapter 2 (VIRDEN et al., 1965). An increase in Arginine kinase could be a downstream effect of the increase in ATPα. As ATPα requires ATP to successfully transfer ions, ATP hydrolysis increases, which consequently triggers Arginine Kinase. These associations make analysis of these remaining identified proteins, which are putatively involved in the pathway as well, even more important.

Sodium-Potassium ATPase is a substrate of Roc2

The protein we chose to investigate in the frame of this thesis is the Sodium-Potassium ATPase, which is an ion pump in the plasma membrane of every cell and is required to maintain the cell's resting membrane potential. To effectively transfer ions against a concentration gradient, energy from ATP is used. In general, the pump has two subunits, which have to be assembled together before leaving the ER to the plasma membrane. Although we only investigated the alpha subunit or ATPα, the role that the beta subunit (ATPβ) plays in our pathway still needs to be addressed, especially because it is an HRP carrying protein. Understanding the role of ATPβ is currently an ongoing project and preliminary studies suggest that there is a slight increase in beta subunit in our mutant. However, it is important to understand how the increase in the alpha subunit does not correspond to the amount of ATPβ in our mutant.

The *roc2*^{ms16} mutant demonstrates that increased ATPα is associated with decreased HRP-epitope. To determine whether this observation is reporting a cause or a correlation, additional experiments are required. The first of these additional studies has already been completed. Namely, adults with decreased ATPα (chromosomal deficiency over a balancer) exhibit increased HRP-epitope. What remains to be shown is that increased ATPα expression in an otherwise wildtype background phenocopies the *roc2*^{ms16} HRP-epitope decrease. To perform this experiment, we will use ELAV-GAL4, which is a pan neural driver, to overexpress ATPα, from an available UAS-ATPα stock in neurons of wildtype embryos (Berger et al., 2007). Using this system, we expect to see the same changes in HRP-epitope as we detected in the *roc2*^{ms16} mutant. Another important question to address is whether the Golgi phenotypes seen in our mutant can be recreated by ATPα overexpression, as this is the major phenotype attributing to our glycosylation defects. These experiments would support our hypothesis by showing a

decrease in ATPα (using the deficiency line) increases HRP (and changes overall glycosylation), whereas an increase in ATPα (using the UAS-Elav system) leads to a decrease in HRP epitope expression. Together, these results would confirm that the *roc2*^{ms16} phenotype is due, at least in part, to a change in ATPα levels.

Staining of mutant and wildtype embryos indicated that ATPα is expressed everywhere; it is seen at the plasma membrane of all cells throughout the nervous system and the ectoderm. Using confocal microscopy, we were able to detect an increase of ATPα in the nerve cord as a result of improper trafficking of the protein in the mutant based on an increase of staining in the axonal plane. Simultaneously, a slight, statistically insignificant decrease in ATPα was observed in the mutant cell bodies. We also observed some vesicular staining accompanying plasma membrane staining, which suggests that ATPα is expressed vesicularly as well. If the *roc2*^{ms16} mutant phenotypes are due to improper trafficking of ATPα, it is essential to understand what the impact of an excess of this pump could do. In order for the pump to transport ions across the membrane against their concentration gradient, it requires energy. ATPα uses ATP for energy and the phosphorylation and dephosphorylation, creates a conformational change in the protein that allows the release of ions. An increase in ATPα should lead to shorter membrane voltage transients; i.e.: excursions of membrane potential away from resting values should be more rapidly corrected in the mutant. Thus, in mutant neurons compared to wildtype neurons, greater pre-axonal depolarization may be required to reach threshold at the axon hillock, and, along the axon, fewer action potentials may be produced by each threshold stimulus. One possibility for linking glycosylation and altered ATPα is to propose that the neuronal trafficking machinery utilizes ionic fluxes as signals for engaging specific modification pathways, such as generation of the HRP-epitope. The mechanistic link between membrane potential and trafficking remains to be determined, but the normal function of ATP(Tian et al., 2006)α may provide a clue.

Since ATPα activity consumes ATP, increased expression of ATPα would be expected to drive ATP levels down and ADP/AMP levels up, a form of cellular stress. To assess whether increased ATPα in *roc2*^{ms16} alters high-energy phosphate stores, the levels of ATP, ADP, and AMP should be quantified relative to wildtype. To do this, the glycolipid fractions obtained from the extracts of both genotypes are cleaned up and analyzed by HPLC. In the mutant, we expect an increase in AMP levels. The most promising approach would be to compare the ratios of each of the nucleotides between genotypes and look for changes. If ATP/ADP/AMP levels are altered significantly, activation of AMP kinase could also be contributing to the Golgi phenotypes as the gamma subunit, where AMP binds to activate the kinase, has been implicated in Golgi assembly/disassembly (Chia et al., 2012). AMP kinase activation and the phosphorylation status of some AMP kinase targets should be investigated. Furthermore, we are interested in examining the ionic environment in depolarized and repolarized cells, and compare this in the mutant where the exchange of ions could cause an accumulation of ions, which could ultimately be the cause of the changes in Golgi architecture as well.

As briefly mentioned in Chapter 2, several kinases have known associations with ATPα. These include Protein Kinase A, Protein Kinase C and Src kinases, which are kinases found around the Golgi and are well-known to affect Golgi architecture. Src kinases are membrane bound tyrosine kinases that localize at the Golgi in its active form (Weller et al., 2010) and control Golgi integrity and function. It has been shown that an increase in Src Kinase activity causes Golgi fragmentation (Bard et al., 2003) and this kinase is also involved in downstream activation of proteins like Arf1 and ubiqtuin ligase, CBLC (Lee et al., 2015). Src Kinase also colocalizes with ATPα at the membrane during which Src kinase stays inactivated (Tian et al., 2006). We envision that in the *roc2*^{ms16} mutant, excess ATPα at the membrane keeps Src Kinase bound and inactivated; and

inactivated Src could lead to improper compartmentalization and polarization of the Golgi subunits, leading to altered Golgi architecture.

Additionally, as part of our current experiments, we are using pharmacological techniques to revert glycosylation in the mutants towards wildtype profiles. Ouabain is a cardiac glycoside (CG) that is responsible for inhibiting the Sodium-Potassium pump (Cherniavsky-Lev et al., 2014; Kulikov et al., 2007). Many studies have demonstrated that ouabain binds to ATPα to trigger signaling events (Cherniavsky-Lev et al., 2014; Tian et al., 2006). We plan to use this in our mutants to rescue overall glycosylation. There are several experiments planned with ouabain treated lines; some of these include monitoring HRP epitope expression by ELISA and western blots, and to analyze overall N-glycosylation in the mutant to verify if wildtype glycosylation could be restored. Finally, we would use these lines to assess the Golgi architecture and integrity. If the Golgi architecture appears to be rescued in ouabain treated lines compared to the mutant, our hypothesis would be supported and show for the first time the role of ATPα in the secretory pathway, suggesting that in excitable cells, changes in glycosylation are a response to changes in ATP and ionic levels.

Since our hypothesis focuses on membrane potential, another future experiment we propose is the use of patch-clamp methods to control membrane potential in neurons. This will be achieved in collaboration with a neuro-electrophysiologist; using a neural cell line and controlling the voltage of neural membranes, we would examine the effects on fluorescent tagged-HRP in real time. Separately, to test whether the phenotypes stay consistent between species, Roc2 could be knocked down in IPS cells. IPS cells that can be differentiated into several lineages is advantageous in looking at the role of ATPα in a cell and tissue specific manner in neural and non-neural backgrounds. Additionally, drug treatments in cells can be used to look at Golgi phenotypes directly associated with changes in ATPα levels. Performing these

experiments in a cell line will also enable resources and techniques for rescue experiments.

Roc2 and Sodium-Potassium ATPase at the NMJ

As discussed above, we expect Roc2 to have different substrates in different tissues; but based on our observations, ATPα is a substrate even at the NMJ. An increase in ATPα at the NMJ gives rise to an increase in receptors on the post-synaptic density (PSD) whereas a decrease in ATPα presents fewer receptors. Therefore, we hypothesize that due to shorter transient times caused by the ATPα increase, the muscle continues to produce more glutamate receptors (DGluR) to enhance the signal transduction passed from the pre-synaptic neuron. However, there is still some work to be done to test this hypothesis. There are well-established protocols and methods to read electrical recordings at the NMJ to test if this is altered at the NMJ, as well as experiments to determine if HRP expression at the NMJ consistently changes with changes in ATPα and DGluR. To augment this further, we can obtain deletion or mutant lines for DGluR and examine HRP-epitope and ATPα expression. The consistency of our data suggest that our phenotypes extend from the embryos to other stages of *Drosophila* as well, including larvae (through NMJ) and adults in which ATPα is increased in the mutant and HRP-epitope levels are decreased.

Closing remarks

As discussed in Chapter 1, glycosylation is a highly complex process, which requires that a whole set of machinery be at the right place, at the right time. Through this research, we hope to have put a dent into the vast field of tissue specific glycosylation by demonstrating how a ubiquitin ligase can alter neural specific glycosylation by influencing synaptic homeostasis and ATP hydrolysis (**Fig 4.1**). There are copious amounts yet unknown, but hopefully this data can shed some light on the highly diverse process of glycosylation. Even though the work described in this thesis

was using *Drosophila* as our model system, we hope be able to perform experiments to test if the role of Roc2 is conserved throughout species. It is possible that the substrates may vary in every organism, but its involvement in regulating glycan expression should be conserved. Overall, our findings for the role of Roc2 and ATPα in regulating glycan expression leave some unanswered questions, but present the first step in showing the involvement of proteins and mechanisms that have never been studied before.

Figure 4.1: Roc2 regulates glycan expression by controlling synaptic homeostasis and neural membrane potential.
Our current model suggests that Roc2, an E3 ubiquitin ligase is the molecular lesion responsible for the *Roc2*^{ms16} phenotype. A decrease in Roc2 causes an accumulation of ATPα in neurons and at the muscles at the NMJ. In the neuron, the increase in ATPα causes a constant repolarization of depolarized cells, which leads to altered Golgi trafficking and mislocalization or dilution of Golgi resident enzymes and glycosyltransferases.. Another possible effect is that the ATP to ADP shift could lead to a decrease in AMP, which causes reduced activity of AMP-kinases, such as *sff*, placing *sff* function downstream of *Roc2*. The increase of Arginine Kinase in our mutant could be explained by the need for excess ATP for energy. Ubiquitin ligases have been implicated in altering Golgi architecture, and we don't rule out the possibility that Roc2 could also be affecting Golgi Organization.

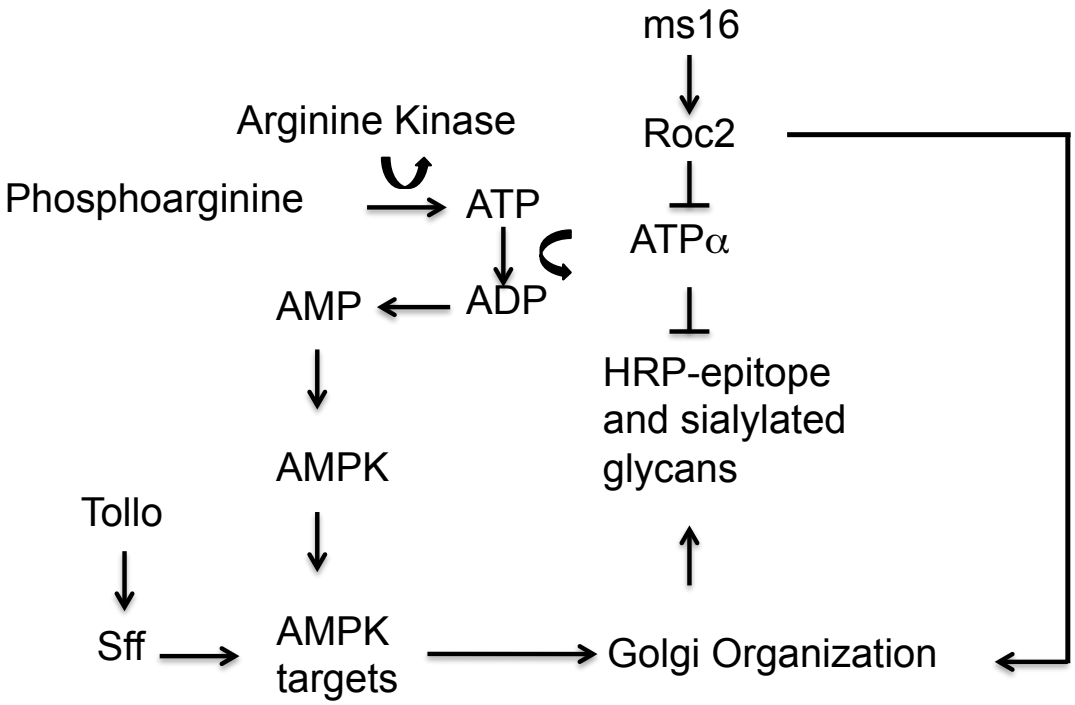

References

Acconcia, F., Sigismund, S. & Polo, S. 2009. Ubiquitin in trafficking: the network at work. *Exp Cell Res,* 315(9)**,** pp 1610-8.

Aoki, K., Porterfield, M., Lee, S. S., Dong, B., Nguyen, K., McGlamry, K. H. & Tiemeyer, M. 2008. The diversity of O-linked glycans expressed during Drosophila melanogaster development reflects stage- and tissue-specific requirements for cell signaling. *J Biol Chem,* 283(44)**,** pp 30385-400.

Bard, F., Mazelin, L., Péchoux-Longin, C., Malhotra, V. & Jurdic, P. 2003. Src regulates Golgi structure and KDEL receptor-dependent retrograde transport to the endoplasmic reticulum. *J Biol Chem,* 278(47)**,** pp 46601-6.

Barr, F. A., Puype, M., Vandekerckhove, J. & Warren, G. 1997. GRASP65, a protein involved in the stacking of Golgi cisternae. *Cell,* 91(2)**,** pp 253-62.

Berger, C., Renner, S., Lüer, K. & Technau, G. M. 2007. The commonly used marker ELAV is transiently expressed in neuroblasts and glial cells in the Drosophila embryonic CNS. *Dev Dyn,* 236(12)**,** pp 3562-8.

Cherniavsky-Lev, M., Golani, O., Karlish, S. J. & Garty, H. 2014. Ouabain-induced internalization and lysosomal degradation of the Na+/K+-ATPase. *J Biol Chem,* 289(2)**,** pp 1049-59.

Chia, J., Goh, G., Racine, V., Ng, S., Kumar, P. & Bard, F. 2012. RNAi screening reveals a large signaling network controlling the Golgi apparatus in human cells. *Mol Syst Biol,* 8(629.

Kimura, T., Han, W., Pagel, P., Nairn, A. C. & Caplan, M. J. 2011. Protein phosphatase 2A interacts with the Na,K-ATPase and modulates its trafficking by inhibition of its association with arrestin. *PLoS One,* 6(12)**,** pp e29269.

Kulikov, A., Eva, A., Kirch, U., Boldyrev, A. & Scheiner-Bobis, G. 2007. Ouabain activates signaling pathways associated with cell death in human neuroblastoma. *Biochim Biophys Acta,* 1768(7)**,** pp 1691-702.

Lee, W. Y., Goh, G., Chia, J., Boey, A., Gunko, N. V. & Bard, F. 2015. The Ubiquitin Ligase CBLC Maintains the Network Organization of the Golgi Apparatus. *PLoS One,* 10(9)**,** pp e0138789.

Nakamura, N., Rabouille, C., Watson, R., Nilsson, T., Hui, N., Slusarewicz, P., Kreis, T. E. & Warren, G. 1995. Characterization of a cis-Golgi matrix protein, GM130. *J Cell Biol,* 131(6 Pt 2)**,** pp 1715-26.

Schwarz, L. A. & Patrick, G. N. 2012. Ubiquitin-dependent endocytosis, trafficking and turnover of neuronal membrane proteins. *Mol Cell Neurosci,* 49(3)**,** pp 387-93.

Tian, J., Cai, T., Yuan, Z., Wang, H., Liu, L., Haas, M., Maksimova, E., Huang, X. Y. & Xie, Z. J. 2006. Binding of Src to Na+/K+-ATPase forms a functional signaling complex. *Mol Biol Cell,* 17(1)**,** pp 317-26.

VIRDEN, R., WATTS, D. C. & BALDWIN, E. 1965. ADENOSINE 5'-TRIPHOSPHATE-ARGININE PHOSPHOTRANSFERASE FROM LOBSTER MUSCLE: PURIFICATION AND PROPERTIES. *Biochem J,* 94(536-44.

Weller, S. G., Capitani, M., Cao, H., Micaroni, M., Luini, A., Sallese, M. & McNiven, M. A. 2010. Src kinase regulates the integrity and function of the Golgi apparatus via activation of dynamin 2. *Proc Natl Acad Sci U S A,* 107(13)**,** pp 5863-8.

APPENDIX TABLES (TABLES S1-S6)

Table S1. NMR acquisition and processing parameters

	1-D		*gCOSY*		*TOCSY*		*gHSQC*		*NOESY*	
	Proto	*Pres*	*F2*	*F1*	*F2*	*F1*	*F2*	*F1*	*F2*	*F1*
HDO	no	yes	no		yes		no		yes	
Presaturati										
Transients	32	32	16		32		256		32	
Mixing time					80				400	
(ms)										
Spectral	2332	2332	233	233	233	233	317	1809	233	233
width (Hz)			2	2	2	2	3	6	2	2
Points	4778	4778	512	800	512	256	635	256	512	256

Table S2. Chemical shift assignments for Standard 107

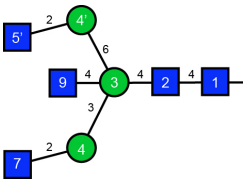

Residue	Chemical shift (ppm)[a]							NOE
	1	2	3	4	5	6	6'	
1a	5.18(2.2)	3.87	3.88	3.63	*nd*[b]	*nd*	*nd*	
	93.1	*56.3*	*72.0*	*82.3*	*nd*	*nd*		
1b	4.688	3.69	3.62	3.63	3.52	3.83	3.64	
	97.4	*58.0*	*76.0*	*82.3*	*77.2*	*62.7*		
2 (a)[c]	4.593(8.0)	3.80	3.73	3.74	3.61	3.87	3.73	1a-4, 1b-4
(b)	4.602(8.4)							
	104.1	*57.7*	*74.6*	*81.2*	*77.2*	*62.7*		
3	4.688(<2)	4.167	3.86	4.069	3.54	3.89	3.89	2-4
	102.7	*73.0*	*81.4*	*74.1*	*77.0*	*68.0*		
4	5.051(<2)	4.241	3.89	3.47	3.70	3.93	3.59	3-3,5-1
	102.5	*79.0*	*72.0*	*70.2*	*76.2*	*64.5*		
4'	4.995(<2)	4.141	3.83	3.48	3.61	3.93	3.62	3-6, 5'-1
	100.4	*78.8*	*72.3*	*70.2*	*76.0*	*64.5*		
5	4.548((8.6)	3.73	3.60	3.48	3.46	3.89	3.78	4-1,4-2
	102.3	*58.0*	*76.2*	*72.5*	*78.6*	*63.4*		
5'	4.539(8.6)	3.69	3.48	3.48	3.40	3.89	3.76	4'-1,4'-2
	102.3	*58.0*	*76.2*	*72.5*	*78.4*	*63.4*		
9	4.458(8.6)	3.70	3.56	3.258	3.41	3.98	3.69	3-4
	103.2	*58.9*	*76.0*	*73.7*	*79.5*	*64.3*		

N-acetyl signals: 2.073/*24.9*, 2.059/*25.2*, 2.050/*24.9*, 2.041/*24.9*, 2.030/*24.7*
[a]coupling constants in parentheses, ^{13}C shifts in italics
[b]*nd*=not determined
[c]α and β of Residue 1

Table S3. Chemical shift assignments for Standard 108

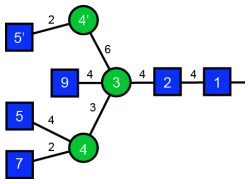

Residue	Chemical shift (ppm)							NOE
	1	2	3	4	5	6	6'	
1a	5.180(2.0)	3.88	3.87	3.63	*nd*	*nd*	*nd*	
	93.1	*56.3*	*71.8*	*82.3*	*nd*	*nd*		
1b	4.688	3.69	3.63	3.63	3.51	3.83	3.64	
	97.8	*58.0*	*76.0*	*82.3*	*77.2*	*62.9*		
2 (a)	4.591(8.2)	3.81	3.74	3.73	3.59	3.88	3.73	1a-4,1b-4
(b)	4.601(8.3)							
	104.4	*58.0*	*74.6*	*81.2*	*77.2*	*62.7*		
3	4.677(<2)	4.138	3.85	4.078	3.53	3.88	3.86	2-4
	102.5	*73.0*	*81.4*	*74.1*	*77.0*	*68.0*		
4	5.049(<2)	4.278	4.037	3.59	3.72	3.80	3.56	3-3,5-1
	102.3	*78.8*	*70.6*	*81.6*	*74.6*	*64.6*		
4'	4.993(<2)	4.139	3.83	3.48	3.61	3.95	3.63	3-6,5'1
	100.4	*78.8*	*72.3*	*69.9*	*76.0*	*64.5*		
5	4.535(8.7)	3.72	3.58	3.48	3.46	3.90	3.77	4-1,4-2
	102.3	*58.2*	*76.0*	*72.3*	*78.6*	*63.4*		
5'	4.536(8.7)	3.69	3.48	3.48	3.40	3.90	3.76	4'-1,4'-2
	102.3	*58.0*	*76.0*	*72.3*	*78.4*	*63.4*		
7	4.508(8.7)	3.75	3.56	3.47	3.51	3.93	3.76	4-6'
	104.4	*58.2*	*76.2*	*72.3*	*78.6*	*63.4*		
9	4.456(8.3)	3.69	3.56	3.263	3.40	3.97	3.69	3-4
	103.5	*58.9*	*76.2*	*73.7*	*79.5*	*64.3*		

N-acetyl signals: 2.075/*24.9*, 2.073/*24.9*, 2.055/*25.2*, 2.049/*24.9*, 2.040/*24.9*, 2.030/*24.7*

Table S4. Chemical shift assignments for Standard 121 without sialic acid

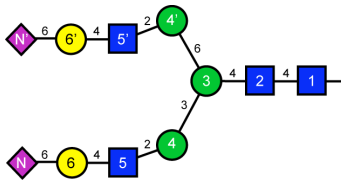

Residue	Chemical shift (ppm)							NOE
	1	2	3	4	5	6	6'	
1a	5.182(3.0)	3.87	3.87	3.63	*nd*	*nd*	*nd*	
	93.2	*56.4*	*72.1*	*82.4*	*nd*	*nd*		
1b	4.687(7.7)	3.69	3.61	3.66	3.51	3.88	3.66	
	97.6	*58.7*	*75.6*	*83.3*	*77.5*	*62.7*		
2	4.59	3.75	3.75	3.73	3.59	3.87	3.74	1a-4,1b-4
	102.1	*57.3*	*74.9*	*82.4*	*77.3*	*62.7*		
3	4.77(<2)	4.251	3.77	3.75	3.63	3.95	3.78	2-4
	103.3	*72.8*	*83.3*	*74.9*	*77.0*	*68.6*		
4	5.126(<2)	4.191	3.89	3.50	3.74	3.87	3.62	3-3,5-1
	102.3	*79.1*	*72.3*	*70.2*	*76.3*	*65.3*		
4'	4.942(<2)	4.110	3.88	3.49	3.61	3.87	3.62	3-6,5'-1
	99.8	*79.1*	*72.3*	*70.2*	*77.3*	*65.3*		
5	4.607(7.3)	3.78	3.73	3.65	3.57	3.97	3.84	4-1,4-2
	102.1	*57.6*	*74.9*	*83.3*	*77.3*	*63.0*		
5'	4.598(7.7)	3.75	3.73	3.65	3.57	3.97	3.84	4'-1,4'-2
	102.1	*57.6*	*74.9*	*83.3*	*77.3*	*63.0*		
6	4.437(8.3)	3.53	3.67	3.92	3.82	3.99	3.54	5-4,5-6
	106.3	*73.5*	*75.4*	*71.2*	*76.6*	*66.0*		
6'	4.440(7.7)	3.52	3.67	3.92	3.82	3.99	3.54	5'-4,5'-6
	106.3	*73.5*	*75.4*	*71.2*	*76.6*	*66.0*		

N-acetyl signals: 2.077/*25.0*, 2.063/*25.2*, 2.059/*25.0*, 2.040/*24.8*, 2.031/*24.8*

Table S5. Chemical shift assignments for Standard 121 sialic acid residues

Residue	Chemical shift (ppm)								
	3	3'	4	5	6	7	8	9	9'
Na, N'a	1.714(12.5)	2.663(4.1)	3.65	3.79	3.70	3.55	3.89	3.91	3.61
	42.8		*70.9*	*54.5*	*75.1*	*71.2*	*74.4*	*64.6*	
Nb, N'b	1.816	2.194	4.01	3.97	*nd*	*nd*	*nd*	*nd*	*nd*
	nd	*nd*	*nd*	*nd*	*nd*	*nd*	*nd*	*nd*	

N-acetyl signal: 2.022/*25.0*

Table S6. Molar response factors, heterogeneity, and mass purity for glycan standards

Malto-Series Standards	Molar Response Factor	
	Measured by HPLC (mvolt·sec/pM, mean±SD, n=9)	Measured by NSI-LTQ/Orbi MS (signal/pM, mean±SD, n=7)
dp3	12.7±0.4	61.6±3.8
dp4	12.9±0.4	79.0±4.3
dp5	13.4±0.5	74.4±4.3
dp6	12.9±0.5	67.8±3.9
dp7	11.4±0.4	68.0±4.1
mean±SD[a]	12.6±0.2	68.1±2.3

N-Glycan Standards	Contribution of Major Component to Total Profile of Standard[b]	Purity by Mass[c]
	Measured by HPLC, MALDI-TOF and NSI-LTQ/Orbitrap MS (%Total Profile, mean±SD, n=9)	Measured by NMR and HPLC (% of Total Mass, mean±SD, n=4)
107	85.7±3.8	104.5±3.9
108	89.7±3.3	86.2±10.8
121	68.0±3.5	83.6±6.0

[a]Mean and standard deviation calculated for dp4-dp7
[b]The expected structure was detected as the major component for all N-Glycan standards
[c]Sum of all glycan components detected in the total profile of the standard

APPENDIX FIGURES (Figures S1-S7)

Appendix Figure S1. Exoglycosidase/HPLC sequencing of Standard 107. An aliquot of N-glycan standard 107 was fluorescently tagged with 2-AB and digested with hexosaminidase from *Streptococcus pneumonia* (GUH). Digested and undigested standards were resolved by HPLC and the structure of the resulting digestion products were elucidated based on elution position relative to standard glucose ladder (GU). GUH digestion removes terminal b-linked GlcNAc residues, but bisecting GlcNAc (b4 to Man) hinders digestion.

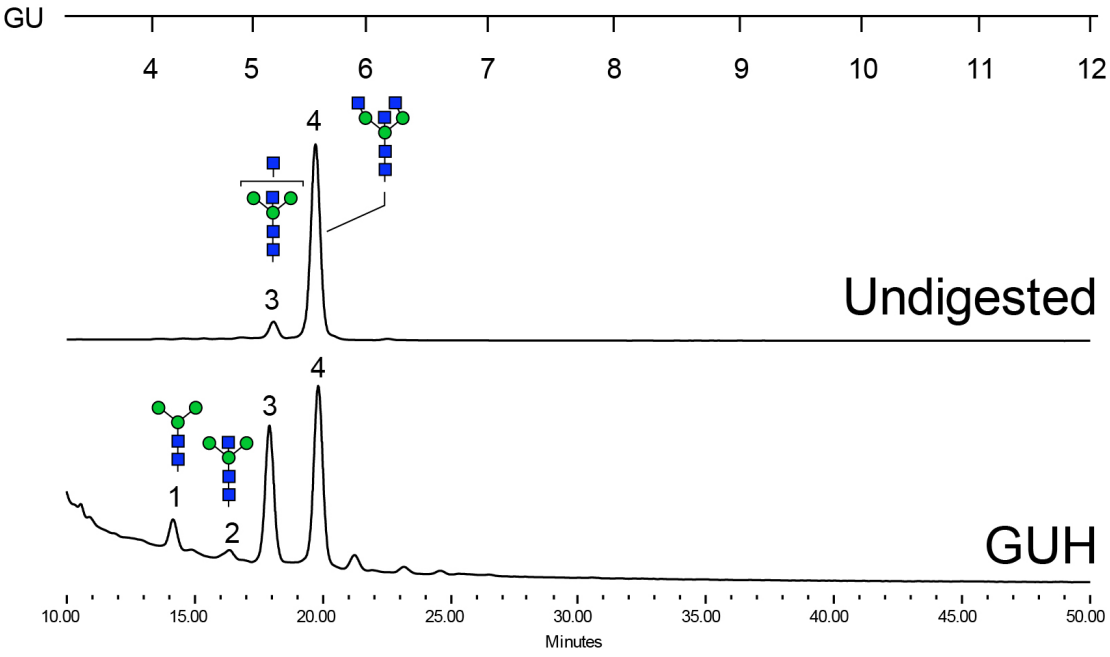

Appendix Figure S2. Exoglycosidase/HPLC sequencing of Standard 108. An aliquot of N-glycan standard 108 was fluorescently tagged with 2-AB and digested with hexosaminidase from *Streptococcus pneumonia* (GUH). Digested and undigested standards were resolved by HPLC and the structure of the resulting digestion products were elucidated based on elution position relative to standard glucose ladder (GU). GUH digestion removes terminal b-linked GlcNAc residues, but bisecting GlcNAc (b4 to Man) hinders digestion.

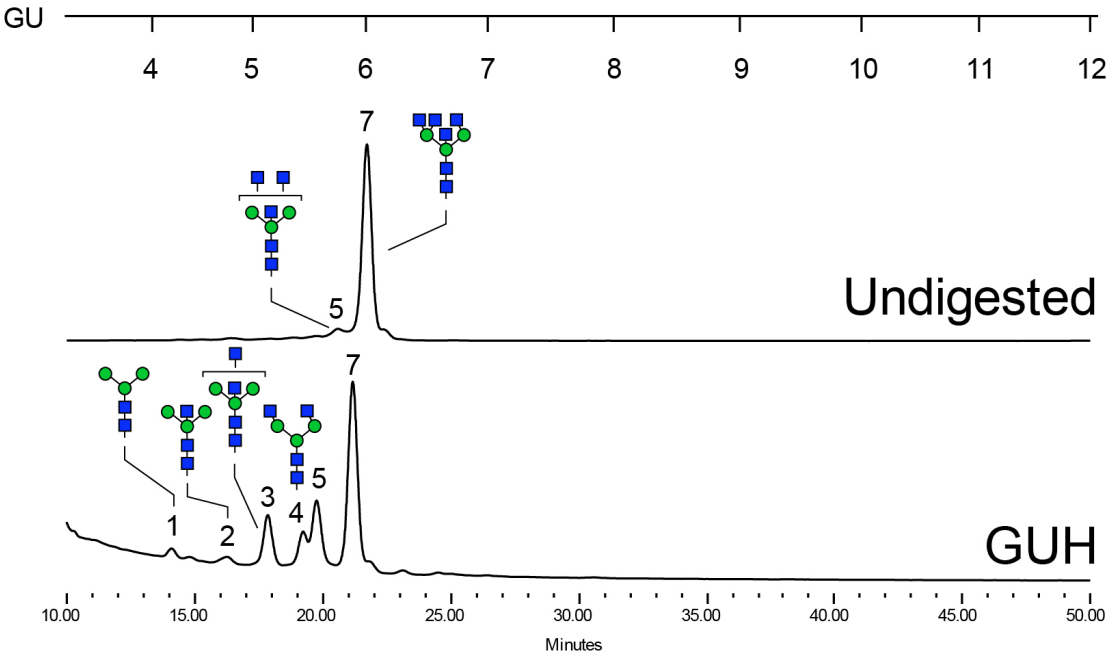

Appendix Figure S3. Exoglycosidase/HPLC sequencing of Standard 121. An aliquot of N-glycan standard 121 was fluorescently tagged with 2-AB and digested a2-6/a2-8 specific sialidase from *Arthrobacter ureafaciens* (ABS) or with ABS plus b-galactosidase from bovine testes (BTG) or with ABS and BTG plus hexosaminidase from *Streptococcus pneumonia* (GUH). Digested and undigested standards were resolved by HPLC and the structure of the resulting digestion products were elucidated based on elution position relative to standard glucose ladder (GU). Sequential sensitivity of standard 121 to sialidase, galactosidase, and hexosaminidase digestion is consistent with the proposed structure for the major component.

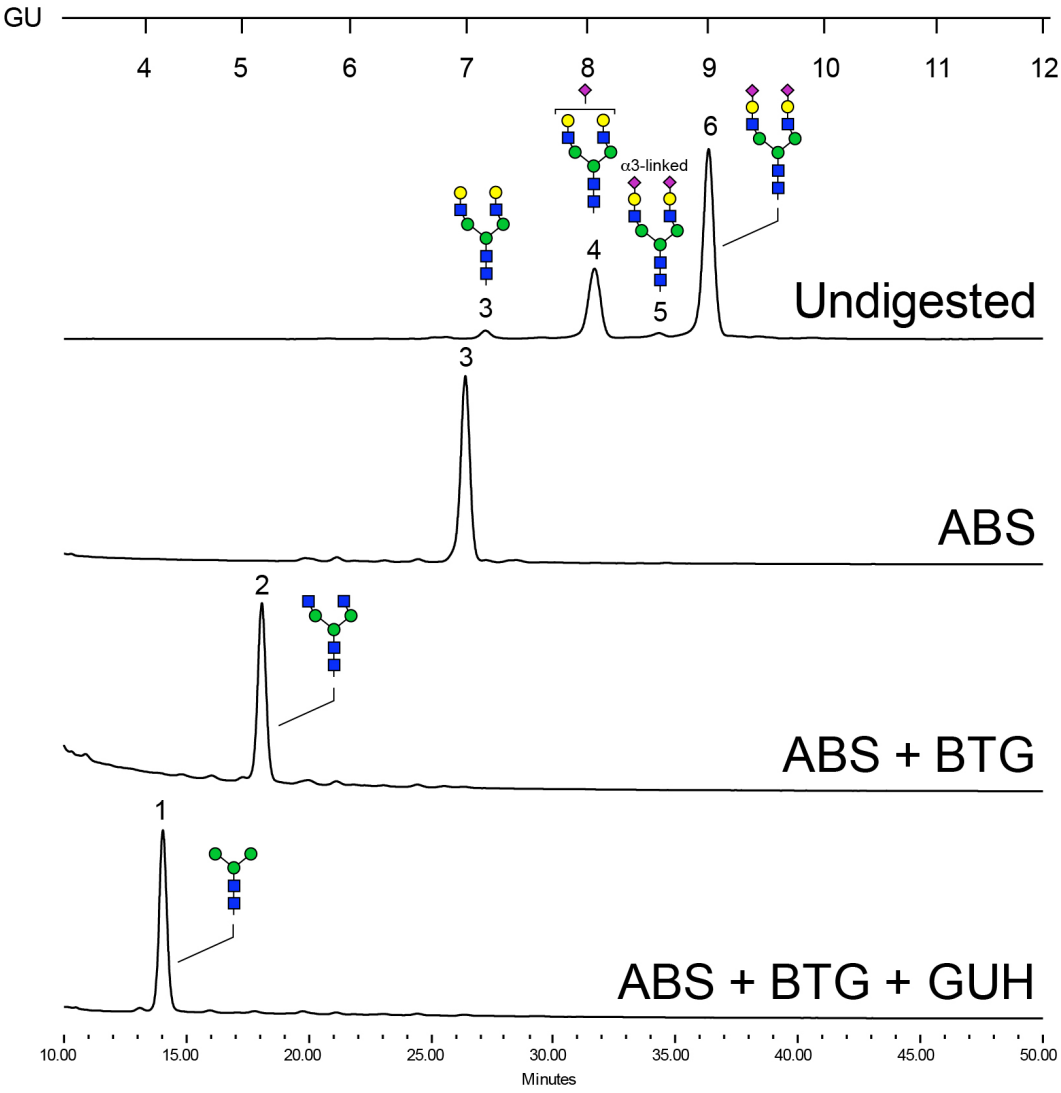

Appendix Figure S4. MALDI-TOF MS of N-glycan standards. An aliquot of each N-glycan standard was permethylated, combined with matrix (α-dihyroxybenzoic acid, 20mg/mL solution in 50% methanol:water), and analyzed in positive mode using a Bruker Microflex LRP operating in reflectron mode.

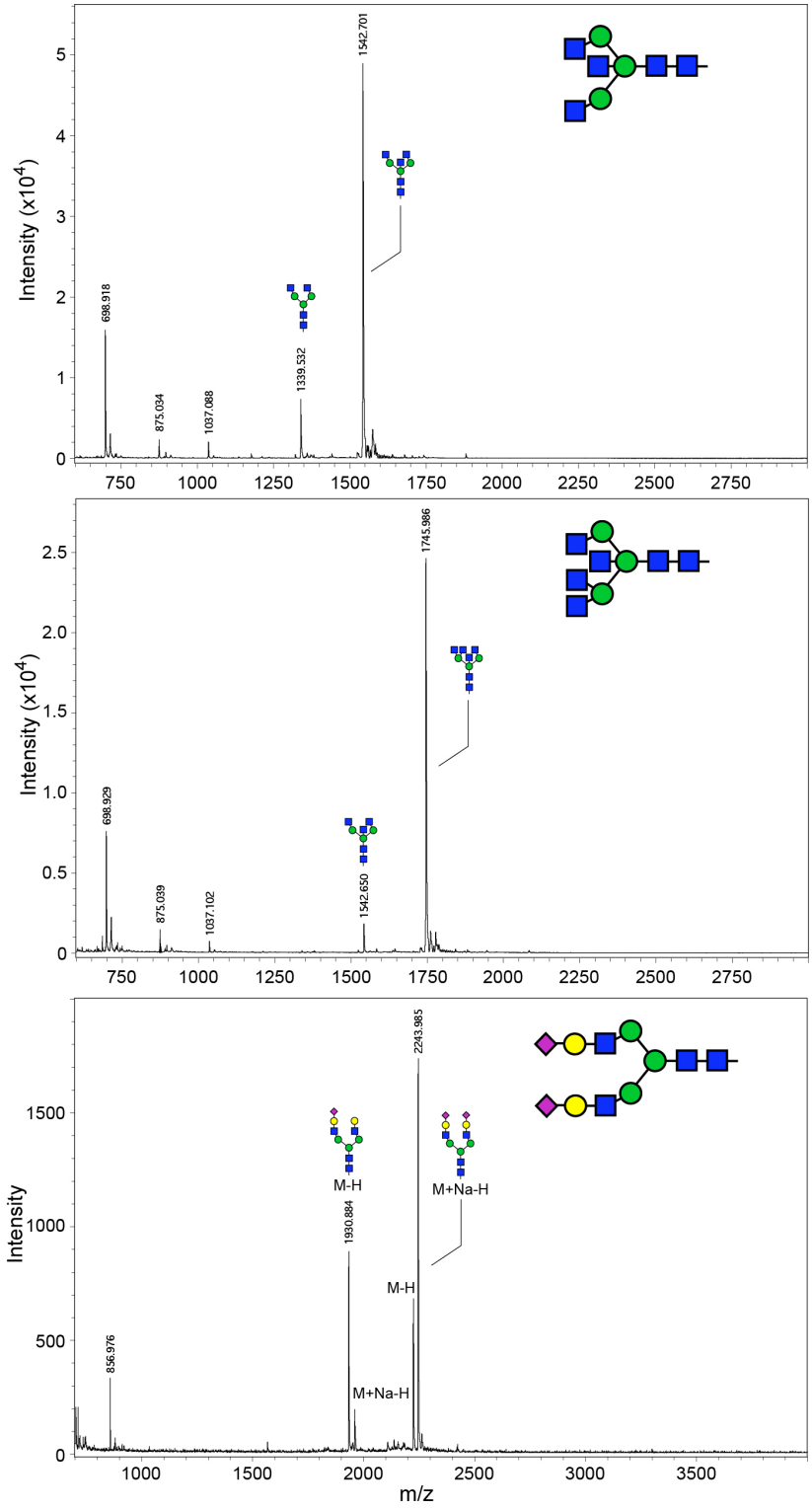

Appendix Figure S5. NSI-LTQ/Orbitrap MS of N-glycan standards. An aliquot of each N-glycan standard was permethylated and infused directly into a Thermo Fisher LTQ/Orbitrap using a nanospray ionization interface. Most permethylated glycan components were identified as singly, doubly, and triply charged, sodiated species [M+Na] in positive mode.

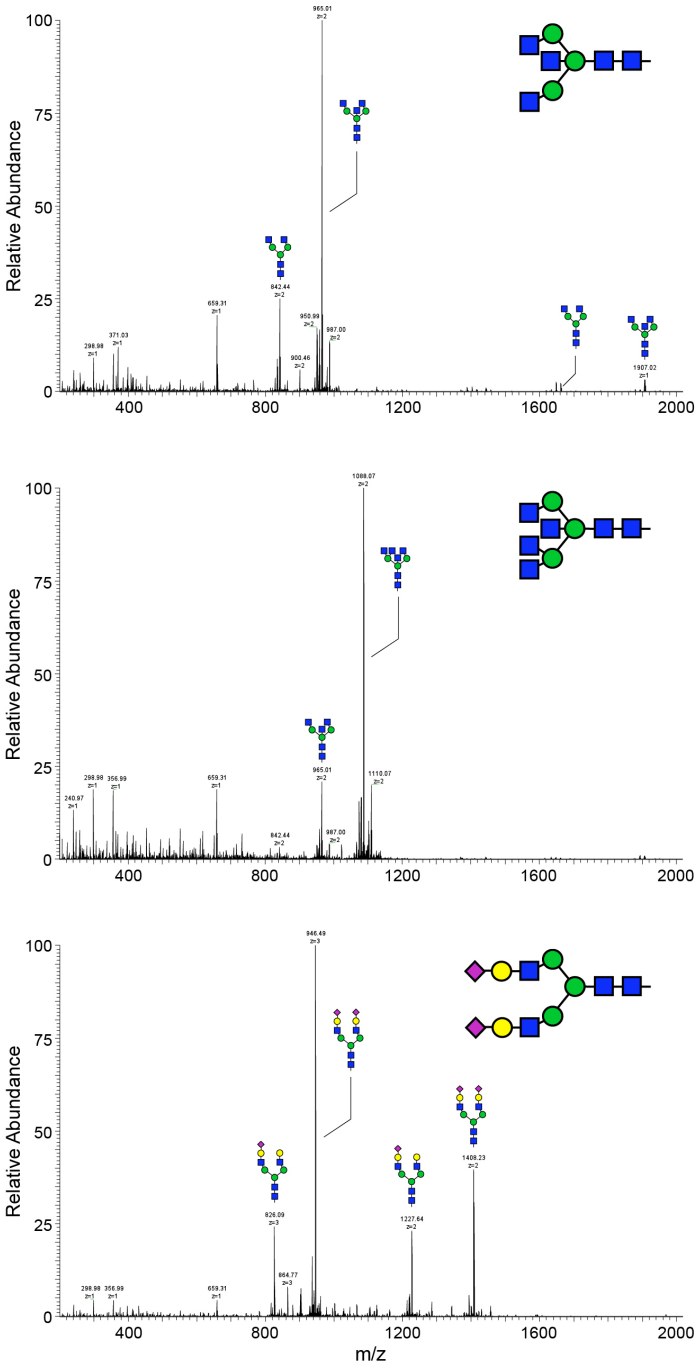

Appendix Figure S6. MS/MS of N-glycan standards. The ions corresponding to the doubly charged species of each of the major components (see Figure S5) of N-glycan standards 107, 108, and 121 were selected for fragmentation by CID in the linear trap of the LTQ/Orbitrap instrument. Doubly charged MS/MS fragments resulting from the neutral loss of 1, 2, or 3 monosaccharide residues as N-acetylhexosamine (HexNAc) or as N-acetylneuraminic acid (NeuAc) from the non-reducing end of the permethylated standards were detectable. Subsequent MSn fragmentation of the remaining cores was consistent with the proposed standard structures.

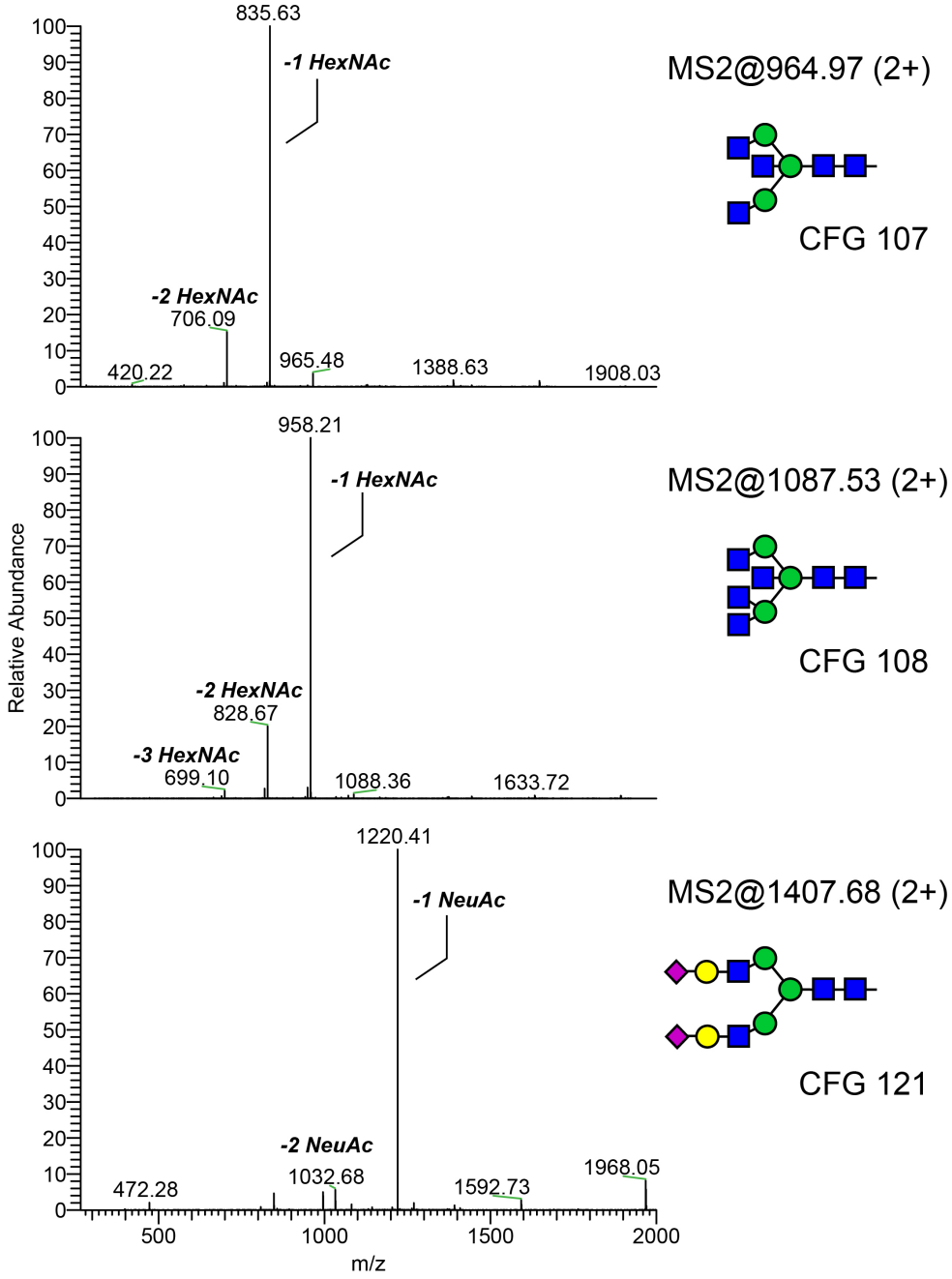

Appendix Figure S7. Reproducibility of fluorescence intensities used to calculate molar response factors for 2-AB labeled malto-series standards. Three chromatographic technical replicates of three independent labeling reactions were analyzed by HPLC. Peak areas were integrated and used to define molar response factors for quantifying N-glycan standards (see Table S6). The percent error associated with technical replicates was 5.6 – 5.7%, while the percent error associated with inter-assay variability was 10.3 – 10.6%. The malto-series standard mixture was prepared with 10% more dp4 than the other malto-oligosaccharides in order to confirm elution positions and standard identities.